POWER EFFICIENCY OF INDUSTRIAL EQUIPMENT

Kirsty Lynn Veale

Submitted in fulfilment of the academic requirements for the degree of Master of Science in Mechanical Engineering

March, 2011

Supervisor: Professor Lance Roberts

Co-Supervisor: Professor Sarp Adali

DECLARATION

I hereby declare that this dissertation presents my own unaided work except where due acknowledgement has been given to others. This dissertation is being submitted to the University of KwaZulu-Natal for the Degree of Master of Science in Mechanical Engineering, and has not been submitted previously for any other degree or examination.

_____   Date   _____

Kirsty Lynn Veale

_____   Date   _____

Professor Lance Roberts

_____   Date   _____

Professor Sarp Adali

ACKNOWLEDGEMENTS

ABSTRACT

Power conservation has become a high priority to South African industries due to recent environmental assessments and electricity price hikes. This research aims to demonstrate to Industry the many simple and cost effective ways to increase their industrial efficiency with simple modifications, as well as making them more aware of common assembly errors that significantly increase power consumption. This has been accomplished with the design, construction and testing of a test rig capable of producing the desired test results which simulate Industry usage.

A test rig was required to test certain energy efficient equipment. This dissertation contains an explanation of the tests required, as well as how they were conducted. These test requirements directed the design outcomes of the test rig. Due to the variety of equipment to be tested, and the accuracy required, the test rig had to be fully adjustable. The design process is explained in this dissertation, along with relevant theory with regard to the testing procedures. The testing procedures were designed to be as accurate as possible. The setup equipment and procedure is briefly explained to ensure an understanding of the capabilities of the test rig.

This dissertation contains the results obtained from testing a variety of couplings, belts and motors under different conditions. The results obtained show the difference between the efficiency of a standard motor and that of a high efficiency motor. The efficiency comparison of the Poly V ^{TM}, Poly Chain$^®$ and SPB V-belts showed very distinct advantages and disadvantages of each belt. The coupling testing was conducted under conditions of misalignment, and resulted in distinct differences in the efficiencies of each coupling at different degrees of misalignments. The couplings tested were the Fenaflex$^®$, the Quick-Flex$^®$, and the Fenagrid$^®$ coupling. All results obtained were analyzed and discussed in the relevant sections.

The results obtained showed that the high efficiency motor is significantly more efficient than the standard motor at full load, although at low loading, the motor efficiencies were very similar. The coupling tests showed the negative effects misalignment has on the efficiency of the Quick-Flex$^®$ and Fenagrid$^®$ coupling as well as the capability of the Fenaflex$^®$ coupling to withstand the effects of large misalignments without significant efficiency loss.

The belt testing revealed the advantages and disadvantages of each type of belt used. This showed that although the synchronous belt did not lose efficiency with decreased tension, it became unstable, and was difficult to keep on the pulley if not aligned correctly. The V-belts can handle low tension well. Prolonged use of the belts can cause them to stretch, lowering the tension into a "danger zone" that will cause the belts to slip. This slip can damage the belt and pulley. At the lower tension of the V-belt, although the efficiency increases slightly, the vibration of the slack side of the belt is significant, and can be dangerous as the belt could jump off the pulley. The Poly V ^{TM} belt has some of the advantages of the V-belt, except that it is unable to maintain its friction at low tension, as the belt width prevents it from being wedged into the grooves like the V-belt.

The fluid coupling tests showed that the shock loading on a high inertia system can be significantly reduced with the aid of a fluid coupling. The reduced shock loading can reduce energy consumption, and increase the life of electric motors and the equipment that they drive by preventing excessive overloading.

TABLE OF CONTENTS

NOMENCLATURE

Symbols

D	–	Distance from centre of rotation to force (m)
E_i	–	Input electrical cost
E_u	–	Useful electrical output cost
F	–	Force applied to load cell (N)
K_t	–	concentration factor for bending
K_{ts}	–	concentration factor for torsion
k_f	–	key factor
M	–	Bending moment (Nm)
M_t	–	Torque (Nm)
m	–	Mass per meter (kg/m)
N	–	Rotation Speed (rpm)
P	–	Power transmitted (kW)
Su	–	Ultimate tensile strength
Sy	–	Yield strength
T_{st}	–	Static tension of belt (N)
V	–	Velocity (m/s)
W	–	Power (W)
η_s	–	Total system efficiency

Abbreviations

BMG	–	Bearing Man Group
DOL	–	Direct On Line
VSD	–	Variable Speed Drive
OST	–	Oscillating System Technology
CNC	–	Computer Numerical Control
PLC	–	Programmable logic controllers
SA	–	South Africa
NEES	–	National Energy Efficiency Strategy
CVT	–	Continuously Variable Transmission

LIST OF FIGURES

CHAPTER 4

APPENDIX B

APPENDIX C

LIST OF TABLES

CHAPTER 1

INTRODUCTION

1.1   Introduction

Due to the current energy crisis in South Africa, energy conservation has become an important factor in people's lives. Industry consumes the greatest part of this energy, and thus needs to establish new ways to reduce power consumption, resulting in reduced expenses. This research has become even more important after the recent announcements of the proposed electricity price hikes that will be occurring over the next 3 years. [1]

This research project was proposed by Bearing Man Group (BMG) to demonstrate that their specialized products can help reduce energy consumption in Industry by a significant amount. BMG required the design and construction of a test rig that was able to determine the efficiencies of their new high efficiency motors, variable speed drives (VSD), fluid couplings, belts under a variety of tensions, and couplings under misalignment.

The test rig designed had to be capable of providing a direct online (DOL) start to test the effect the fluid coupling had on the start-up efficiency. The system also had to be able to simulate a soft start with the use of VSD's. The soft start was used to test the efficiency of equipment under running conditions, without the initial damaging shock of start-up.

The results obtained in this project gave an accurate comparison of the equipment efficiencies under different loading conditions. The conclusions drawn from these results either proved or disproved the claims made by the BMG marketing department. Further research into this topic will improve the understanding and importance of correct alignment procedures within Industry.

The design of this test rig incorporated the capacity to test a variety of equipment, including components that may not be specified in this dissertation. This ensures that any testing of additional equipment can be conducted under the same conditions. The flexibility of the test rig was an important factor in the design process, and had to be considered before any design choices were made.

1.2   Power consumption in South Africa

It is well known that South African electricity production is dominated by coal-fired power stations. This is due to the abundant supply and low cost of local coal supplies. The Digest of South African Energy Statistics 2006 [1] showed, in 2004, 68% of the total electricity in South Africa was produced by coal-fired power stations. Coal will remain the preferred source of energy production in South Africa into the foreseeable future. This is due to the availability of coal from local mines as well as the well established coal-fired plants within the country. Figure 1-1 below shows a comparison of the capacities of the different sources of electricity generated in South Africa in 2004. It is clear that coal produces the greatest part of electricity in SA. There are thirteen coal-fired power plants in South Africa, three were previously shut down due to excess power generation capacity, and are now currently under repair due to the energy shortage. Three others were in working condition but were not functioning, and have recently been brought back into production to relieve the electricity shortage.
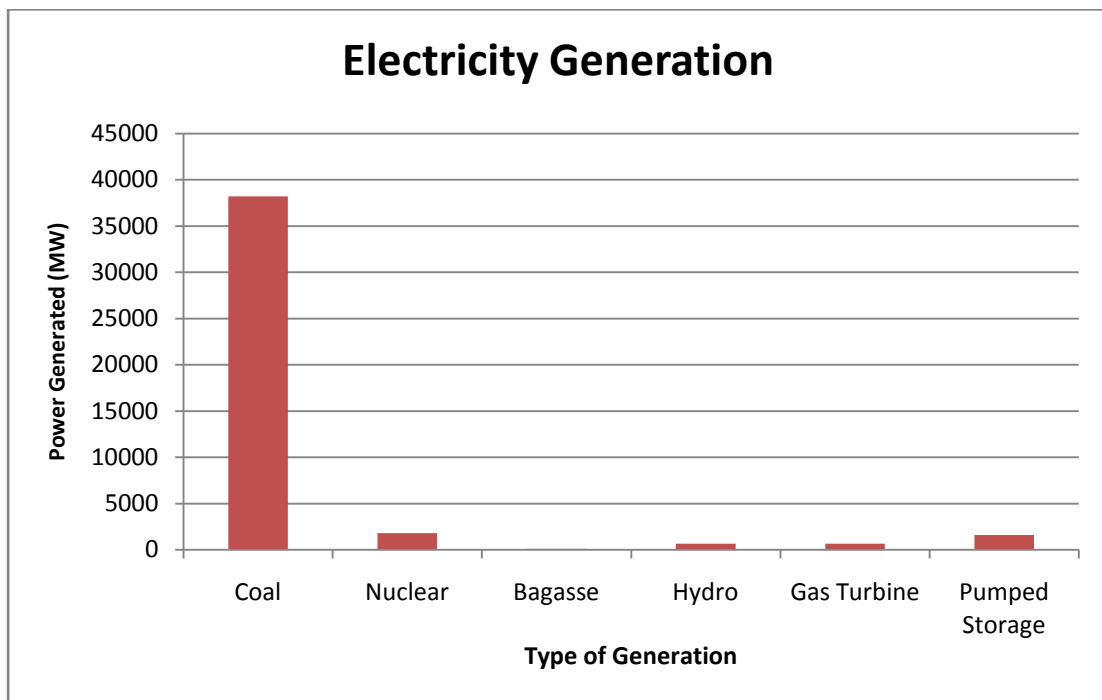
Figure 1-1: Source of electricity generation in South Africa [1]

This section of the dissertation focuses on coal power due to the air pollution the combustion process produces. It causes the greatest part of air pollution compared to the other sources, and needs to be reduced to stall the onset of global warming. Coal combustion can lead to particulate matter being present in the air, as well as contributing to acid rain. As it is impossible to immediately change South Africa's electricity source due to its almost total dependence on coal, the next logical choice is to reduce emissions until a new source can be established. To reduce emissions, electricity usage must be reduced. In 2004 it could be seen that 36.2% [1] of electricity was consumed within Industry, including mines. This was the most any single sector consumes, and is thus a good place to start reduction.

South Africa previously produced some of the cheapest electricity in the world, with the result that Industry was not as energy efficient as reasonably possible as it was cheaper to ignore efficiency and pay the electricity bill. It has now become extremely important for Industry to reduce consumption as there have been two recent electricity price hikes, and a further three are expected within the next three years. There is an opportunity for simple efficiency improvements in Industry due to aspects previously neglected, as well as many more improvements due to recent technological advances.

1.3   Existing steps to reduce consumption

South Africa has a strategy in place to reduce energy consumption. It is called the National Energy Efficiency Strategy (NEES) [2,3], which was drafted in 2008. This strategy showed the proactive involvement of government in reducing energy consumption, as well as the importance of finding a solution for this ongoing problem. The NEES acknowledges the potential that was available to improve efficiency in all sectors. It was also aimed at creating affordable energy while reducing health and environmental impacts. The main aim of this strategy was to reduce industrial consumption by 12% by 2015.

The Kyoto Protocol (1997) was created to reduce the effect of climate change on the world. It was only compulsory for Annex 1 (first world) countries to join, but SA joined as they understood the importance of cooperating. This protocol aimed to reduce the CO_2 levels by 5% by 2012. This protocol became legally binding in 2005. The NEES goes beyond this target, and has a plan of action for the country to achieve this goal.

A less successful solution was implemented in previous years called the Power Conservation Programme. This was caused by the insufficient energy supply and was more commonly known

as load shedding. Unfortunately it had a negative impact on production and needed to be discontinued. As this solution was not ideal, the Department of Minerals and Energy then drafted the NEES. Energy efficiency is the preferred choice as opposed to load shedding as it has a positive impact on production and keeps costs down.

Some of the proposed actions in the NEES are:

- Efficiency Labels
- Performance Standards
- Energy Management Activities
- Energy Audits
- Promotion of Efficient Practices

As South Africa is a developing nation with a large number of heavy industrial areas, it is very energy intensive. It is one of the highest emitters of CO_2 per capita in the world, and uses 40% of the energy used in the whole of Africa. This needs to be reduced. South Africa will always have high energy consumption due to the rich mineral deposits, resulting in a well developed mining sector. Mining is heavily dependent on energy, but due to previously cheap electricity, energy efficiency has been neglected. This new strategy will promote efficiency norms on all industrial equipment. The solutions proposed by the NEES will pay for themselves over a very short time period (3-5 years), and then continue to save the company money in the long run.

The strategy consists of 8 simple goals. These are as follows:

1. Improve health of the nation
2. Job creation
3. Alleviate energy poverty
4. Reduce environmental pollution
5. Reduce CO_2 emissions
6. Improve industrial competitiveness
7. Enhance energy security
8. Reduce the necessity for additional power generation capacity

There have been some barriers preventing the implementation of this strategy. The previously low electricity price made Industry reluctant to pay for efficiency. The situation has changed as the electricity prices have been increased by a significant amount. There was also a lack of knowledge within Industry about energy efficiency, resulting in a reluctance to change the previous standards. The lack of investor confidence in energy efficiency also slowed down the

implementation of the strategy. The strategy claims that 5-15% can be saved through proven no/low cost techniques. A further 11% can be saved easily with known low/medium cost technical interventions.

1.4   Efficiency of industrial equipment

The word efficiency is defined as the ratio of the output to the input power of any system [12]. Improved efficiency in Industry will result from reducing power losses in a system to reduce total power consumption. Efficiency of an entire plant can be improved significantly by increasing the efficiency of the more common inefficient systems within the plant.

Previously, efficiency in Industry was ignored, and corners were cut as often as possible to keep costs down. A common error in Industry was the lack of maintenance of equipment. This includes correct belt tension and shaft alignment. Incorrect maintenance can cause premature failure of bearings, and unintentional heating causing further damage to the system. The simple use of VSDs can increase efficiency and reduce shock loading on a system dramatically increasing the life of the system.

Correct installation and alignment of couplings can significantly increase efficiency and reduce running temperature. Most energy that is lost in a system is through heat loss; therefore heat generation is not a desirable product of a system. Reducing heat generation due to misalignment will increase efficiency.

Correct belt selection, alignment, and tensioning are simple techniques that can reduce power loss in a belt driven system. These factors are often overlooked in Industry. Temperature increase is the result of inefficiencies in the system, and therefore to increase the efficiency of a belt drive system, and increase the life of the belt, temperature has to be kept to a minimum. Misalignment and incorrect tension can significantly increase the temperature of a belt, and thus reduce the efficiency.

1.5   Importance of efficiency in South Africa

South Africa's energy supply is dangerously close to maximum capacity, and the effects of demand going beyond maximum capacity have been experienced recently during the load shedding incidents in 2008. This was not a desirable situation, and a solution needed to be found before all South Africans were subjected to load shedding again. ESKOM managed to overcome load shedding previously as there were various measure in place to temporarily solve the problem [4]. These measures took time, and load shedding was still suffered by all South Africans throughout the year. There were three power plants on standby, which were put into production as soon as was possible. ESKOM also initiated power saving interventions such as handing out free power saving light bulbs to households, and holding energy saving campaigns in an effort to reduce consumption and raise awareness of the problem at hand. All these actions helped, and the country was eventually fully powered again, but not without the potential threat of further blackouts.

Efficiency is extremely important to all South Africans as it may keep our electricity demand below the generating capacity, and prevent further blackouts. Industrial efficiency is even more important, as Industry consumes the most energy, and thus an efficiency improvement in this sector can relieve the energy crisis significantly. It is for this reason that this research focused on industrial efficiency. An increased efficiency will result in a decrease in electricity demand, and thus a decrease in pollution caused by the by-products of electricity produced by our coal-fired power plants.

CHAPTER 2

TESTING

2.1   Testing requirements

BMG required the efficiency of a selection of products to be tested under various loads and different levels of misalignment. The products proposed were advertised by the BMG marketing department as energy efficient products, and the purpose of this project was to determine the actual energy saving to verify these claims. Belts were to be tested using different tensions, and couplings were to be tested under misalignment. The purpose of this was to emphasize the importance of correct installation procedures and the use of correct alignment and tensioning equipment.

The products tested include:

- Fenner® Eff1 electric motors
- Fenner® standard electric motors
- Fenner® SPB V-belt drives
- Poly V ™ drives
- Poly Chain® GT2 drives
- Transfluid couplings
- Quick-Flex® couplings
- Fenaflex® couplings
- Fenagrid® couplings

The system required that the electrical and mechanical powers be accurately measured in order to obtain the precise efficiencies of the motors. Electrical power was read from the supply, and a gimbal mechanism was designed to measure the mechanical torque output. A more detailed explanation of the gimbal will follow later in this dissertation.

The system had to be able to run the motors at a specified speed, as well as applying any specified load. This was done using two identical opposing motors, one as the drive motor, and one as the load motor. The load motor applied the load onto the drive motor, and re-circulated the power generated back into the drive motor. This concept will be discussed further in the next section of this dissertation.

In order to test the effects of belt tension, a lay shaft was required. Two different belt drives were used in the system; the belt to be tested was placed on the drive side, and a Gates® Poly Chain® GT2 was used to connect the lay shaft to the load. The GT2 was used because of its high efficiency and non slip properties. The belt ratios are 2.5:1 step down, and 2.5:1 step up, thus keeping the programming simple by maintaining equal speed on both motors. As two different belts were used, with different centre distances, the system would need to be adjustable. Slots were machined into the base plate on which the gimbal would sit so as to slide the motors back and forth in order to give each belt the correct tension. A layout can be seen in Figure 3-1.

To test the motors and couplings, a shaft was designed to directly couple the drive motor to the load motor by means of a Quick-Flex® coupling on the drive side with the coupling to be tested on the load side. This can be seen in Figure 3-15 on page 40.

BMG also required a Transfluid fluid coupling to be tested. This was achieved by using a second, shorter shaft which coupled the motors by means of the fluid coupling on the drive side, and a Quick-Flex® coupling on the load side.

2.2   Testing theory

2.2.1   Motors and variable speed drives

Electric motors are the backbone of modern Industry and a small increase in the efficiency of each electric motor can result in a significant difference to the total electricity consumption of the country. Electric motors account for 60% of all industrial consumption and using well known, low cost efficiency techniques can save up to 18% [6]. There are a few simple ways to increase the efficiency of Industry with regard to electric motors. These include using specially designed high efficiency motors as well as using VSDs. The load requirements of the task should be assessed before a motor is purchased and the correct motor size should be used for maximum efficiency [5]. Rewound motors should be avoided as efficiency can be lost due to incorrect winding, as well as using substandard material in the new windings [5].

A squirrel cage induction motor, as seen in Figure 2-1 below, consists of a rotor and a stator. These motors do not have brushes, and rely on contactless magnetic induction to transmit torque. A 4 pole, 3-phase squirrel cage motor, as tested for this project, has 12 stator coils. These coils are positioned at equal angles around the rotor.
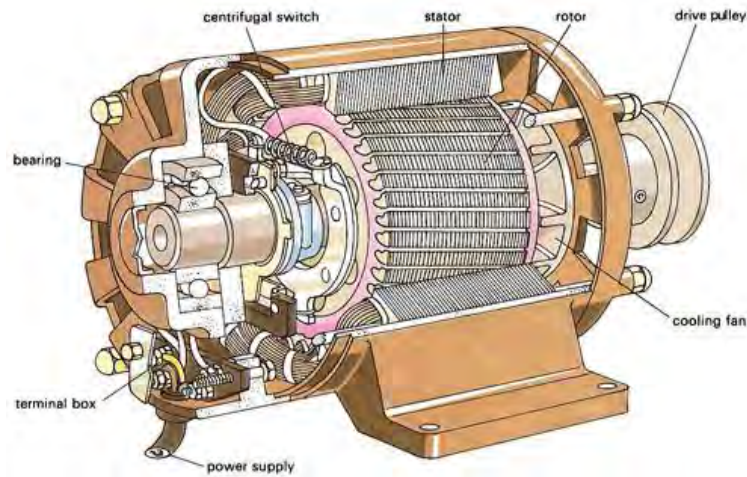
Figure 2-1: Squirrel cage induction motor [30]

A current is allowed to flow through the stator coils. This current creates a magnetic field at the stator, which induces a current at the rotor. This induced current then creates a magnetic field in the rotor, which interacts with the magnetic field of the stator. These same polarity magnetic fields will repel each other, resulting in rotation. The AC current changes the direction of the current flow in each cycle, and thus the polarities of the poles are continuously alternated, causing constant rotation.

Figure 2-2 below shows a 4 pole, 3-phase electric motor. It clearly depicts the stator coil timings, which are dependent on the phase of the AC current. The maximum speed of an electric motor depends on the number of stator poles, i.e. a 3-phase motor with 6 poles will rotate slower than a motor with 2 poles. This is because a 6 pole motor at 50Hz will only rotate 60° per pole, while a 2 pole motor will rotate 180°. This is due to the equal spacing of each pole around the rotor. Figure 2-2 depicts a 3-phase, 4 pole motor, with 12 stator coils.
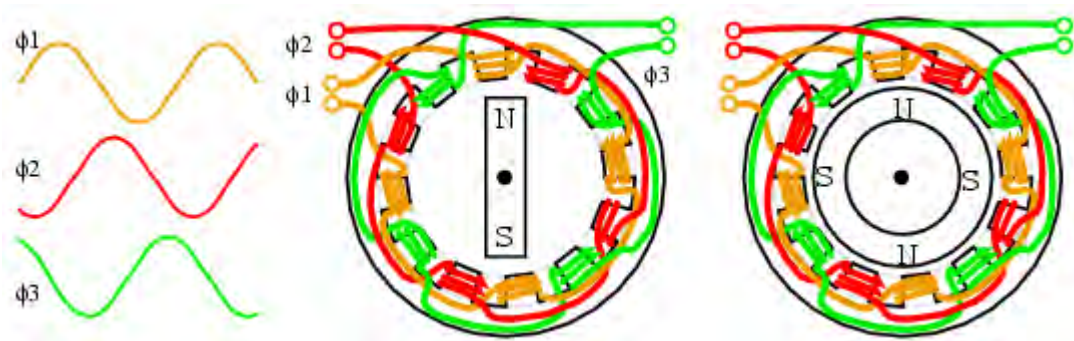
Figure 2-2: Schematic of 3-phase, 4 pole electric motor [31]

Motor losses consist of fixed losses and variable losses. Variable losses are dependent on the load, while fixed losses are independent of load. Fixed losses consist of magnetic core losses or iron losses, friction and windage losses. Variable losses consist of stator and rotor losses and stray load losses. [5]

Iron loss is the energy required to magnetize the core material, and includes losses caused by eddy currents flowing in the core. This loss is found in the rotor and stator magnetic steel, and is caused by the hysteresis and eddy current effects. Iron losses constitute 20-25% of the total motor losses. Friction losses are caused by the friction of the bearings within the motor. These losses are independent of the load on the motor. Windage losses are caused by the circulation of air through the motor. These losses account for 8-12% of the total losses.

Stator losses are caused by the heating of the windings due to the current flow through the stator (I^2R) and are dependent on the load on the motor. This loss constitutes 50-60% of the total losses. Rotor losses are similar in that they are caused by the heating up of rotor windings. This loss can be decreased by increasing the size of conductive bars. Stray load losses are caused by the leakage fluxes through the resistance of stator windings but only when the motor operates under load. This loss constitutes 4-5% of the total loss. [6]

High efficiency motor manufacturers use several techniques to increase motor efficiency. High efficiency motors consist of higher grade steel in the rotor to allow for thicker laminations, thus reducing iron core losses. These motors also reduce resistance by increasing the amount of copper in the stator windings. [7]

When a motor starts under load, the initial power required can be greater than the maximum power rating of the motor. This is due to the torque required to accelerate the motor to maximum speed as soon as possible. The torque applied can be up to 3 times the maximum continuous running torque of the motor and can cause serious damage to the equipment, as well as increase the power consumption of the motor. Variable speed drives (VSDs) allow motors to start-up under load without applying this increased torque. This is achieved by regulating the frequency applied to the motor, and allowing the motor time to ramp up to speed, thus overcoming the inertia of the load.

Depending on the number of start-ups in a plant, a VSD can improve the energy consumption just by preventing this initial overload. The unseen damage caused by this shock loading will be radically decreased, and unplanned maintenance can be reduced. VSDs are known to significantly increase the life of electric motors and other related equipment.

2.2.2 Belts

2.2.2.1 V-Belts

Belt transmissions are used in about one third of all electric motor transmissions in Industry. This makes efficiency of belt drives an important feature in this research. V-belts are an important aspect of this research as they are the most common type of belt used in Industry due to the simplicity involved in use and their low price. It is well established that V-belt efficiency drops dramatically if the load goes below or above the design load. The efficiency also degrades with extended use due to wear and stretching, and requires frequent maintenance. [8]

A belt drive system works with the transmission of torque from the drive pulley to the driven pulley. There is frictional contact between the flanges of the pulley and the sides of the V-Belt. There is a tensional difference in the belt as the belt drive runs under load. The tight side occurs at the exit of the driven pulley, and the slack side occurs at the entry side of the driven pulley. If the cross sectional area of a V-Belt is examined, in Figure 2-3 below, it can be seen that there is a tension member near the top of the belt, which takes up to 95% of the torque load, while the rest of the rubber layer of the belt is for friction and shock absorption. [9]
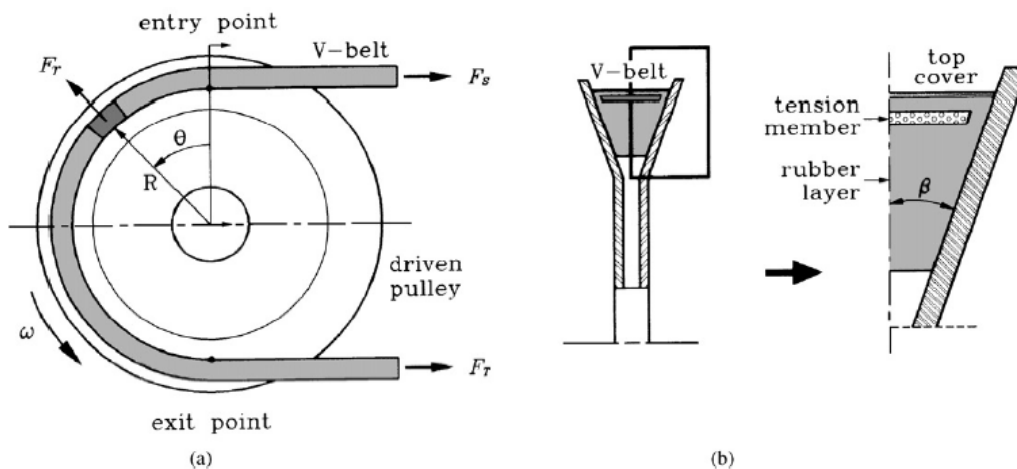
Figure 2-3: (a) Side view, (b) cross section of a V-belt drive system [9]

Belt losses consist of a combination of torque and speed losses. Torque losses include the hysteresis loss, frictional loss and windage loss. Speed losses include slip losses and creep losses. The hysteresis loss depends on the thickness of the belt and pulley diameters. This loss is caused by the bending and straightening of the belt around the pulleys, which creates a stress on the belt materials. The use of cogged V-belts can reduce the hysteresis loss by allowing the belt to bend more easily [23]. Frictional losses are created when the belt slides in and out of the groove. The loss is the energy required to overcome friction as the belt enters or leaves the pulley. Windage losses are caused by the resistance of the air around the belt as it moves, therefore the smoother the belt, the less the resistance. [8]

Slip losses occur if the belt tension is below the amount specified in the operation manual, reducing the static friction and thus causing slippage. If the belt is tensioned correctly and this tension is maintained, slippage losses are kept to a minimum. If the belt tension is set too high, it can cause bearings to become damaged. Significant slip loss can occur if the belt is overloaded or if the pulley grooves are worn. Creep losses are caused by the difference of the belt elongation before entering and after exiting the pulley. The tension on each side of the pulley is different. The belt entering the driven pulley is under less tension, and is thus shorter and wider than the belt leaving the driven pulley. These small differences cause the belt to creep around the pulley, reducing the speed of the driven pulley. These losses cause the belt to heat up, leading to an increase in the degradation of the belt materials. [8]

An experiment was conducted on the efficiency of V-belt CVT (continuously variable transmission) [10]. This experiment focuses on the CVT, but the information discovered on belt drive reactions to pulley sizes is important for this research. Firbank [11] found there to be a speed loss between the two pulleys caused by the creep of the belt around the pulley. The experiment conducted in Firbank's research consisted of a test rig on which numerous tests were conducted on V-belts. Their results acknowledged the existence of hysteresis losses, and found that the losses were dependant on the belts elastic properties. Figure 2-4 below illustrates the creep loss of the belt around the pulley, due to the elasticity of the tension member.
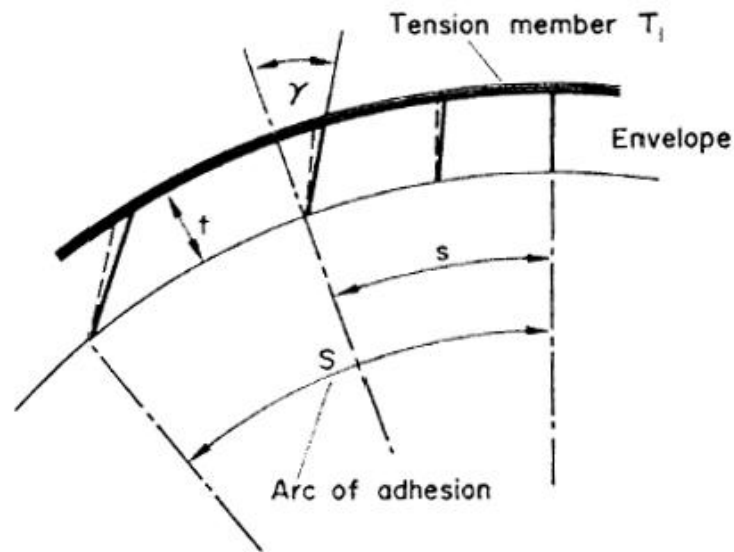
Figure 2-4: Effect of elasticity of tension member [11]

Frictional losses also played an important role in their research as the belt was reluctant to enter and exit the pulley, thus energy was required to overcome the resistant friction. They showed that belt slip and creep losses can be reduced to an insignificant percentage of the losses, but still cause premature wear if not kept at its absolute minimum. This is due to the deformation of the belt.

The effects of belt misalignment should also be investigated to ensure that the alignment will not affect any of the results. It is understood that V-belts are commonly used within Industry due to their tolerance of shaft misalignment. The required tests investigated the effects of belt tension on efficiency, and thus any other effects on efficiency should be removed from the system. Moon and Wickert [17] investigated the vibration effects of misaligned V-belt drives. This study showed that slippage was caused by two types of relative motion between the belt and sheave. These consisted of tangential slippage, along the circumference of the sheave, and radial slippage, along the radius.

The tangential slippage occurs when the torque capacity of the belt is reached. This is most likely to occur on the smaller diameter pulley, due to the reduced friction area. This slippage contributes to accelerated wear, fatigue and friction induced squeal and vibration. [18]

Radial slippage increases the belt vibration and noise. This occurs at higher frequencies and misalignment. This reduces the efficiency of the belt drive system, increases wear and vibration, and can lead to eventual fatigue failure.

When misaligned, V-belts demonstrated stick slip behaviour. This is when the belt gradually moves up the groove, then rapidly settles back into position. This process causes sound bursts, which do not occur when the belt is aligned correctly. This behaviour is caused by the misalignment of the two pulleys. During operation, the V-belt favours one side of the groove. This causes the belt to climb up the groove as the pulley rotates. The belt then becomes supported by only the one side. When the belt reaches a critical angle, it will rapidly slip back into the fully seated position [18].

Investigation into the journal article by Connel and Rorrer [18] shows the importance of alignment on the belt drive for the tension testing as overload conditions will be reached. This will result in damage to the belts and will cause discrepancies in the results.

The Fenner® SPB Wedge belts, seen in Figure 2-5 below, were used for this testing. Pulley diameters of 200mm and 500mm are used, giving a belt ratio of 2.5:1. The belt length is 2990mm, resulting in a 933mm centre distance. This is within an adjustable range of the test rig with a targeted 950mm centre distance. [26]

Figure 2-5: V-belt [32]

2.2.2.2 Synchronous belts (timing belts)

As the majority of belt efficiency loss is due to the lack of maintenance on a belt system, the use of a synchronous belt can significantly reduce this loss, as much less maintenance is required. Synchronous belts do not rely on friction or wedging for power transmission like V-belts. They have teeth that fit accurately in grooves on the pulley resulting in a positive engagement. This can be seen in Figure 2-6 below.

Figure 2-6: Synchronous belt [33]

A comparative lab test conducted by Gates® [19] concluded that in most situations a synchronous belt will have a higher efficiency than a properly maintained V-belt. Synchronous belt efficiency remains constant at about 98% at rated load. This is a significant increase from the 93% of a V-belt. This high efficiency is mainly due to the lack of slip of the synchronous belt. Slip will only occur if a tooth "jumps" a groove, but this is uncommon, and will only occur if the belt is significantly worn or damaged. This can also be seen as a disadvantage as the synchronous belt offers no protection from overloading and torque spikes.

In high torque applications, synchronous belt efficiencies remain relatively constant compared to the V-belt drive, which undergoes slippage as the static tension is overcome. At low speeds the synchronous belt can transmit more power than a V-belt. Commonly, if V-belts are selected, they are usually over or under rated for the power transmission required, resulting in a decreased efficiency, while synchronous belt efficiency remains constant.

The sudden application of excessive torque onto a system that offers no slip protection can result in the belt teeth being sheared off or significant damage to the rotating machinery coupled to the motor via the belt drive. If the equipment being driven is sensitive to torque spikes, synchronous belts are not recommended.

A main advantage of the synchronous belt is that it does not stretch significantly in its life time, and therefore does not need to be re-tensioned as often as a V-belt. If the V-belt tension is not maintained, a resultant efficiency loss of up to 10% can be observed. Synchronous belts are most suitable for areas where maintenance is difficult. Unfortunately, synchronous belts produce more noise than standard V-belts, and therefore, in certain situations, cannot be used in noise sensitive areas.

As discussed previously, hysteresis loss is a major contributor to the efficiency loss in belt drive systems. Due to the thinner profile of the synchronous belt, the bending stresses within the belt are significantly smaller than that of the V-belt [20]. This reduced the affect of flexing on the belt material, thus reducing the internal stresses. This reduced hysteresis loss can result in smaller pulleys being used for synchronous belts than V-belts.

There is minimal frictional and creep loss in a synchronous belt, as it does not rely on wedging in grooves to transmit power. The only friction component exists as the belt enters and exits the pulley, but this is minimal compared to a V-belt.

The main disadvantage of synchronous belts is the small misalignment tolerances. Due to the direction the teeth run on the belt, small misalignments and manufacturing inaccuracies can cause the belt to run off the pulley. This increases the manufacturing cost of the pulley. Improper installation of the pulley (e.g. high running keys) can result in the pulley not running true. The maximum angular misalignment for synchronous belts is 1/4°, which is a difficult range for a normal technician to correct without the proper tools.

A paper produced by the Advanced Engineering Research, Belt Testing Centre [25] discussed a method of testing a large variety of different belts. The design of their test rig was very similar to the design discussed in this dissertation.

 The design used by the Belt Testing Centre can be seen in Figure 2-7 below. This system uses a regeneration system, and allows the motor to rotate about its axis, thus measuring an accurate output torque of the motors.
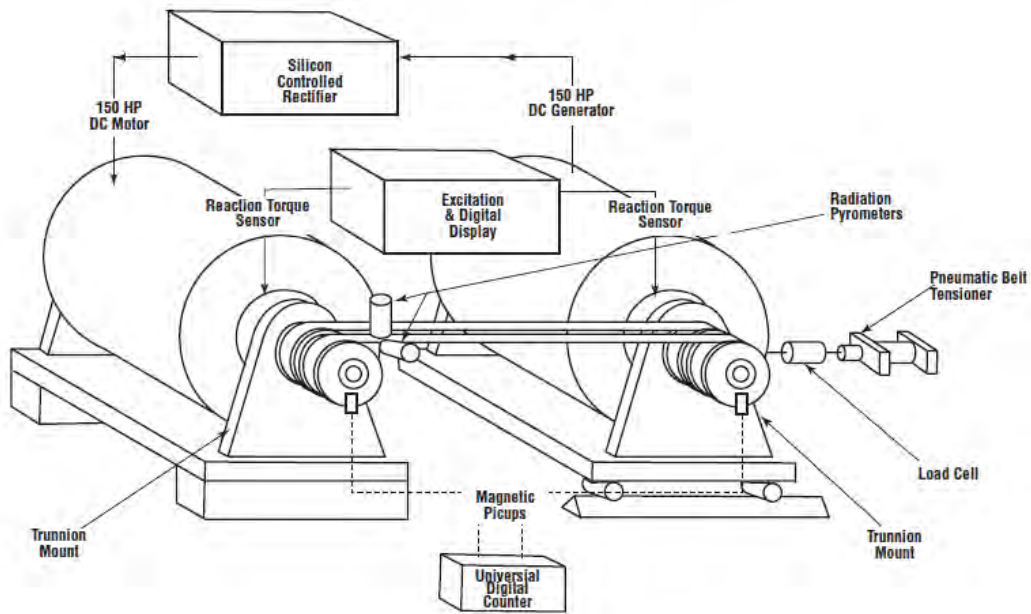
Figure 2-7: Belt testing centre belt test rig [25]

The testing methodology was discovered to be similar to the testing methodology contained in this dissertation. This included adequate run-in time for each belt to reach stable temperatures. The test run time was also similar, and an average of the last few minutes of results was taken as the data point. The results obtained show efficiencies of belts similar to the efficiencies measured in this dissertation. The results of the Advanced Engineering Research paper are for a much larger variety of belts, but did not focus adequately on belt tension. This dissertation will focus more on the effects of belt tension on commonly found belt drives.

The Gates® Poly Chain® GT2 synchronous belt was used for this belt testing. The number of teeth per pulley was selected to be 56 and 140, with a belt length of 2600mm, resulting in a 901.6mm centre distance, and a 2.5:1 reduction ratio. [28]

2.2.2.3 Poly V ™ belts (joined-V)

Poly V ™ belts, as seen in Figure 2-8 below, are a number of small V-belts joined together. This type of belt adaption gives advantages of both the V-belt and the flat belt. This belt still has V's, which have to wedge into the grooves on the pulley. This increases the frictional area, and thus allows the belt to transmit more load than a standard flat belt. This belt is also able to withstand small amounts of misalignment, similar to the V-belt.

Figure 2-8: Poly V ™ belt [34]

The Poly V ™ belt has a much flatter cross section which, like a flat belt, reduces the hysteresis loss in the system. This reduced hysteresis loss results in a lower running temperature. At lower temperatures, belt life increases dramatically. For every 7°C increase in belt temperature, belt life is cut by half [21]. A further advantage of the Poly V ™ belt is its ability to run over pulleys on its flat back. This allows the belts direction to change by being wrapped around multiple idler pulleys.

The Poly V ™ belt tested was the Fenner® PL16 as this is the correct belt selection for the full load specs of the test rig. The pulley diameters selected were 140mm, and 315mm, resulting in a belt ratio of 2.25:1. This is not an ideal ratio, as 2.5:1 was the target, but due to stock constraints, this was accepted. A belt length of 2515mm resulted in a centre distance of 950mm. [26]

2.2.3 Couplings

This section of the dissertation looked at two different aspects of coupling efficiency which are the effect of misalignment of couplings, as well as the use of soft start fluid couplings. Correct alignment and soft-starts can significantly reduce energy consumption as well as preventing damage caused by shock loading.

2.2.3.1 Fluid coupling

A fluid coupling is used to prevent sudden shock loading when starting up machinery under load. This sudden power shock loading causes the initial torque of the electric motor to jump up to three times its maximum power capacity. Although this high torque is short lived, the power spike results in increased energy consumption and the damage it can cause to the motor is high. Testing of the fluid coupling will compare the effect and price of using a fluid coupling as opposed to a VSD. This research will find which is better to use depending on the number of stops and starts in a day, as well as the torsional loading on a system. There will also be an investigation into whether the fluid coupling loses efficiency during long runs and how it is affected by heating.

A simple fluid coupling consists of three components. These are the housing, the drive pump and the driven turbine. The drive shaft is coupled to the drive pump of the fluid coupling, and the driven shaft is connected to the turbine with an oil tight seal. The turbines can be seen in the cross section in Figure 2-9 below.

Figure 2-9: Fluid coupling [35]

19

When the system is started up, the drive motor rotates the pump blades. This allows the drive motor to get up to speed with much less initial power as it will only have to overcome its own inertia, and the inertia of the fluid in the coupling. The pump would then direct the fluid towards the turbine, rotating it in the same direction as seen in Figure 2-10 below. This lag reduces the shock on the driven equipment significantly.
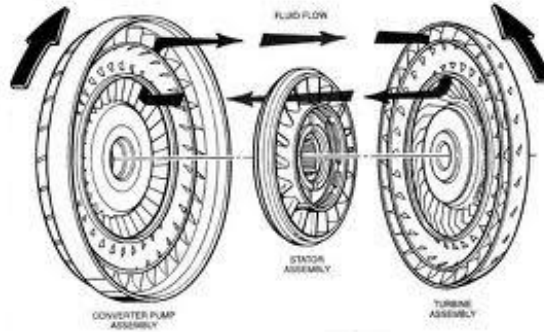
Figure 2-10: Fluid flow within a fluid coupling [36]

Fluid couplings should be used in high inertial systems, where the inertia of the coupling itself does not significantly affect the total inertia of the system. These are to be used in systems where VSD cannot be used and where the system is not run for extended periods of time. This is due to the reduced running efficiency. Delay chambers can also be included within fluid couplings to further reduce the start-up torque of the system.

The fluid coupling tested in this dissertation was the Transfluid 13 CKRG. This coupling has one delay chamber which further reduces the start-up torque. [27]

2.2.3.2 Flexible couplings

Shaft misalignment is simply the offset of the two centrelines of two coupled shafts. Misalignment, although normally measured when equipment is stationary, should be measured while equipment is running under normal conditions at the point of power transmission. There are two types of misalignment in couplings; these are angular and axial misalignment. For a coupling to accommodate these misalignments there must be at least two points of flexibility. The misalignment should be measured by projecting the centrelines of each shaft to the transmission point as seen in Figure 2-11 below. [13]
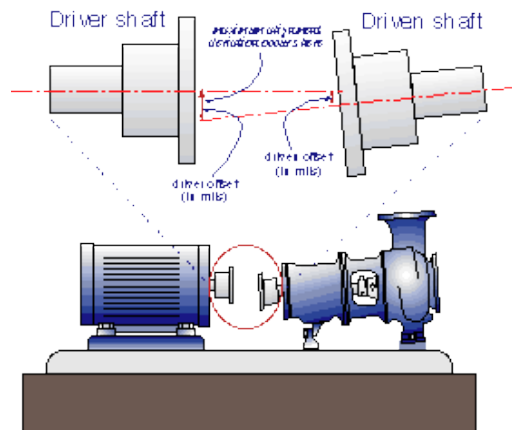
Figure 2-11: Typical misalignment condition [13]

A typically overlooked aspect in shaft misalignment is the effect the running of the equipment has on the alignment of the shafts. When the equipment is started, the shafts move into different positions. This movement is commonly caused by temperature changes due to friction in bearings and any play in the system.

The correct alignment of shafts is important as it will increase the operational life of rotating machinery. Bearings, seals, couplings and shafts are the components most likely to fail. Correct alignment can achieve the following results: [13]

1. Reduces excessive axial and radial forces on bearings
2. Minimizes shaft deflection
3. Minimizes wear on the coupling components
4. Reduce seal failure
5. Maintain correct internal rotor clearances
6. Reduces the possibility of cyclic fatigue in shaft
7. Reduces vibration

There has been significant research into the damage caused by misalignment, but much less into the effect on power consumption. After reviewing The Journal of Sound and Vibration [14, 15] it was clear that the focus in coupling misalignment is towards vibration and stability. It is understood that the effect of faster rotating machinery needs to be researched in this regard, as well as from a power consumption angle, to avoid unnecessary machine damage. This journal referenced a test completed by Lorenzen et al. [16], which compared the effect of critical speeds on different types of couplings.

2.2.3.3   Quick-Flex® coupling

Quick-Flex® couplings are an insert based flexible coupling. These couplings have a high quality urethane insert, and two separate steel hubs [26]. It can be seen in Figure 2-12 below that the two hubs have teeth which, when aligned, hold a toothed urethane insert. The main advantage of this coupling is its ease of installation, and its ability to withstand small amounts of misalignment. This coupling offers a small amount of shock loading protection, but may fail if this is exceeded. The effect of misalignment on the running efficiency of this coupling was investigated. The Quick-Flex® coupling has two different types of urethane inserts. These are the red low torque insert, and the blue high torque insert. The QF50 coupling with the blue high torque insert was selected for these tests. [26]
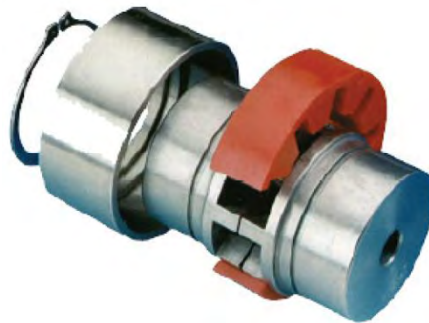
Figure 2-12: Quick-Flex® coupling [37]

2.2.3.4   Fenaflex® coupling

The Fenaflex® coupling is a tyre type coupling, as seen in Figure 2-13 below, which is known for its misalignment capabilities. The Fenaflex® coupling is capable of accommodating a large range of misalignment without causing excessive loads on nearby bearings. This coupling is also excellent for shock absorption in a system. The Fenaflex® F80 F type coupling was selected for this dissertation. [26]

Figure 2-13: Fenaflex® coupling [38]

22

2.2.3.5 Fenagrid® coupling

The Fenagrid® coupling consists of two hubs, mounted opposite each other. These hubs are placed only 3mm apart, and a steel grid is placed around them, meshing the hubs together. This can be seen in Figure 2-14 below. These couplings offer very little misalignment tolerance and very little shock load absorption. The advantage of this coupling is the high torque transfer. This torque transfer is far higher than any other flexible coupling. The grid coupling chosen for this dissertation was the Fenagrid® TH 1070. [26]

Figure 2-14: Fenagrid® coupling [39]

2.3 Testing procedure

2.3.1 Motor testing

The motor testing measured the overall efficiency of the motors. The two motors tested were a standard 30kW squirrel cage induction motor and a high efficiency motor in the Fenner® range. The efficiencies of each motor were compared to each other, and thus the test procedures were identical. These tests resulted in a standard power efficiency graph of percent load vs. percent efficiency.

The graphs were plotted by running the motors at synchronous speed at set loads until a stable temperature was reached. The percentage loads to be plotted on the graph were 50%, 60%, 70%, 80%, 90% and 100%. The test system was able to calculate the efficiency from the power input, measured from the mains, and the power output, measured from the gimbal. These tests were conducted three times per motor to ensure accurate repeatable results.

2.3.2 Belt testing

The belt testing procedure was designed to investigate the effects of tension on belt drive efficiency. The effect of belt tension was investigated on three different belts types. These were V-belts, Poly V ^{TM} belts, and synchronous belt drives. Each belt was tested in a similar manner, but due to the different tension values, the results are plotted as a percentage of the correct stationary tension.

Firstly, the belt was tensioned once at the beginning of the testing procedure, and run for a set amount of time, depending on the belt type, to ensure adequate run in. The belt was then re-tensioned, and allowed to run for 20 minutes. An average of the efficiency readings during the last 2 minutes of the 20 minute test was taken. This test was then repeated twice more to ensure consistency. If the values were not consistent, the entire set of three tests was conducted again until the results were consistent. Temperature readings of the belt surface were taken at certain intervals to ensure that the temperature has reached a stable level before the readings were taken.

The belt tension was then reduced by a percentage of its correct stationary tension. The tests were then repeated following the same procedure as above, at the reduced tension. This process was repeated until the belts either failed, became too dangerous to run, or were unable to transmit the required torque.

2.3.3 Flexible coupling

There were three different types of couplings that were tested under misalignment and load. These couplings were the Fenner® Quick-Flex®, Fenaflex® and Fenagrid® couplings. The coupling efficiencies were compared to each other during the testing procedure. The efficiency was tested under full load and speed as this would be the worst case of torque transfer. These tests were run for an initial warm up time, which varied depending on the coupling. After the couplings were warmed up, the 20 minute run time began, and the average of the last two minutes of readings was recorded as the efficiency. Numerous tests were conducted on each coupling to ensure repeatability.

Misalignment was then introduced into the system to view the effects it had on the efficiency of the couplings. The misalignment values tested for each coupling may not have been identical as each coupling had specific misalignment limits. At least three misalignment values were chosen within the recommended range of the coupling, and further testing was conducted beyond that range until failure occurred. Failure includes coupling destruction or excessive noise and

vibration. Both angular and radial misalignments were tested separately on each coupling to ensure an adequate understanding of the losses.

2.3.4   Fluid coupling

The fluid coupling was designed to reduce the start-up torque on a system required to start under load. The use of fluid couplings will conserve energy and the life of the motors running the system by preventing shock loading. The testing procedure involved the motor being started DOL, to view the difference between the start-up torque of a solid coupling and a fluid coupling. This initial increase in torque of a DOL can be up to 3 times the normal full load torque of a motor. The fluid coupling test was conducted at both cold start and warm start to see the difference between the start-up load of warm and cold oil. This was conducted three times to ensure consistency. The fluid coupling was then replaced with a standard Quick-Flex®️ Coupling, and the tests repeated. These results were then compared to each other and the advantages and disadvantages discussed.

The running efficiency of the fluid coupling was also investigated. This was important as the running losses of a fluid coupling may make it inappropriate for certain situations. These tests show under what conditions a fluid coupling can be beneficial to a system depending on the number of start-ups and the length of run time. It is safe to assume that due to the nature of this coupling, the running efficiency will be lower than that of a solid coupling, and thus is not a practical choice if the machinery is expected to run for long periods of time.

CHAPTER 3

TEST RIG DESIGN

3.1   Design requirements

Based on the testing requirements discussed above, a test rig was designed. The fundamental requirement of the rig was the ability to test motors, belts and coupling while keeping costs to a minimum. The ability to apply misalignment on the couplings as well as varying the belt tension was included in the design. The test rig had to be fully adjustable to allow for different sized couplings, and have the ability to tension different belt lengths.

The motor tests required the ability to apply different loads and speeds to the tested motor. The motor speed and torque output needed to be measured accurately. To ensure the tests were conducted under correct conditions, the voltage and current of the motor needed to be continuously measured and displayed.

The belt testing required the test rig to be able to tension different types of belts with different centre distances. The centre distances chosen had up to a 150mm difference. The adjustment in the system was designed to allow the belts to be easily positioned on the pulley, and allow for adequate tensioning.

The coupling testing required the test rig to accurately apply angular, axial and radial misalignment on the couplings. This ability for adjustment was also used to ensure accurate alignment, by overcoming any misalignment errors caused during manufacture. Vibration was kept to a minimum to prevent any incorrect readings.

The control system designed for the testing was able to apply any load and speed to the tested component. These loads were applied in both soft start and DOL starts. The dynamometer system chosen was able to measure the input and output power of the equipment tested.

3.2 Loading system

As this project was initially started to provide information to Industry to help save energy, it was decided that the testing processes should use as little energy as possible. The system used was developed by a company called Exigo, which uses frequency inverters to control the speed of the motors as well as recycle the power from the generator (load motor) back to the drive motor.

This system was ideal as all it required was a second identical motor to act as the generator. A layout is shown in Figure 3-1 below. The load motor (generator) applied a load on the drive motor, and the power generated was fed back into the drive motor. The system still drew power from the mains, but this was a small percentage of the total power used to make up for the losses within the system. The advanced software based control program was specially designed to produce the testing sequences that were required in this project. The program, developed by Exigo, featured a user-friendly software interface which allowed for easy data monitoring and testing.
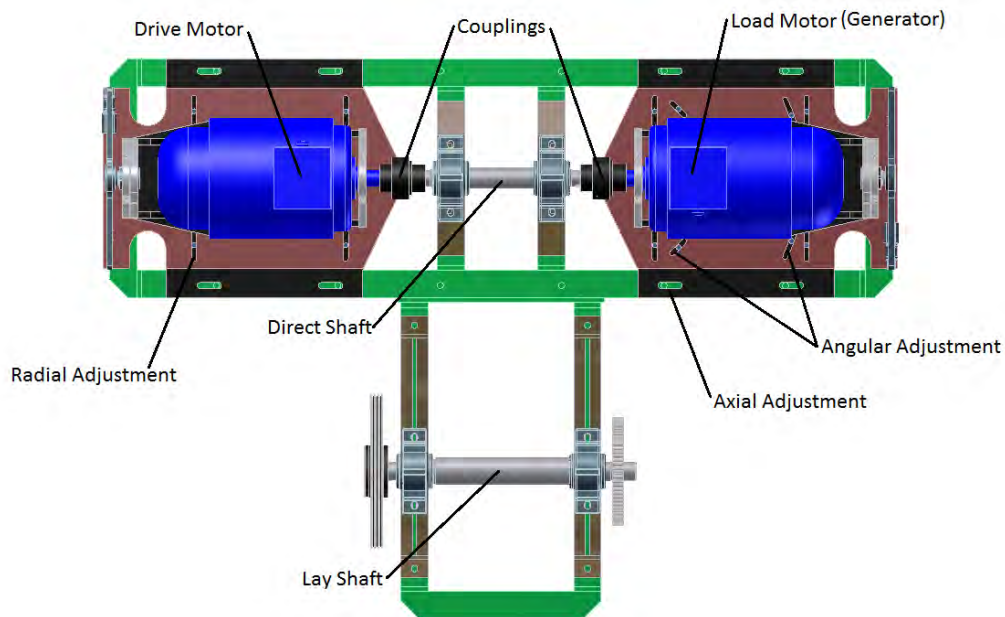
Figure 3-1: Test rig layout

The control system was designed to conduct different tests under varying conditions in order to simulate a wide range of scenarios found within Industry. Creating a test procedure began with choosing either VSD dynamic load or DOL inertia loading on the software interface. If VSD was selected, the test parameters could either include a set supply frequency or a variable speed, and then any load was then applied on top of this. If DOL was selected, the number of starts, duration and rest time can be set. This allowed the test to be run continuously without constant supervision.

The system software automatically recorded values for power, speed, efficiency and temperature and was also capable of high speed data capture. The high speed capture could be set to record any of the existing variables at a 1ms sample rate as opposed to the one sample per second in the standard recorded values, producing a much more accurate graph. The high speed capture however was very limited, as it could only take 750 readings at any time. This was due to the programmable logic controllers (PLC) being saturated before the reading could be sent to the software.

Figure 3-2 below is a diagram briefly illustrating how the Exigo EcoDyn system works. The component labelled Exigo EcoDyn is the controller consisting of PLC and software which is responsible for making the system run as required. This controller maintains the power input to the drive motor at the correct levels by taking power from the generator, and adding the power from the main supply to compensate for the losses. The controller has total control over the two frequency inverters, Danfoss VLT Type IP21 30kW. These frequency inverters provide the power to the drive motor as well as receiving power from the generator.
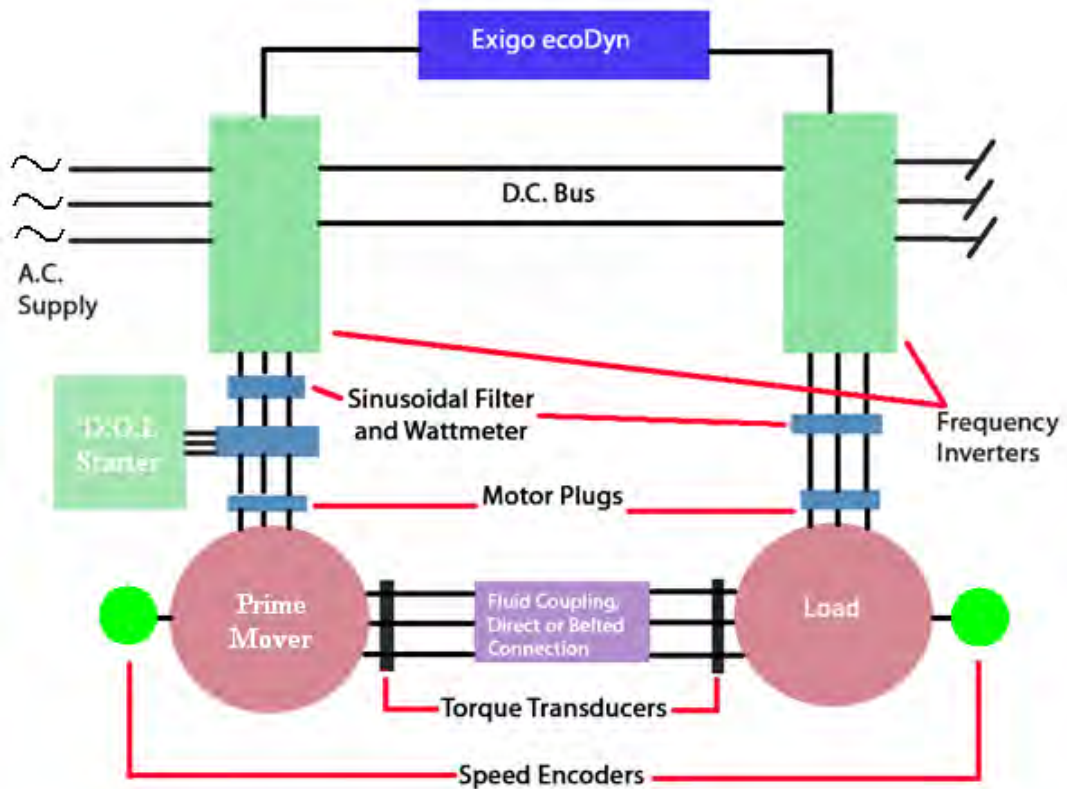
Figure 3-2: Exigo EcoDyn schematic

The frequency inverters are responsible for transferring the power from the generator to the motor. This occurs by using inverters to convert the generated power from AC to DC. This DC is then transmitted to the Drive inverter, which then converts it back to AC to supply the drive motor. Using this method simplifies problems that would have occurred with phase mismatch, as well as matching the frequencies of the generated power with the main power. The EcoDyn uses inputs from the Watt meters, sine wave signal filters, torque and speed sensors to control and maintain the correct power at all times.

The Watt meter is placed directly before the drive motor to allow for the most accurate control of the drive, by measuring and controlling the power received by the drive motor. The sine wave filter is placed before the Watt meter to convert the square waves to natural sine waves to ensure an accurate reading from the Watt meter.

3.3   Frame design

The base frame, as seen in Figure 3-3, was constructed from 300WA structural steel channel sections. These channel sections were sand blasted to remove any uneven paint surfaces, and straightened out to ensure no inaccuracies in the system. The entire frame was then painted to prevent further corrosion. The sections of the channel were bolted together using class 8.8 M20 bolts, and then bolted to the floor using class 8.8 M30 studs.
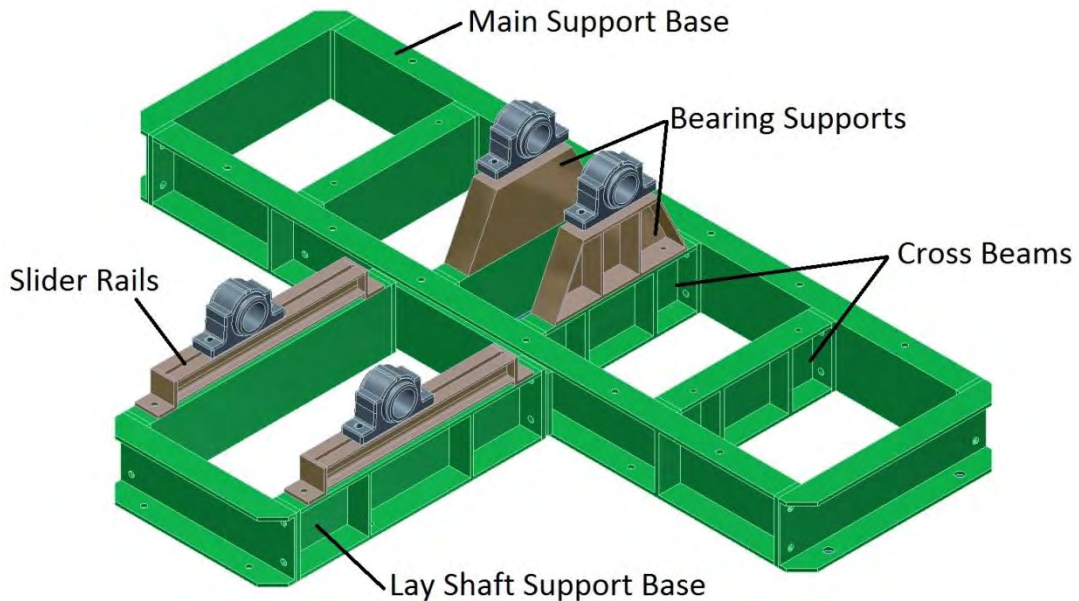
Figure 3-3: Test rig base frame design

A large rectangular main support base was used to support the two motors in the correct positions. The distance between the motors was selected due to existing studs in the workshop floor, as well as the required separation distance of the bearings from the couplings and pulleys, allowing for adequate assembly space.

The lay shaft support base, designed to hold the lay shaft, was intended to allow for a variety of different belt centre distances, and ratios. This section was bolted to the floor at the end with two M20 8.8 studs, and bolted to the main support base using four M20 8.8 bolts. This section was bolted to the main support base via a 10mm steel end plate welded onto the main support base. Both the main support base, and lay shaft support base sections had flanges welded inside the „C' section to reduce the effect of vibration, and thus reduce the interference caused by vibration on the sensitive measuring equipment.

The same channel sections used in the base frame were used to create four cross beams inside the main support base. These cross beams had flanges welded inside the „C' section for additional support and vibration dampening. The cross beams were machined accurately to a length of 605mm, to ensure accurate spacing throughout the frame. The tops were also machined to the same height to ensure the two direct shaft support bearings sat at the same height. They were then bolted between the sides of the main support base, ensuring the sides of this frame were evenly spaced throughout its entire length.

In order to connect the two motors, a direct shaft was placed between them. Two 55mm diameter tapered plummer block self-aligning ball bearings were incorporated to hold the direct shaft to prevent unnecessary vibration within the system, and to prevent excess deflection of the shaft. Two A-Frames, constructed from the same 300WA channel as the frame, were placed on top of the two centre cross beams to hold the bearings for the direct shaft. Both the A-Frames have flanges welded into them to reduce the effects of vibration and deflection on the test rig.

The symmetrical spacing of the bearing supports in the rig design prevented the fluid coupling from fitting between the drive motor and the bearing. Additional holes were drilled in the base frame to allow the drive side bearing support and cross beam to be moved, allowing adequate space for the fluid coupling.

The lay shaft was supported in two 70mm diameter plummer block self-aligning ball bearings. These bearings were bolted directly onto two "slider rails". The slider rails were designed to allow for large movements with regard to belt length adjustment. The slider rails were constructed from 100mm channel sections, which were welded back to back, a set distance apart. A bolt from the bearings was then placed between the channel sections, and allowed to slide freely. When the required position was reached, the bolt was tightened. The slider rail was bolted to the frame via two M20 8.8 bolts at each end. The design centre distance for the belt drives was 950mm, but the incorporation of the slider rails allows this value to be changed.

The distance between the sides of the frame required a plate to be manufactured to support the motors. Figure 3-4 below shows the frame with the motor support plates bolted on. It can be seen that there were two separate plates on each side. This was to allow the motors to be fully adjustable on the horizontal plane, ensuring that they can be aligned accurately. Figure 3-4 below shows the capability of the bottom plate to move the motors axially towards each other, and the capability of the top plate to move the motors radially relative to each other.
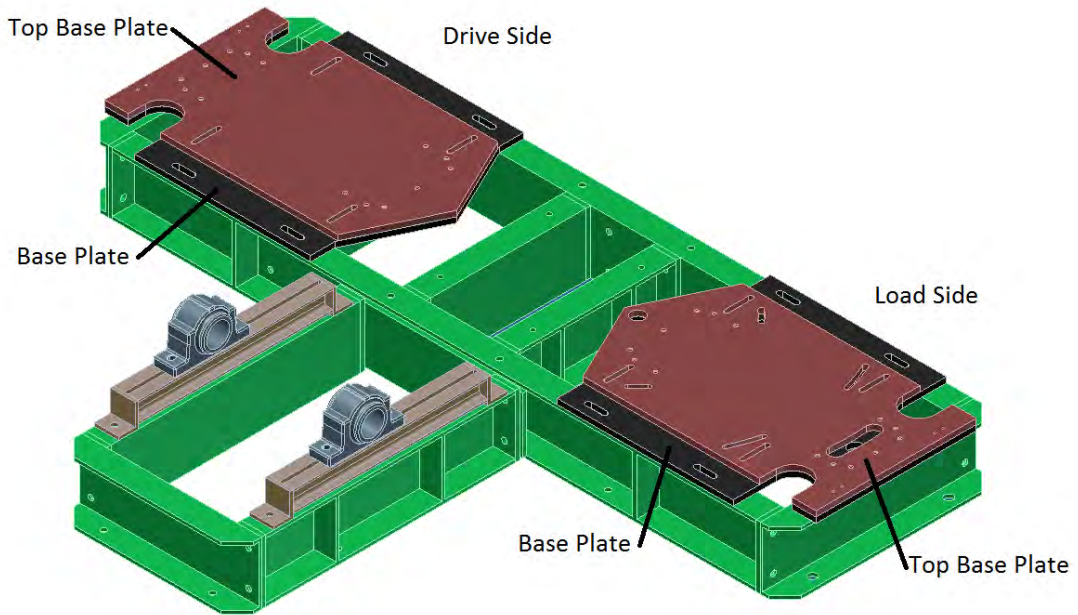
Figure 3-4: Test rig frame with motor support plates

Figure 3-5 and Figure 3-6 below show the two base plates on the drive side. Both these plates were made from 20mm thick mild steel. The steel plate was ground to a flat finish before machining occurred, to ensure easy sliding surfaces, and to reduce the probability of an uneven surface, resulting in inaccurate alignment. The base plate had four parallel slots machined to allow for axial motion of the motor. These slots were bolted directly onto the frame with M20 8.8 bolts when the desired axial position was reached. The base plate also had four 16mm holes drilled through to bolt the top plate onto it. These slots and holes were machined accurately using a CNC mill, and the plates were then painted with an anti rust paint to prevent corrosion.
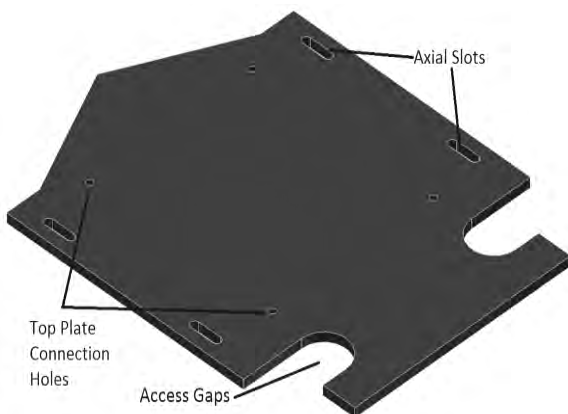
Figure 3-5: Base plate drive side

Figure 3-6: Top base plate drive side

The top plate had four radial slots machined into it. These slots were bolted to the base plate, to allow for radial movement of the motor relative to the frame. The top plate had an array of 12mm holes with a 21mm countersink to attach the motor supports. This will be explained in more detail in the next section. The holes were countersunk to allow cap screws to bolt the motor supports underneath the top plate, while still allowing smooth sliding of the plates on top of each other without interference from the cap screws.
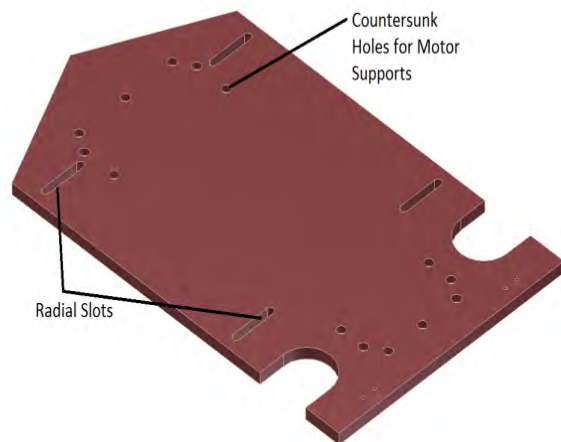
Figure 3-7 and Figure 3-8 below show the two base plates on the load side of the test rig. They were similar to the drive side base plates, but with the addition of the freedom of angular rotation. The base plate had four additional 16mm holes drilled. These holes were positioned in such a way that the four angular slots machined in the top plate could move freely about the large 50mm pin hole, and still be bolted down to the base plate when the correct positioning was achieved. These angular slots allowed for up to 5° angular rotation. This angular misalignment was used for the efficiency testing of couplings. The slots are placed on the load side only of the test rig as the misalignment only had to be applied to one coupling at a time.
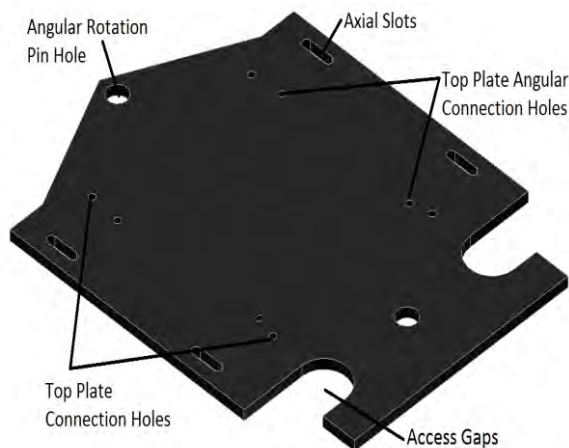
Figure 3-7: Base plate load side   **Figure 3-8: Top base plate load side**
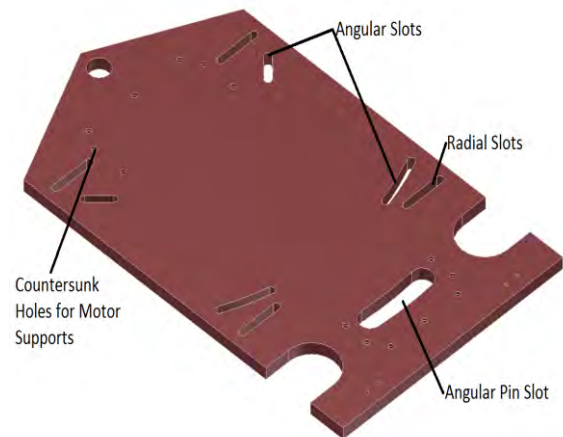
For rotational movement to occur, the bolts allowing radial motion were removed, and put into the angular slots. These angular slots were machined to rotate about the front pin hole. A 50mm pin was placed in this front hole to ensure smooth rotation. This point of rotation was centred at the end of the motor shaft. Another 50mm pin was then placed in the back pin slot to assist with smooth motion. When the desired position was reached, the plates are bolted together with the bolts in the four angular slots. Both the plates on the drive side and load side had access gaps machined in them to allow bolts to be tightened from underneath.

3.4   Torque measurement

In order to accurately measure the torque at set points on the test rig, a gimbal mechanism was designed and used. This mechanism suspended the motors through their shaft, and allowed them to rotate freely. This free rotation was then resisted by load cells placed at a set distance from the centre axis. The design theory behind the gimbal was that as the motor experienced a torque, the motor body transmitted this torque to the feet of the motor, which were bolted down, creating a reaction force. In this situation the motor was suspended by the shaft, and thus the load cell resisted the torque of the motor, reading the applied force. If the distance from the centre, and the force generated was known, the torque could be calculated.

It was the original intention that the motors would be mounted by bearings on either end of their shafts. Figure 3-9 below shows the support designed to hold the motor shaft at either side of the motor. This stand was machined from 20mm thick mild steel plate. Large gaps were cut into the plate to assist ventilation of the motor and prevent any possible overheating. A separate cap was used to hold the bearing in position, and to simplify the process of changing or removing the motor. A sealed single row deep groove ball bearing was placed on the shaft before assembly. This bearing runs in the groove machined out between the cap and stand. A 2mm lip is left to hold the outer race of the bearing in position.

Figure 3-9: Motor shaft stand

The motors supplied for testing did not have shafts protruding beyond the fan covers. In order not to affect the normal operating conditions of the motor, it was decided not to cut the fan cover, and thus an alternative solution was decided upon. This solution was to introduce a dummy shaft.

In order to suspend the back of the motor about its shaft axis, an accurately aligned back shaft had to be created. A cradle base for the motor to bolt on to, and a back stand supporting the back shaft was used. Figure 3-10 below shows a diagram of this mechanism.
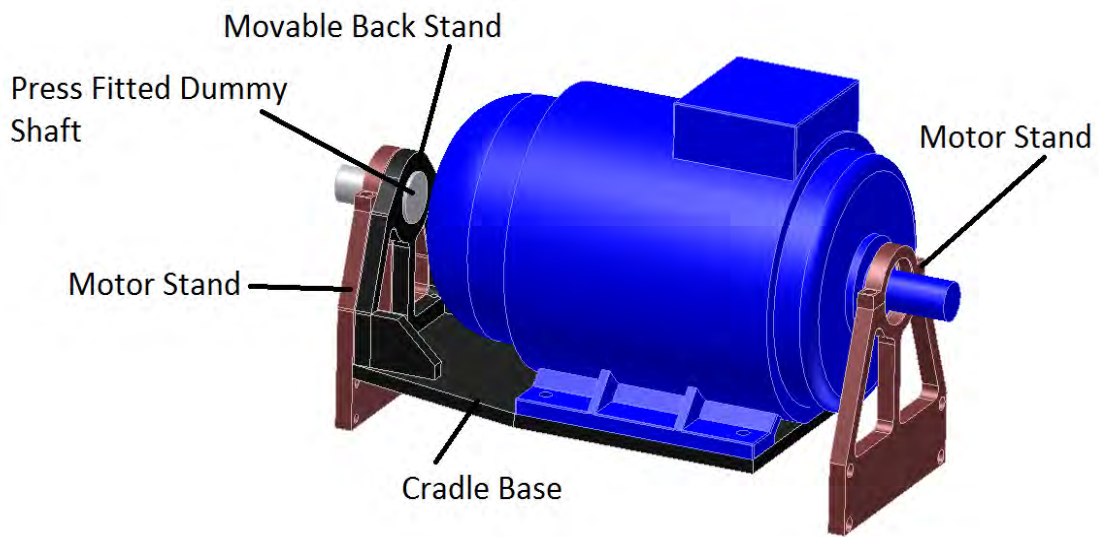
Figure 3-10: Cradle mechanism

The motor was bolted onto the cradle base, and the movable back stand was mounted perpendicular to this. This movable back stand was made from 20mm thick mild steel plate, and was held upright by three cap screws underneath and two supporting wedges. The dummy shaft was then press fitted into a hole with a 0.1mm interference fit, which was more than sufficient to transmit the required torque. This system allows the cradle base and the movable back to rotate, relative to the motor stand, as a torque is applied, thus turning the dummy shaft. The motor stands and the movable back stand for the dummy shaft were ground down to 20mm before manufacture, and then machined using a CNC mill

The complete gimbal assembly, shown in Figure 3-11 below, allowed the motor to be suspended about the centre of its shaft. The gimbal stands, on either side of the motor, were mounted to the motor shafts and dummy shaft by means of deep groove ball bearings to allow the shafts to spin freely within the gimbal stands. As seen in Figure 3-11, the load cells were attached to the dummy shaft on one side of the motor, a known distance from the centre of the shaft, thus giving an accurate torque measurement. The centre of mass of the motor was found to be just below the centre axis of the shaft. This was due to the extra weight of the feet of the motor, which was small in comparison to the weight of the rotor and stator. The effect of the offset centre of mass of the motor did not affect the torque measurements of the gimbal as a load was placed on the lever arm to prevent significant rotation of the motor when a torque was applied. The deflection of the load cells themselves was also very small when under load, and thus rotation of the motor was negligible.

Figure 3-11 below illustrates of the final gimbal system on the drive side of the test rig. The gimbal was mounted onto the top base plate with cap screws countersunk underneath the plate. These plates had adjustment slots machined in them. The adjustment was used to either tension the belts using hydraulic jacks, or move the motor to allow the direct shaft to be mounted with the correct spacing between the couplings.
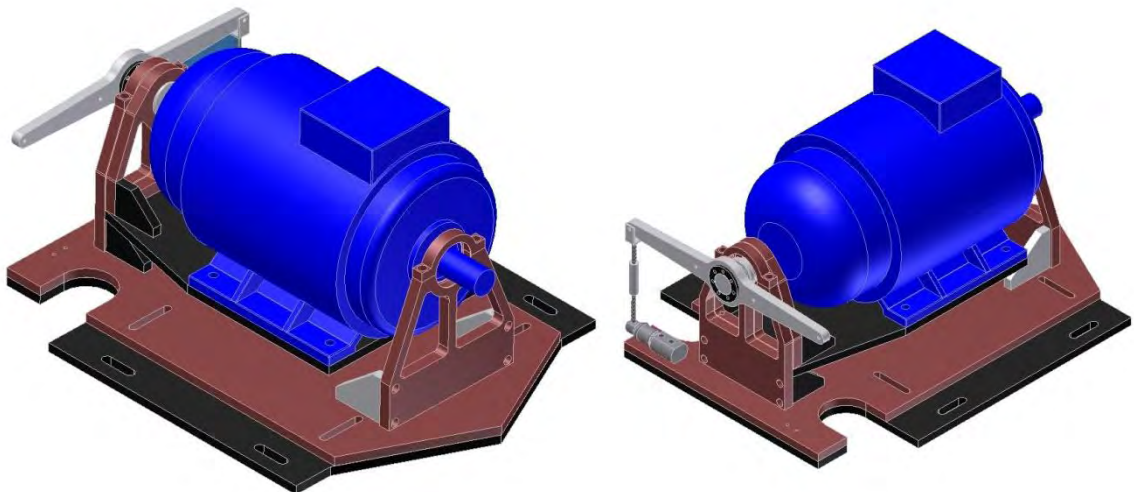
Figure 3-11: Front and back view of the drive motor on gimbal

Figure 3-12 below shows the gimbal system on the load side of the test rig. As discussed previously, this system was slightly different to the drive side as it had angular slots machined. There were still radial slots machined to allow for belt tensioning. This adjustment is important as the centre distances of each belt may not be the same, and thus each belt had to be tensioned

independently of each other. The angular slots were rotated about the hole centred below the end of the motor shaft. These slots allowed the motor to be twisted about its shaft end for testing coupling angular misalignment efficiencies. It can be seen that the angular misalignment of the motor does not affect the torque measurement, and the whole gimbal mechanism rotates with the motor.
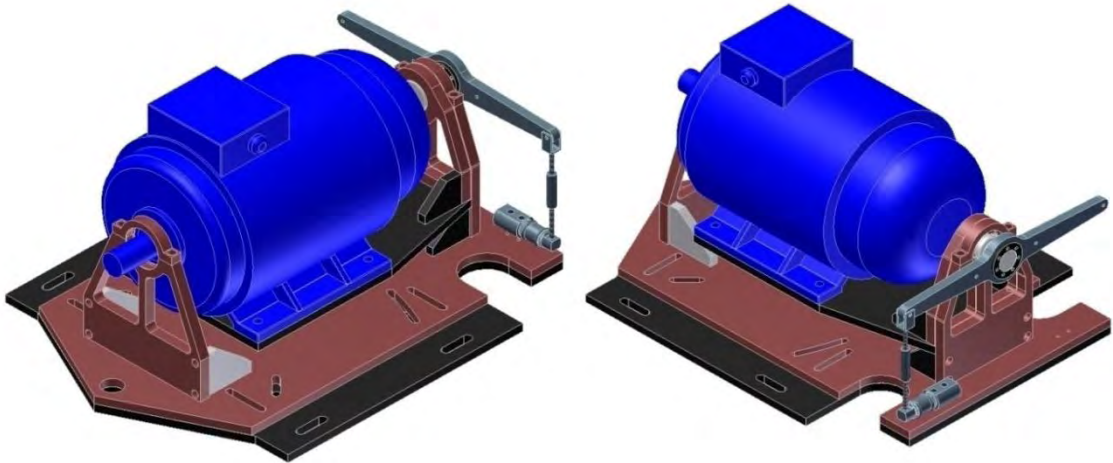

Figure 3-12: Front and back view of the load motor on gimbal

The torque on the motor was applied to the load cells by means of a load arm mounted on the dummy shaft. The load arm, Figure 3-13 below, was fixed to the dummy shaft by means of a taper lock bush. This arm was designed to transmit the torque as a vertical force onto one load cell in tension. The distance the load cells was mounted from the centre of the shaft was set to allow the full potential of the load cells to be utilized thus preventing readings either below or above the accurate range of the load cells. The calculations for the load arm can be found in Appendix A-1.

The load cells were connected to the load arm by means of a turnbuckle, which was pinned to the load arm, and bolted to the load cell. The threaded sections of the turnbuckle had reverse threads to allow for pre-tensioning of the load cell, preventing any play in the mechanism resulting in incorrect readings. The load cells were mounted solidly to the top base plate using two cap screws. The load cell offered minimal deflection, so very little movement was expected within the system. A counter weight was placed on the other side of the load arm to ensure that any "slack" in the system was taken up.

Figure 3-13: Load arm on dummy shaft

The load cells used in this dissertation were the Avery Berkel T203 super precision beam cell. These load cells were used due to their high accuracy, and small size. The 250kg beam was chosen as it covers the load expected, including overload during DOL starts. This shear beam consists of a single high precision strain gauge, which was protected from any environmental factors. Figure 3-14 below shows the load cell used in the system.

Figure 3-14: Avery Berkel load cell [17]

The efficiency of the test rig itself was not calculated. There were many variables in the system where losses may have been present. All bearings used were high performance bearings, which had a negligible efficiency loss when compared to the losses of the tested components themselves. The losses within the gimbal mechanism were reduced as all readings were taken when the gimbal mechanism was in its neutral position. This prevented there from being any inaccuracies with regard to the rotation of the centre of mass, and restricted the load to always act perpendicularly upwards. The stiffness of the gimbal bearings can be neglected as the vibration induced while running would allow the bearings to move freely.

3.5   Shafts

To complete all the tests required in this project, three different shaft designs were required. These were the direct shaft for the misaligned couplings, the direct shaft for the fluid coupling, and the lay shaft for the belts. To make manufacturing simple, it was calculated that having a straight 55mm diameter shaft for both direct shafts was sufficient to handle the stresses created during testing. This also simplified the selection of the support bearings, as they could be used for both direct shafts. The calculation of the direct shaft can be found in Appendix A-2.

An added advantage of using the same bearings for both direct shafts is the separation function of the plummer block bearings. This means that the shaft can be removed and replaced without moving the bearing feet. This resulted in the shaft alignment remaining correct when the shaft was removed, reducing changeover time. The shaft had to be removed every time the coupling was changed, and therefore the plumber block bearing housings were a great advantage.

As there were no abutments, the bearings on the direct shaft were held in position with taper lock sleeves. These sleeves slid onto the shaft, and when in the correct position, the tapered bearings were tightened on with a nut. This caused the bearing to be forced higher on the taper, resulting in the sleeve tightening onto the shaft. This ensured a simple tight fit to the shaft.

The lay shaft was slightly more complicated due to the higher torque transmitted as a result of the belt ratio. The size of the pulleys and bearings were also a restricting factor in the design of this shaft. The end of this shaft had a diameter of 60mm. The shaft was then stepped up twice to a diameter of 70mm on which the bearing sat. A threaded piece was included in this section to secure the bearing against the locating abutment with a nut. The shaft was then stepped up again to give the bearing an abutment to sit against. The calculation of the lay shaft can be found in Appendix A-3.

3.6   Final layout

A representation of the final layout of the test rig is shown in Figure 3-15 below. It can be seen that the design allowed for direct testing of different couplings as well as a lay shaft for belt tension testing. The entire frame, as discussed above, was designed to be adjustable to accommodate varying levels of misalignment and tension of the shafts, pulleys and belts during testing.
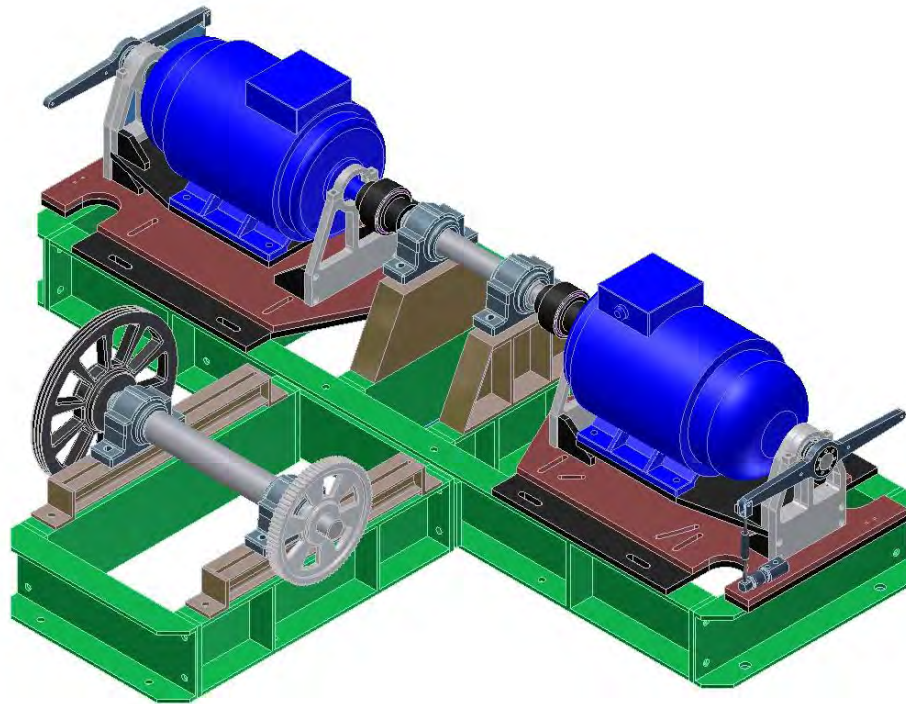

Figure 3-15: Frame layout

Power measurements were measured at the input of the drive motor (electrical power input), the output of the drive motor, and the input of the generator. Power measurements at these points were sufficient to measure any component in this system. A Quick-Flex® coupling was used on the drive side of the system during all the coupling tests. During belt testing the direct shaft was removed, and the belts were connected. The belt on the load side was always the Poly Chain® GT2. This was due to the high efficiency of this belt under all conditions.

3.7 Setup

Due to the importance of accuracy in the setup of the rig, special alignment tools were purchased. A shaft alignment tool, called the Leonova ^{TM} Infinity came with two laser line detectors, which were connected on either side of the coupling. The lasers had built-in inclinometers, so the inclination of the lasers were always known, and were wirelessly connected to each other. The software included in this package can accurately determine the height adjustment required under each foot of the motors. It showed angular and axial misalignment in both the horizontal and vertical directions.

The Belt alignment was also of great importance. This was done using a simple laser alignment tool. The laser is placed on one pulley, and the receivers are placed on the opposite pulley. The lasers had to be aligned by eye, but the accuracy was significantly better than without the tool. Belt tension was measured using either the Gates$^{®}$ sonic belt tensioner, or a standard force-of-deflection gauge. The sonic belt tensioner was programmed with the belt specifications as well as the centre distance. When the belt is struck, the sonic tensioner measures the frequency at which the belt vibrates, and determines the tension. The force of deflection gauge measures the force required to apply a certain deflection on the belt. The deflection and force are calculated depending on the belt and centre distance of the pulleys. The sonic tensioner was used for the Poly Chain$^{®}$ GT2 belt, and the deflection gauge was used for the V-belt and Poly V ^{TM} belt.

The belts were tensioned using a hydraulic cylinder jack and hand pump to push the motor, and screw threads to twist the motor if it was pulled out of alignment during tensioning. The cylinder and screw threads were mounted on a bracket, bolted onto the main frame of the test rig.

CHAPTER 4

EXPERIMENTAL TESTING

This chapter of the dissertation will explain how each test was completed in more detail. The results were discussed and the necessary conclusions were drawn.

4.1   Motor testing

4.1.1   Testing procedure

A comparison of the difference in efficiency between a standard Fenner® 30kW induction motor and a 30kW high efficiency motor was required. To ensure compatible results motor efficiencies were tested at stable winding temperatures. In order to obtain a steady temperature, the motors were run for a set length of time of 2 hours before testing began. It was decided that readings would be taken at load intervals of 10%, starting at 50% of full load. Each test would be run for 20mins, with readings taken very 1 second. The average of the last 200 readings was used. All data was recorded and reviewed after the test was completed to ensure that they were satisfactory before accepting the results. Each set of tests was conducted three times per motor to ensure consistent results. Figure 4-1 below shows the set up of the test rig with the high efficiency motor on the right, and the standard efficiency motor on the left.

Figure 4-1: High efficiency motor test setup

4.1.2   Test setup

Before the motor testing could start, the motors had to be aligned accurately. This was done using the Leonova ™ Infinity alignment tool, as discussed in section 3.7. The two motors were aligned by eye, and then the load motor was bolted down and used as the reference point. The Leonova ™ was then connected to the two motors, and the drive motor was correctly aligned relative to the load motor. Any height inaccuracies were overcome by shimming the feet by the amount specified by the Leonova ™. The motors were aligned to within 0.01mm in the horizontal and vertical directions. This was well within the acceptable range stated in the Leonova alignment instructions. The connecting shaft was then placed between the two motors, and aligned to the load motor to within 0.02mm. The Leonova ™ infinity produces alignment certificates after each setup. These can be seen in Appendix C.

The load cells were then calibrated to ensure that any changes with shaft alignment and motor adjustment did not affect the torque readings. The calibration consisted of preloading the load cells with up to 10 kgs to put an initial tension on the load cell. The load cell was zeroed, and a load of 65kgs was applied to the load cell, and then set. This drew a linear loading graph for the load cell between the zeroed point and the loaded point.

As stated previously, for the motor efficiency to be tested accurately, the motors had to be running at a stable temperature before the efficiency was recorded. The temperature was recorded using a thermal camera from the outside of the motor. Figure 4-2 below shows progressive temperature readings taken from the side of the drive motor. Once the temperature had stabilised, the motor was then set to the desired load, and the test was run.
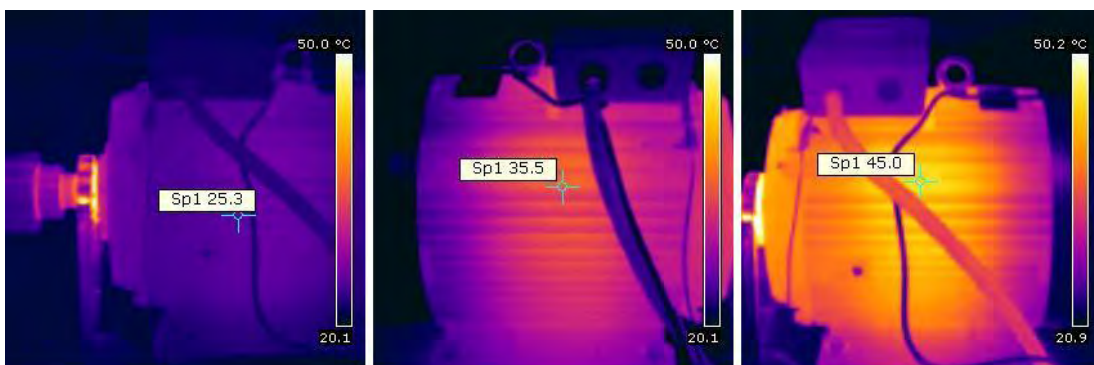

Figure 4-2: Motor temperature at 20 minute intervals

4.1.3 Results

The graph below (Figure 4-3) illustrates the averaged results for the efficiency tests of the standard motor, and the high efficiency motor. It can be seen that at 50-60% load, the motors have similar efficiencies. If the motors are run at a higher load, although a drop is expected, it is clear that the high efficiency motor remains significantly more efficient than the standard motor. This reduced drop in efficiency resulted in a 2% improvement at 100% load of the high efficiency motor over the standard efficiency motor, and thus, depending on the run time of a motor, can result in a noticeable decrease in energy consumption. It should also be noted that even if a variable load is applied to the motor, the high efficiency motor will still operate significantly more efficiently than the alternative.
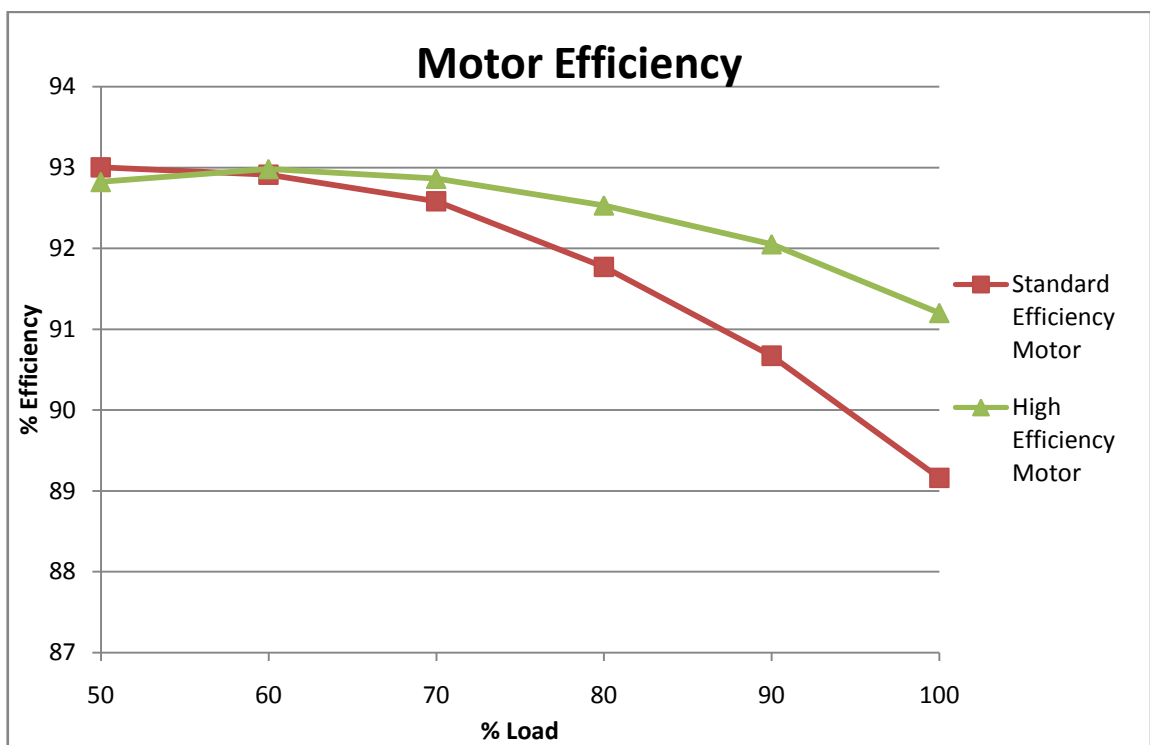

Figure 4-3: Graph of efficiency of high efficiency motor and standard efficiency motor

The motors require a 400V supply to run at full capacity, but the supply in the Mechanical Engineering workshop is restricted to 360V. This caused the control system to increase the current supply to obtain the desired loading. It can be noted that the motors have a peak efficiency at 50-60% load as opposed to the expected 75% due to the reduced voltage supplied to the motors at the time of testing. Due to this reduced voltage, it would be more correct to take this motor as a 27kW motor and not a 30kW motor, but as this is a comparative test, the required results were obtained.

The voltage, current and speed values were recorded throughout the testing process. These tables can be found in Appendix D. It is important to note that these values are instantaneous values, and therefore the power, torque and efficiency values may not be what are reflected on the graphs. As stated previously, the efficiency values were taken as an average of the last 200 readings. These tables clearly show the reduced operating voltage, and the resultant increased current.

Each motor test was run three times to ensure consistent results. These graphs can be found in Appendix B, Figure B-1.

4.2   Coupling testing

4.2.1   Testing procedure

As alignment is an important factor in coupling efficiency, it was necessary to ensure that the shafts were correctly aligned before testing began. Although this was a tedious job, it was achieved successfully. This coupling testing consisted of an efficiency comparison test of the Quick-Flex® coupling, the Fenaflex® coupling, and the Fenagrid® coupling. All these tests were conducted at full load (30kW). These couplings have different misalignment tolerances, so each coupling was tested at a different set of misalignment values. This was done to ensure that there was enough detail for each coupling to draw an accurate graph. Each coupling was tested at 25% steps of their recommended misalignment, up to their maximum recommended misalignment value in both angular and radial directions. The recommended maximum misalignment for each coupling was then exceeded until failure was reached. Failure was defined as excessive damage to the coupling or test rig and dangerous levels of vibration or temperature. Excess noise, vibration and heat generation caused by the misalignment was noted. Each test was run three times to ensure consistent results.

Figure 4-4 below shows a Quick-Flex® coupling set up on the test rig. The figure shows the use of a dial gauge to test the concentricity of the bore of the coupling. Figure 4-5 shows a Fenaflex® coupling setup on the test rig.
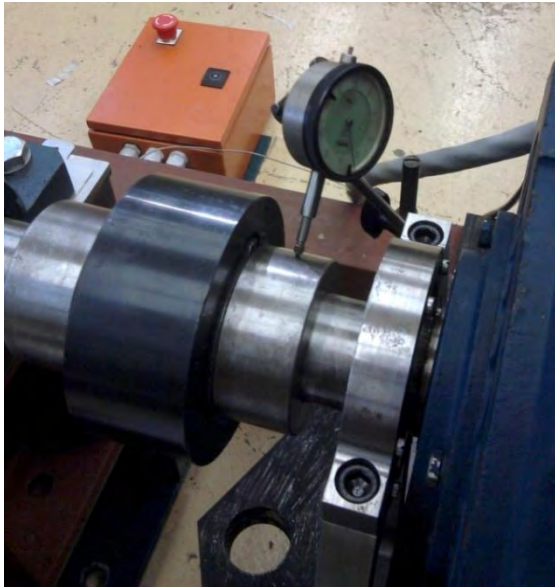
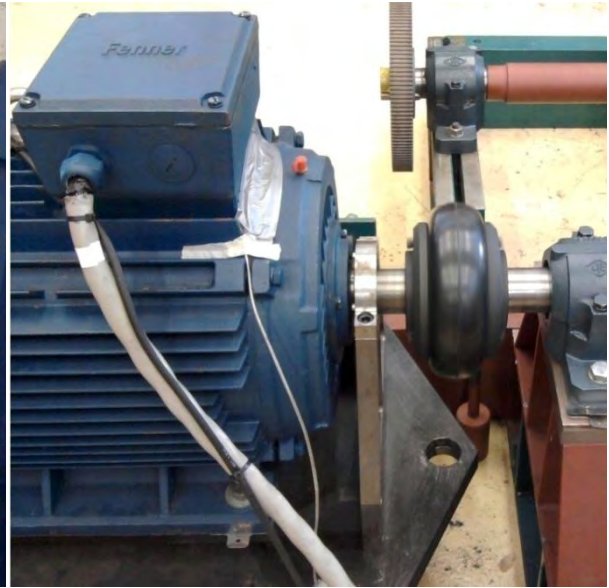**Figure 4-4: Quick-Flex® coupling setup on test rig**   **Figure 4-5: Fenaflex® coupling setup on test rig**

4.2.2   Test setup

To test the effect of misalignment on the efficiencies of the selected couplings, the misalignment had to be accurately known. This was done using the Leonova ™ Infinity alignment tool. The couplings were accurately aligned, and then three tests were conducted. The alignment tool was then used to misalign the couplings accurately. Care was taken to ensure that the couplings were not set with both angular and radial misalignments simultaneously during testing. The set misalignment was checked after each test was conducted to ensure that the misalignment remained at the set value, and was not altered by vibration or heat. The alignment certificates can be found in Appendix C.

The coupling efficiency could only be determined when the coupling had reached an equilibrium temperature. This ensured accurate and consistent results. As a temperature rise was expected as the misalignment increased, the couplings were run until a stable temperature was reached. This length of time varied for each coupling. The couplings were then allowed to cool before retesting.

4.2.3 Results

As couplings have two different modes of misalignment, radial and angular, both were tested. Radial misalignment was imposed by keeping the centre axes parallel to each other, while off-setting them by a certain distance. Angular misalignment was achieved by keeping one shaft axis fixed, and setting the other at an angle to the first.

4.2.3.1 Radial misalignment

Quick-Flex® coupling

The Quick-Flex® coupling radial misalignment efficiency was measured at 0.3, 0.6, 1, 1.3 and 1.5mm. This coupling had a maximum recommended radial misalignment of 1mm, so these values are both within and outside the recommended range. Figure 4-6 to Figure 4-11 show the temperature rise of the coupling as the misalignment was increased. The temperature value displayed is the maximum temperature within the square. The temperature of the coupling within the recommended misalignment range changes very slightly, but as the misalignment is pushed beyond this limit, the temperature increased significantly. This temperature rise shown should relate to the efficiency loss of the coupling.
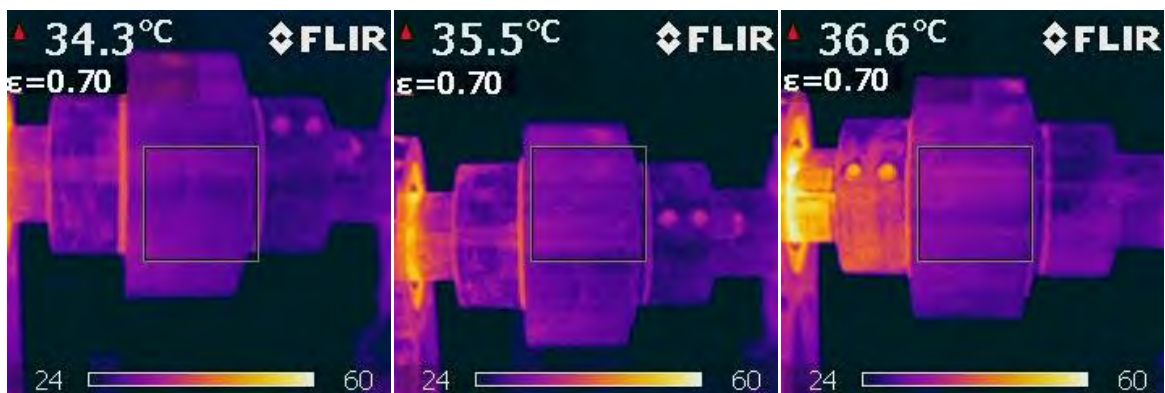
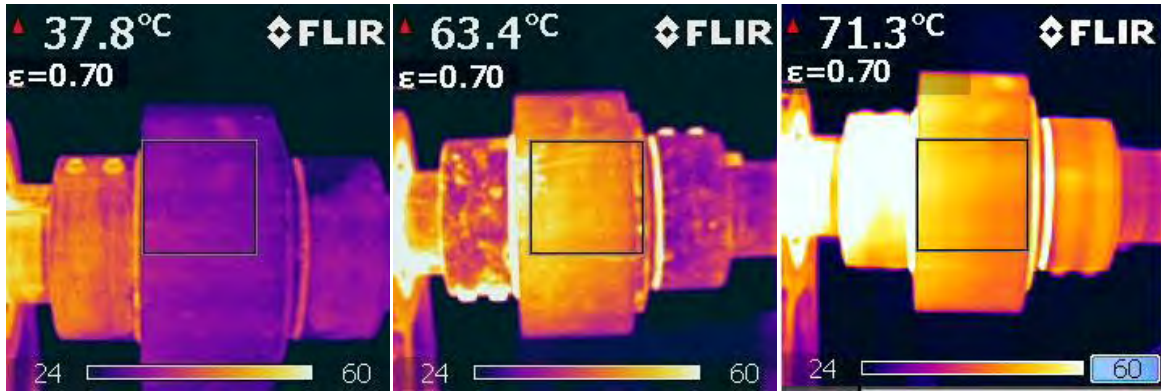| Figure 4-6: Temperature of Quick-Flex® coupling, no misalignment | Figure 4-7: Temperature of Quick-Flex® coupling, 0.3mm radial misalignment | Figure 4-8: Temperature of Quick-Flex® coupling, 0.6mm radial misalignment |

| **Figure 4-9: Temperature of Quick-Flex® coupling, 1mm radial misalignment** | **Figure 4-10: Temperature of Quick-Flex® coupling, 1.3mm radial misalignment** | **Figure 4-11: Temperature of Quick-Flex® coupling, 1.5mm radial misalignment** |

These temperature figures show a distinct temperature rise on the left hand side of the coupling. This was a result of the excess loading applied to the motor support bearing when the coupling was under radial misalignment. The total temperature increase of the Quick-Flex® coupling over the tested radial misalignment range was 37°C, which resulted in a significant energy loss. An interesting characteristic of this temperature rise was that for the first 1mm misalignment, the temperature rise was only 3.5°C. The temperature then increased significantly beyond this level of misalignment.

Figure 4-12 below shows a graph of the temperature increase versus the radial misalignment. If this graph is compared Figure 4-13, it can be seen that the temperature spikes as the efficiency drops. This shows that a significant amount of the energy lost was due to heat.

It can be seen from Figure 4-13 below that the efficiency is relatively unchanged within the acceptable misalignment range. When the misalignment is forced beyond this range, it is very clear that the efficiency drops significantly. Although there was an increase in noise, it was not excessive. Each test was conducted three times, to ensure consistent results. These graphs can be found in Figure B-2 in Appendix B.
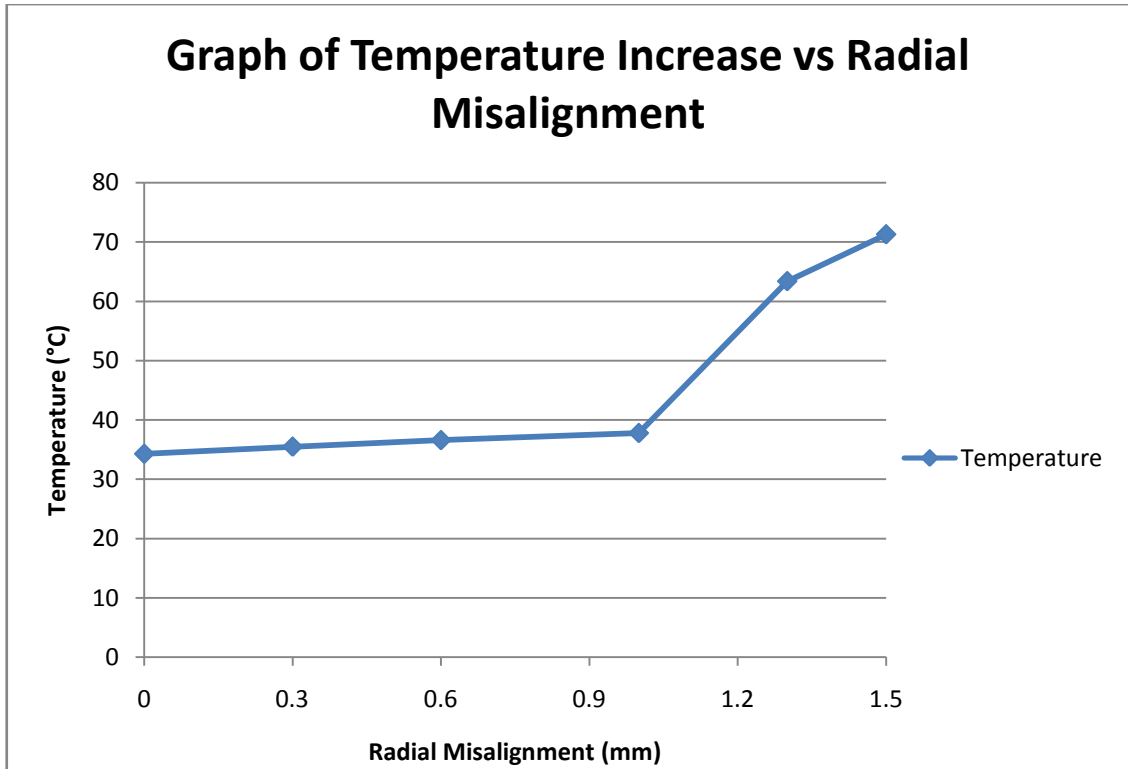
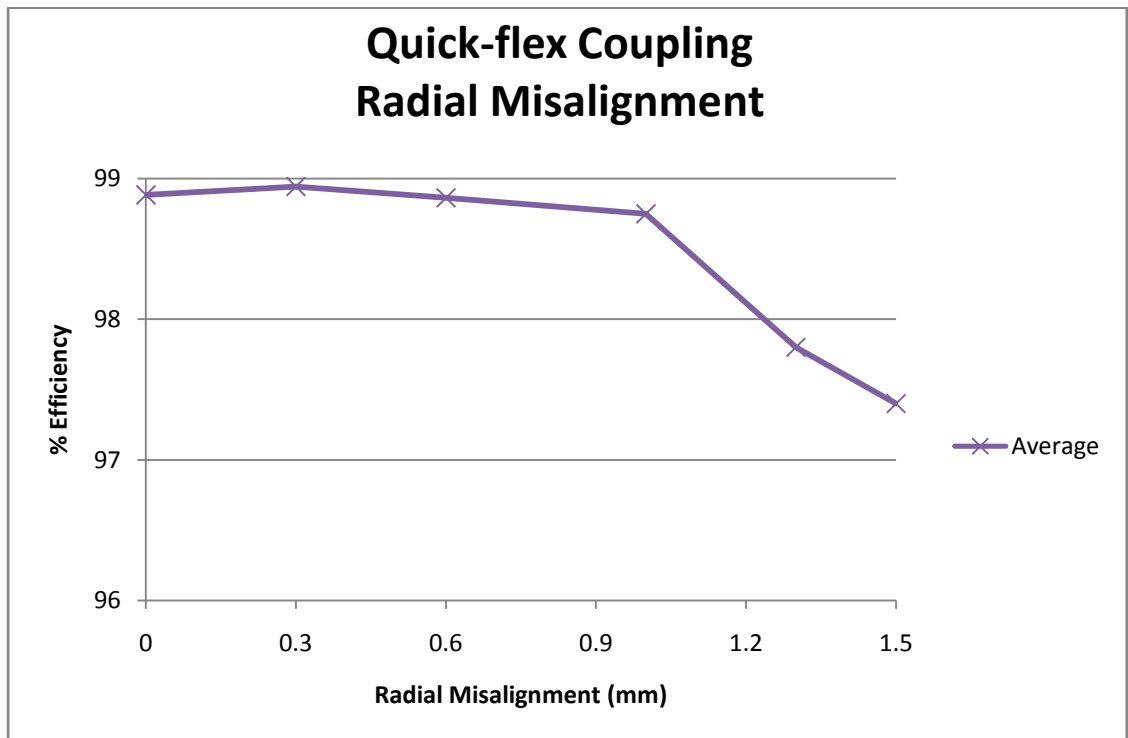**Figure 4-12: Graph of temperature increase vs. radial misalignment of the Quick-Flex® coupling**

Figure 4-13: Graph of radial misalignment vs. efficiency of the Quick-Flex® coupling

The significant efficiency loss observed at 1.2mm misalignment, as opposed to at 1mm, can be attributed to hysteresis loss within the rubber element. As the coupling was rotated, the element was compressed and relaxed continuously. This excess energy was lost as heat, and therefore, less power was transmitted through the coupling. This did not occur at the lower misalignment values as there was play within the element, reducing the compression effects.

The 1.5mm misalignment test for the Quick-Flex® coupling resulted in a significant temperature increase, and it was observed that the element was "smoking". This smoking was later identified as rubber dust as the element was wearing excessively due to the misalignment. This was accepted as a failure, and no further tests were conducted. Figure 4-14 and Figure 4-15 below show the coupling element after the maximum misalignment test.

Figure 4-14: Blackened element of Quick-Flex® coupling   **Figure 4-15: Indentations inside element teeth of Quick-Flex® coupling**

In Figure 4-14, it can be seen that the coupling element was blackened from the temperature as well as the dust that was produced from wear. This element was originally a bright blue colour. Figure 4-15 shows indentations from the coupling teeth inside the element. The indentations support the previous statement about excessive compressions while running, resulting in a hysteresis loss in the element. Figure 4-16 below shows the Quick-Flex® coupling, with the element removed, under 1.5mm radial misalignment. The element shavings can still be seen on the hub teeth.
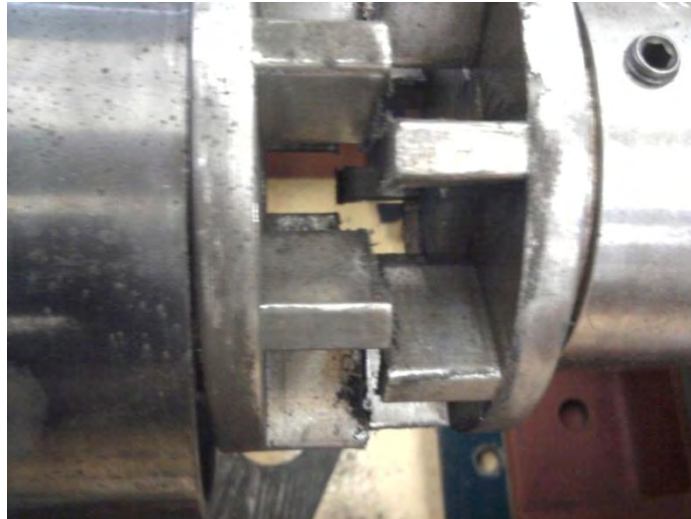
Figure 4-16: Radial misalignment of Quick-Flex® coupling with element removed

Fenaflex® coupling

The Fenaflex® catalogue does not state a recommended radial misalignment value, but due to the nature of this coupling, it was safe to assume it was quite high. The tests were conducted at misalignment values of 0.5, 1, 1.5, 2, 2.5 and 3.5mm. Figure 4-17 shows an efficiency graph of the Fenaflex® coupling under different misalignment values. All the tests were conducted three times to ensure consistent results. These graphs can be found in Appendix B Figure B-3
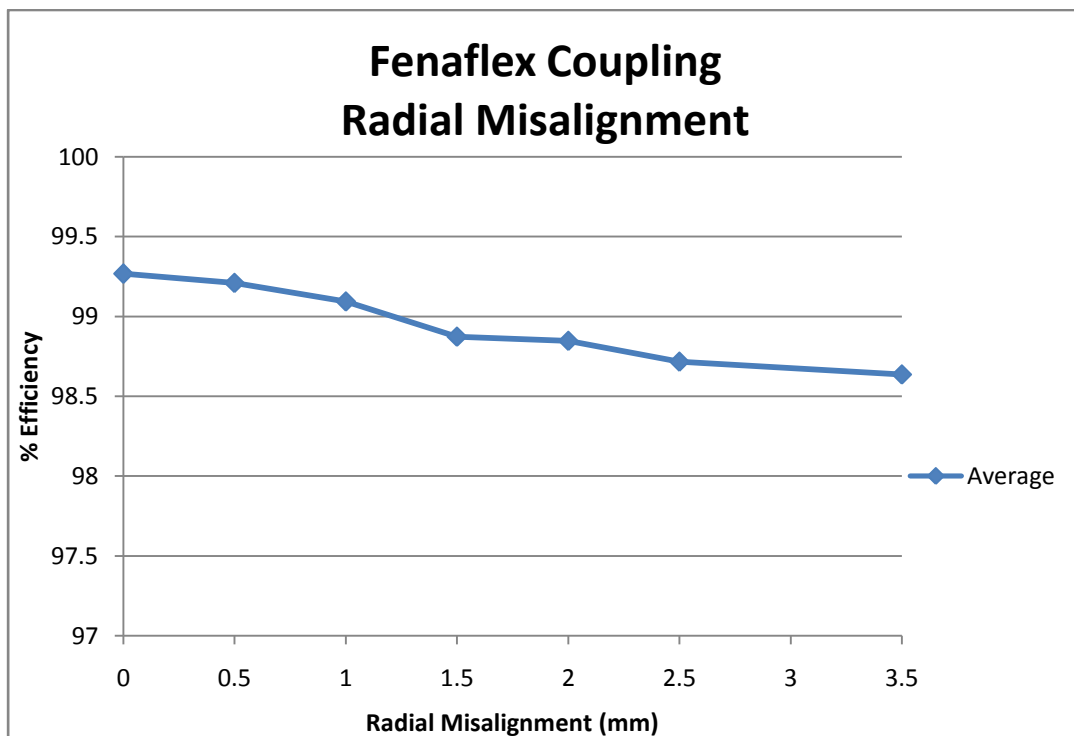
Figure 4-17: Graph of radial misalignment vs. efficiency of the Fenaflex® coupling

It is clear from this graph that the Fenaflex® coupling was able to withstand high levels of misalignment without a significant decrease in efficiency. At 3.5mm misalignment, efficiency loss was still less than 1%. This coupling exceeded the capabilities of the test rig, and could not be run to failure. The temperature of the Fenaflex® coupling did change at the higher misalignment values, but not as excessively as the Quick-Flex® coupling. The temperature increase was related to the hysteresis loss within the coupling as it was compressed and relaxed during misaligned rotation. The loss was reduced due to the thin cross section of the tyre. It is noted that any misalignment beyond 3.5mm will be clearly visible to an operator.

The temperature readings of this coupling at different misalignment values can be seen in Figure 4-18 to Figure 4-24 below.
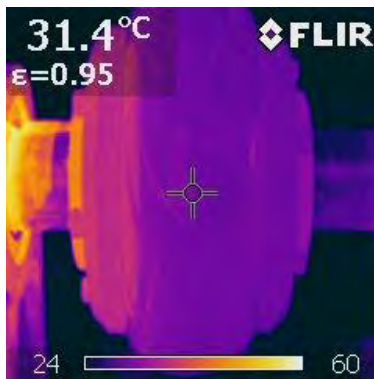
Figure 4-18: Temperature of Fenaflex® coupling, no misalignment
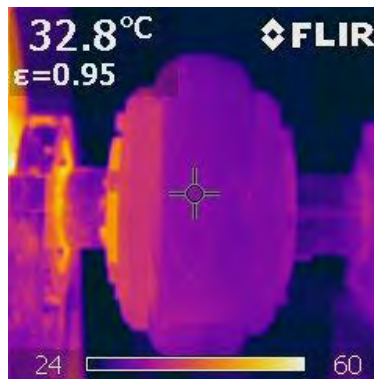
Figure 4-19: Temperature of Fenaflex® coupling, 0.5mm radial misalignment
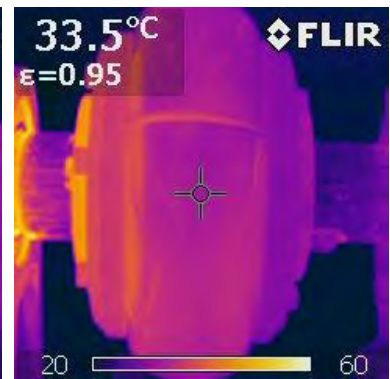

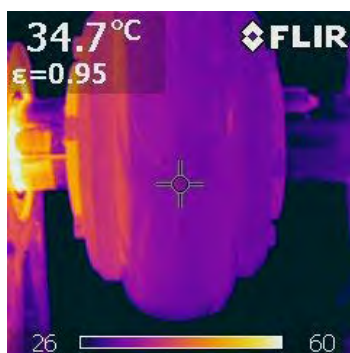**Figure 4-20: Temperature of Fenaflex® coupling, 1mm radial misalignment**

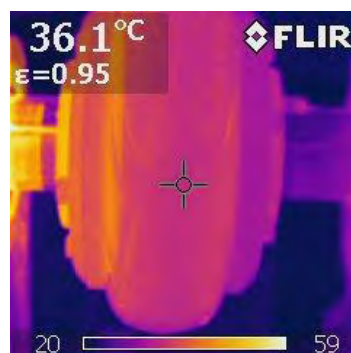**Figure 4-21: Temperature of Fenaflex® coupling, 1.5mm radial misalignment**

Figure 4-22: Temperature of Fenaflex® coupling, 2mm radial misalignment
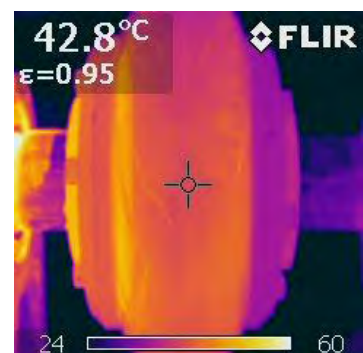

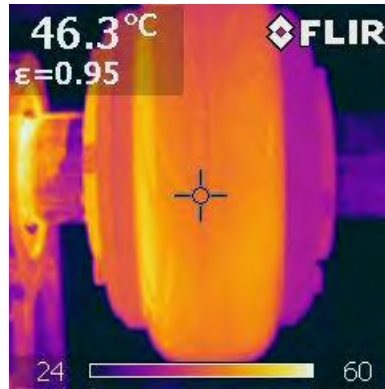**Figure 4-23: Temperature of Fenaflex® coupling, 2.5mm radial misalignment**

Figure 4-24: Temperature of Fenaflex® coupling, 3.5mm radial misalignment

The figures above clearly show a much smaller temperature increase of the tyre than that of the Quick-Flex® coupling. The total temperature increase over the 3.5mm range is only 15°C. The heat generated by the motor support bearing remained low as the misalignment did not cause a load on the motor shaft. The coupling showed very little wear after the testing was completed. The edges of the coupling tyre looked slightly smoother than they were when they were new, but this is more likely due to the compression of the sides in the flanges during assembly of the coupling. Figure 4-25 below shows the small amount of wear on the edge of the rubber tyre.

Figure 4-25: Rubber tyre of Fenaflex® coupling with minor wear

Fenagrid® coupling

The Fenagrid® coupling has a maximum recommended misalignment was 0.4mm. These tests were therefore not conducted over as large a range as the others. These tests were conducted at 0.3, 0.6, and 0.9mm misalignment. This was because the vibrations generated under even slight misalignment were extreme. This vibration can damage machinery quickly, and result in major failure. These tests were conducted until it was deemed unsafe to continue misaligning the coupling. The results in Figure 4-26 show that the efficiency was dropping off, but the main concern in this test was the noise and vibration generated. It is thought that radial misalignment of the Fenagrid® coupling can cause massive failures of rotating machinery, resulting in excessive repair costs.
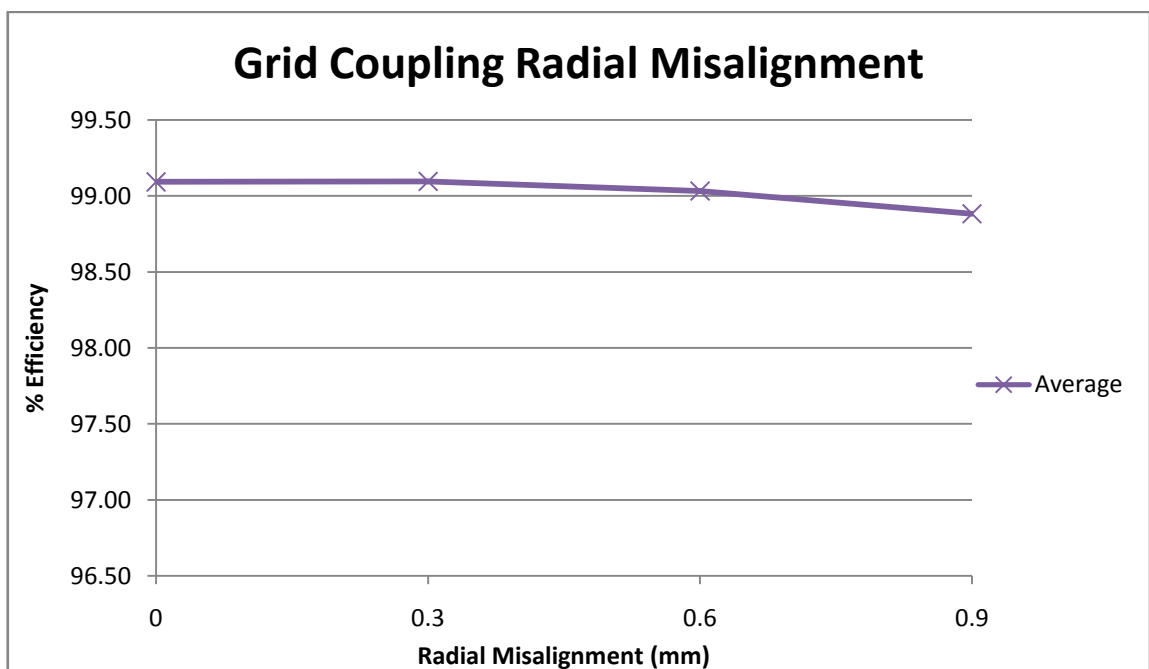

Figure 4-26: Graph of radial misalignment vs. efficiency of the grid coupling

Each test was conducted three times to ensure consistent results. These graphs can be found in Appendix B Figure B-4. The temperature change for this coupling was recorded. It was noted that the temperature did not rise by more than 2° over the entire test duration. This was due to the tests being stopped before a significant efficiency loss was noted. The vibration caused by the misalignment was seen to be worse for an industrial process than the efficiency loss of the coupling, thus the testing was halted.

Figure 4-27 and Figure 4-28 below show the very small temperature increase though the full misalignment test range.
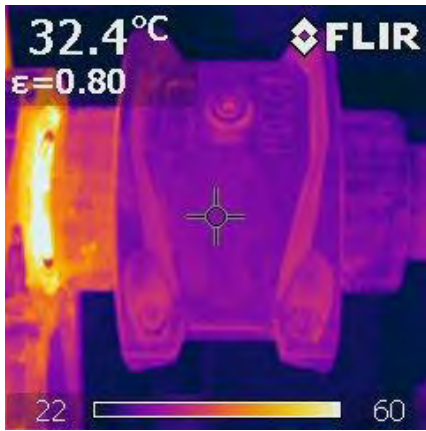

Figure 4-27: Temperature of grid coupling, no radial misalignment
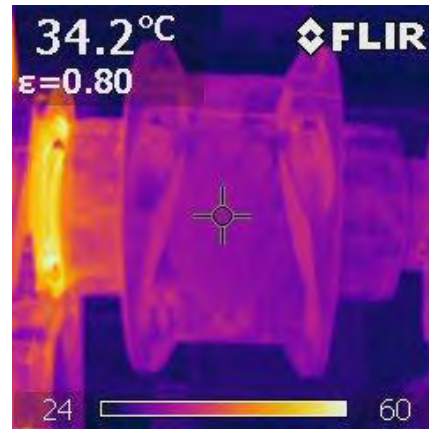

Figure 4-28: Temperature of grid coupling, 0.9mm radial misalignment

Figure 4-29 shows a comparison of the efficiency of each coupling under the different radial misalignment values. It is clear that each coupling reacts differently under radial misalignment, due to the specific properties of each coupling.
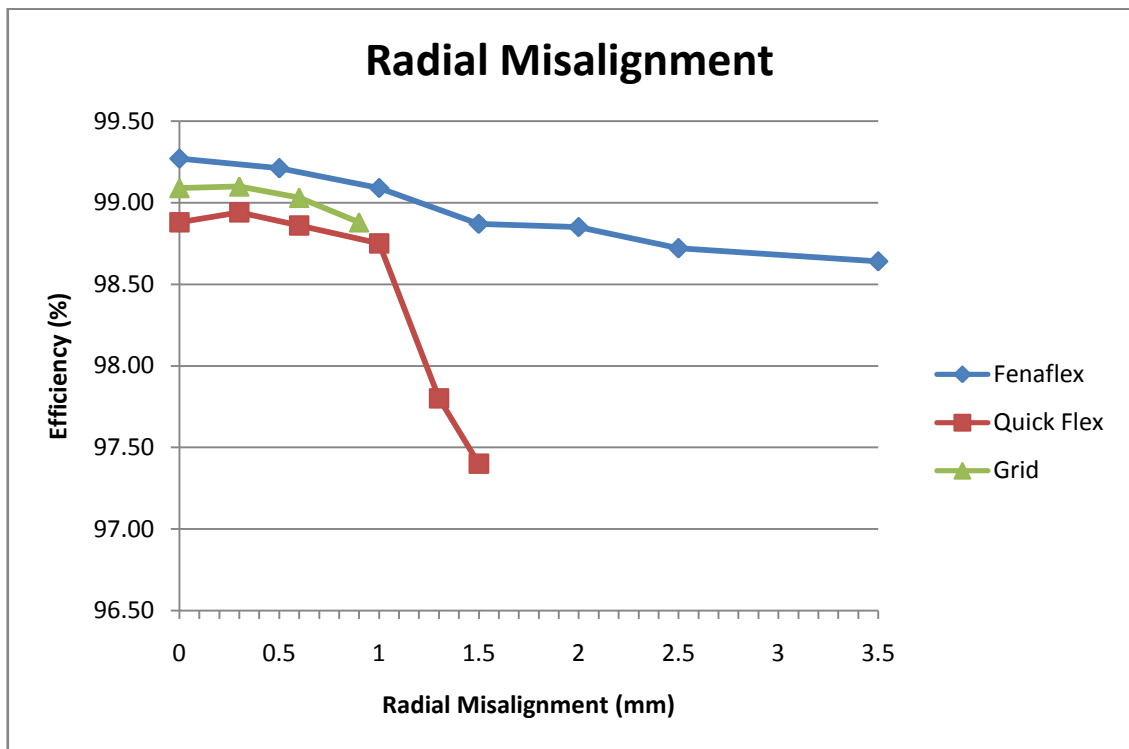

Figure 4-29: Graph of radial misalignment vs. efficiency

The Fenaflex® coupling loses very little efficiency over a large range of radial misalignment. The initial efficiency of this coupling was also very high. The Quick-Flex® coupling on the other had had a lower initial efficiency, which dropped off under slight misalignment. The Quick-Flex® coupling was very easy to install, as opposed to the Fenaflex® coupling, and therefore, the efficiency difference when correctly aligned may be overlooked when compared to ease of installation. The Quick-Flex® coupling and the Fenaflex® coupling both have high vibration dampening properties due to the rubber inserts used. The grid coupling on the other hand does not have this advantage, and any vibration will be carried through to the sensitive equipment on the other side.

4.2.3.2   Angular misalignment

Quick-Flex® coupling

The Quick-Flex® angular misalignment test was conducted at 0.5, 1, 1.5, and 1.9°. The maximum recommended angular misalignment of this coupling was 2°, although the rubber insert prevented misalignment of more than 1.9° without moving the two coupling hubs beyond their recommended spacing. Another factor preventing misalignment from occurring beyond 2° is the teeth of the coupling. Figure 4-30 below demonstrates this. It can be seen that, after the element is removed, the teeth are almost touching on one side.

Figure 4-30: Angular misalignment of Quick-Flex® coupling with element removed

Figure 4-31 below shows the graph of the efficiency of the Quick-Flex® coupling at different angular misalignment values. This graph clearly shows a linear decline in efficiency after 0.5° misalignment. This reduction was caused by the energy required to compress and relax the element as it rotates. This sliding motion of the teeth inside the element resulted in the inner surface of the element being worn significantly. Each test was run three times to ensure consistent results. These graphs can be viewed in Appendix B Figure B-5.
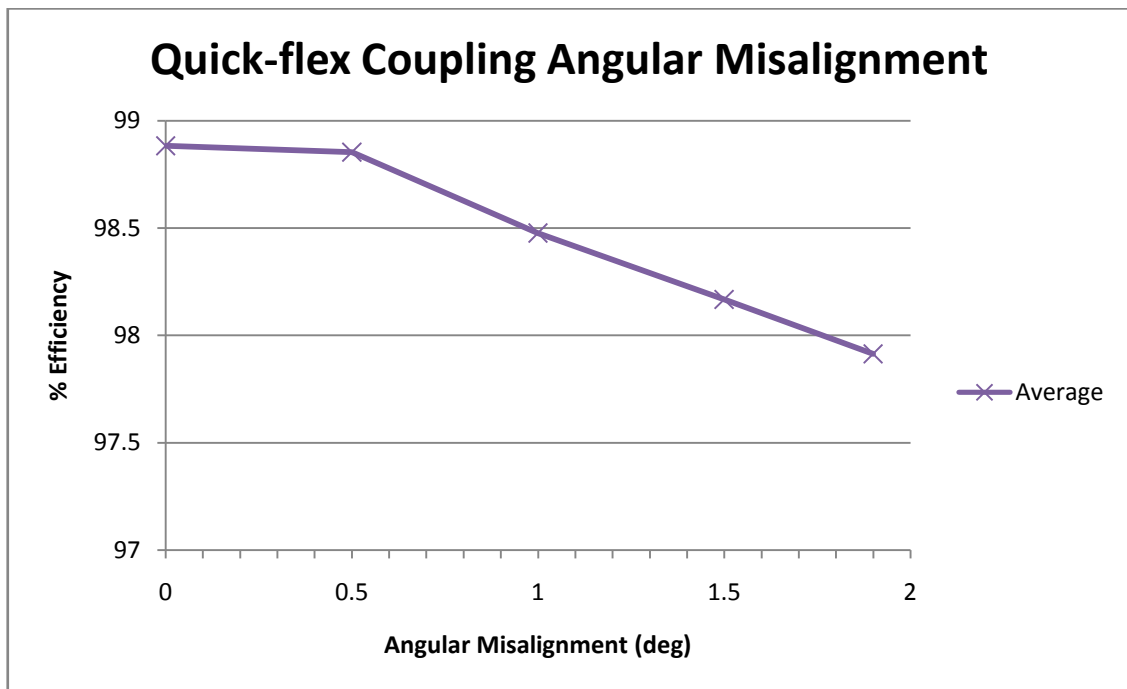

Figure 4-31: Graph of angular misalignment vs. efficiency of the Quick-Flex® coupling

During the misalignment testing, all temperature changes were recorded. The temperature increase, which was measured as the maximum temperature in the square, was clearly visible in Figure 4-32 to Figure 4-35 below. The aligned temperature reading can be seen in Figure 4-6 in the previous section on page 47 of this dissertation. Although there was a noticeable temperature increase of 20°C, it was much less than the increase in temperature during radial misalignment.
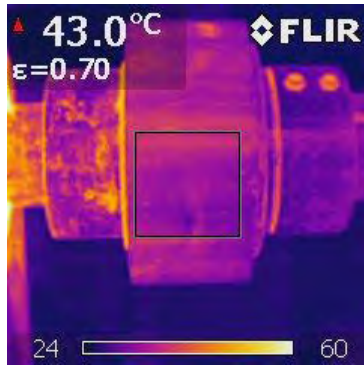
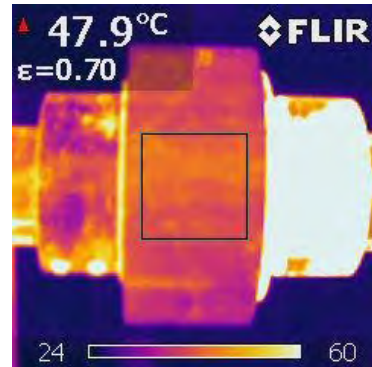**Figure 4-32: Temperature of Quick-Flex® coupling, 0.5° angular misalignment**

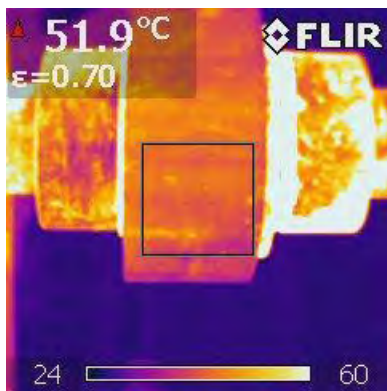**Figure 4-33: Temperature of Quick-Flex® coupling, 1° angular misalignment**

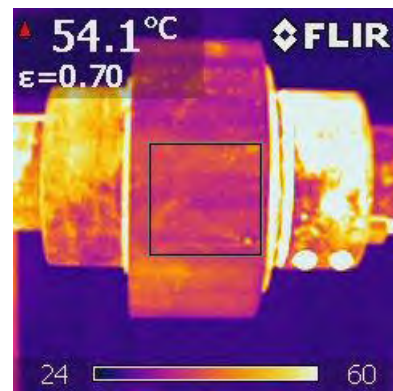**Figure 4-34: Temperature of Quick-Flex® coupling, 1.5° angular misalignment**

Figure 4-35: Temperature of Quick-Flex® coupling, 1.9° angular misalignment

As previously stated, the repetitive sliding of the teeth in and out of the element resulted in excessive wear to the element. At 1.9° misalignment, rubber shavings could be seen between the teeth of the coupling. This was deemed a failure, and the testing was halted. It can be seen from Figure 4-36 and Figure 4-37 below that the element was being shredded between the teeth as it rotated. The temperature increase was again significant at this level of misalignment.
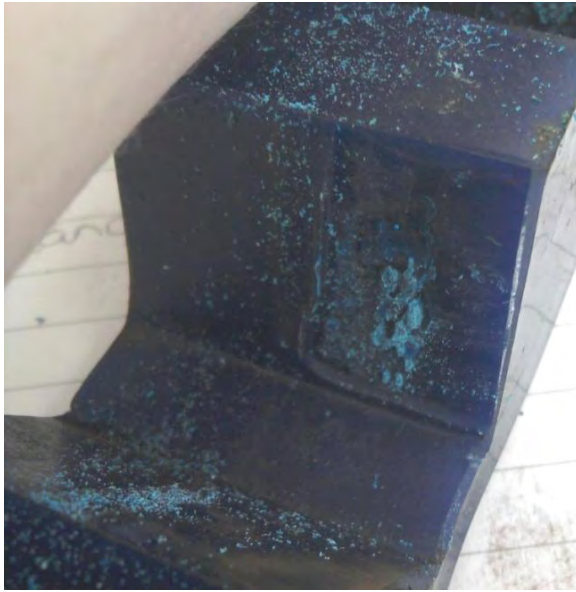
Figure 4-36: Indentation in Quick-Flex® coupling element

Figure 4-37: Shredded element of Quick-Flex® coupling.

The thermal images of this mode of misalignment clearly showed that the right hub had a higher temperature than the left. The difference between this test, and the radial misalignment test, was that the warmer hub was not near the motor support bearing, and thus was not a result of the heat being conducted along the shaft. After analysing the failure of the coupling element, it could be seen that the deep indentations only occurred on right side of the coupling element. This lead to the conclusion that the coupling element sat in the correct position on the left hand side hub, while the right hand side hub was forced to slide in and out of the element as it rotated. This resulted in the excessive damage on one side of the coupling, and the heating of the right hub.

Fenaflex® coupling

The Fenaflex® coupling was tested at misalignment values of 0.5, 1, 1.5, and 2°. The maximum allowable misalignment stated in the catalogue was 4°, but this level would be very noticeable to an operator. Figure 4-38 below shows a graph of the change in coupling efficiency over the different angular misalignment range. The graph clearly shows very little decrease in efficiency over the tested range. The small increase at the beginning of the test could be a result of inaccuracies in the test rig.
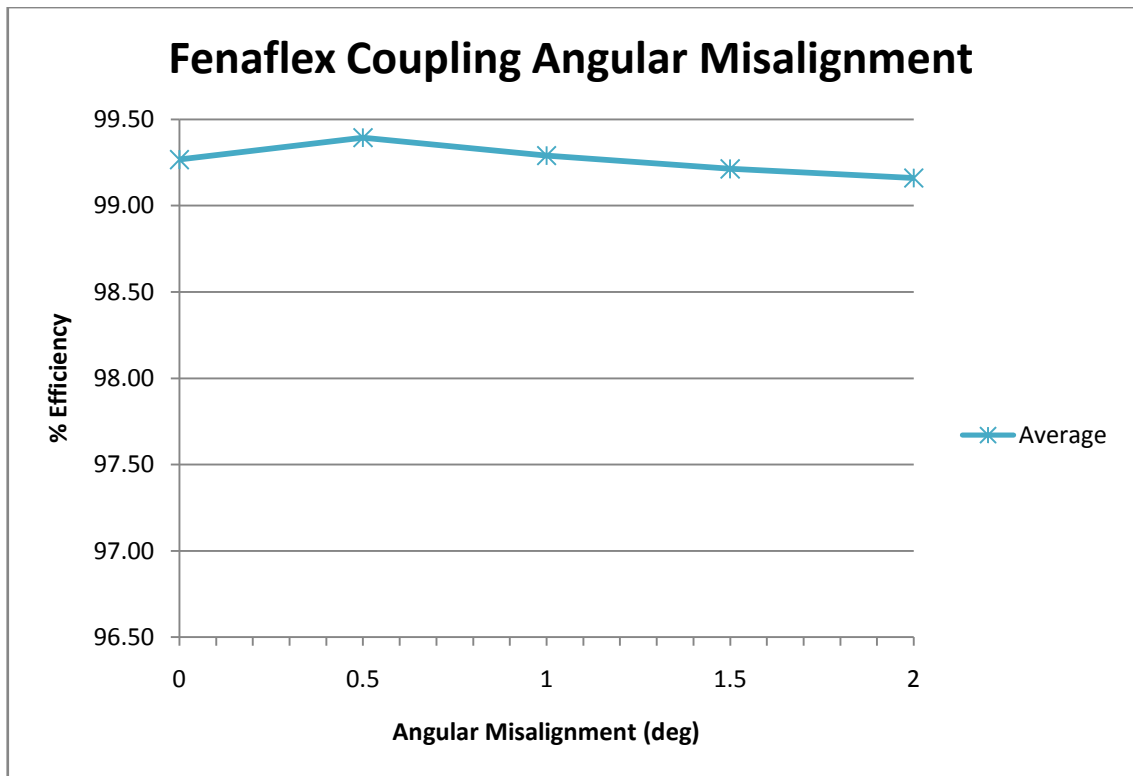
Figure 4-38: Graph of angular misalignment vs. efficiency of the Fenaflex® coupling

Each test was conducted three times to ensure consistent results. These results can be found in Appendix B, Figure B-6.

Figure 4-39 to Figure 4-42 below show the temperature increase of the Fenaflex® coupling over the angular misalignment range. It can be seen that the temperature of the coupling increases as the misalignment increases, and the efficiency decreases. There was a total temperature increase of 15°C over this range of angular misalignment. This seems quite high especially as the efficiency remains relatively unchanged. Analysing of the thermal images shows that the temperature of the Fenaflex® coupling tyre was originating from the left hand side. A clear temperature gradient can be seen over the width of the tyre. This shows that the temperature increase is not entirely a result of the loss of the coupling, but that of the heat generated from the running of the bearing.
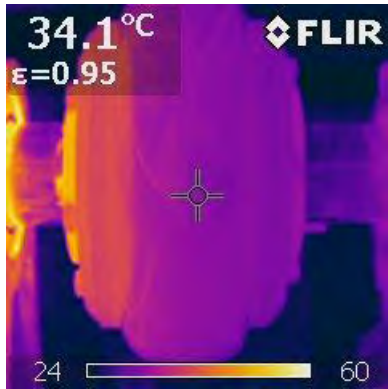
Figure 4-39: Temperature of Fenaflex® coupling, 0.5° angular misalignment

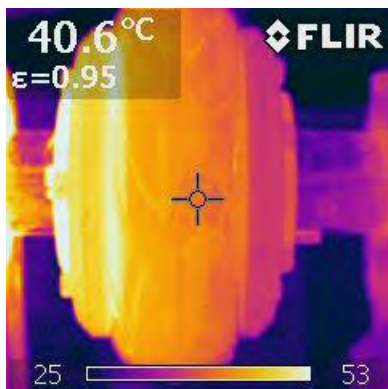**Figure 4-40: Temperature of Fenaflex® coupling, 1° angular misalignment**

Figure 4-41: Temperature of Fenaflex® coupling, 1.5° angular misalignment
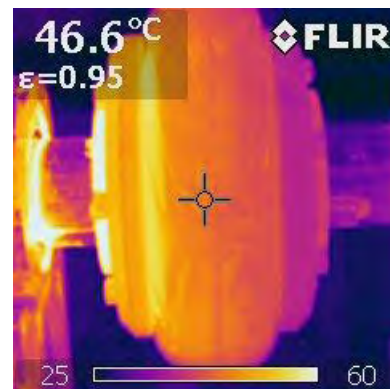

Figure 4-42: Temperature of Fenaflex® coupling, 1.9° angular misalignment

A comparison of the radial and angular misalignment modes of the Fenaflex® coupling shows that although they have a similar temperature increase, the efficiency loss of the radial misalignment is double (1%) that of the angular misalignment (0.5%). A closer look at the thermal images of these two cases shows that the there is no temperature gradient on the rubber tyre during the radial misalignment test, and there is during the angular misalignment test. This shows that the temperature readings from the radial misalignment test is a result of the loss in the flexing of the rubber tyre, while the temperature increase in the angular misalignment test is a result of the heat generated from the bearing being conducted along the shaft and flanges.

Fenagrid® coupling

The Fenagrid® coupling had a maximum recommend angular misalignment of 0.3°. The misalignment tests were conducted at 0.1, 0.2, 0.3, 0.5 and 0.7° misalignment. Figure 4-43 below shows a graph of the efficiency of the coupling at the different misalignment values. The graph shows very little efficiency loss of the grid coupling over the tested range, but as with the radial misalignment, the testing was stopped due to excessive vibration. Each test was conducted three times to ensure consistent results. These results can be found in Appendix B, Figure B-7.
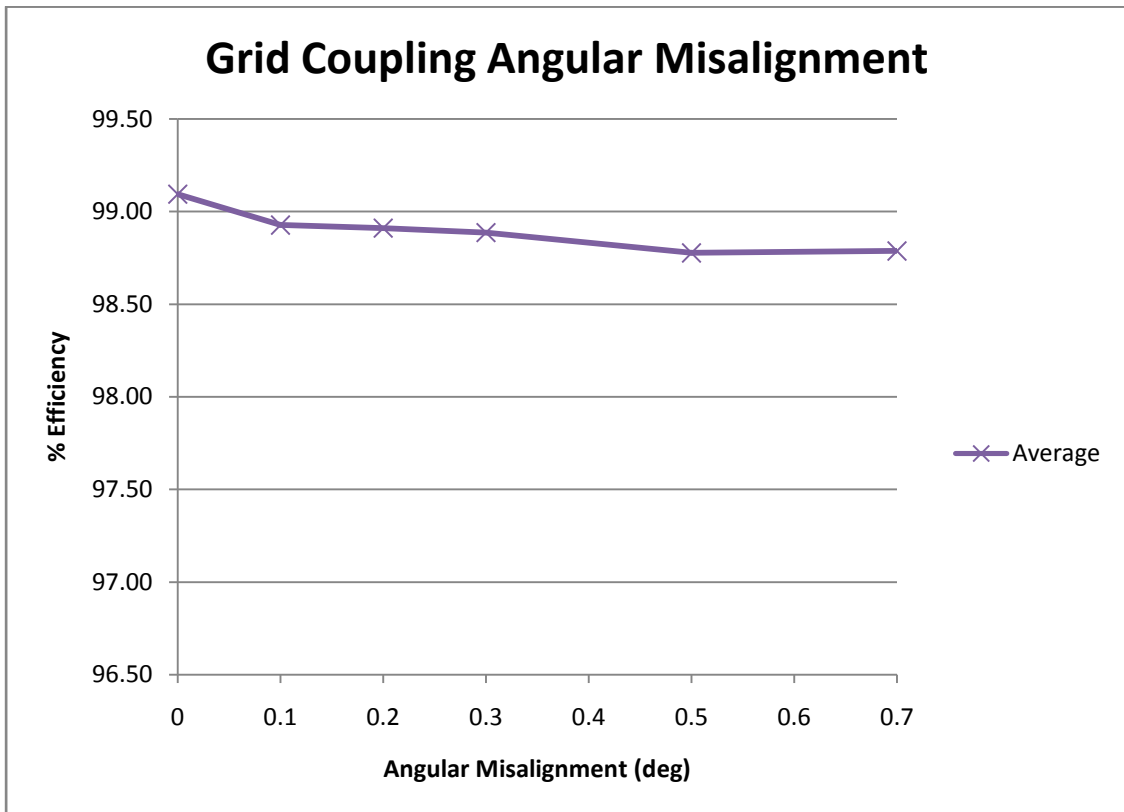

Figure 4-43: Graph of angular misalignment vs. efficiency of the grid coupling

The temperature increase of the grid coupling over this angular misalignment range was small. This can be seen in Figure 4-44 and Figure 4-45 below.
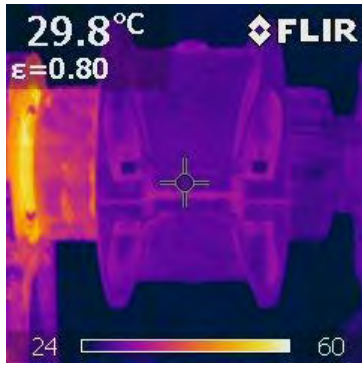
Figure 4-44: Temperature of Grid coupling, 0.1°
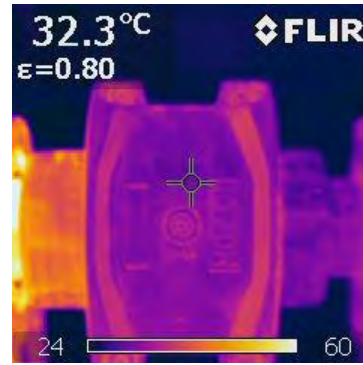**angular misalignment**

Figure 4-45: Temperature of Grid coupling, 0.7°
angular misalignment

Figure 4-46 shows a graph of the angular misalignment of each coupling against efficiency. Again it can be seen that the Fenaflex® coupling lost very little efficiency under angular misalignment, and could not be tested further as the misalignment capabilities of the machine were reached. The grid coupling did not show a significant drop in efficiency before the tests had to be halted due to excessive vibration. The Quick-Flex® coupling under angular misalignment showed a more gradual efficiency loss than when under the radial misalignment.
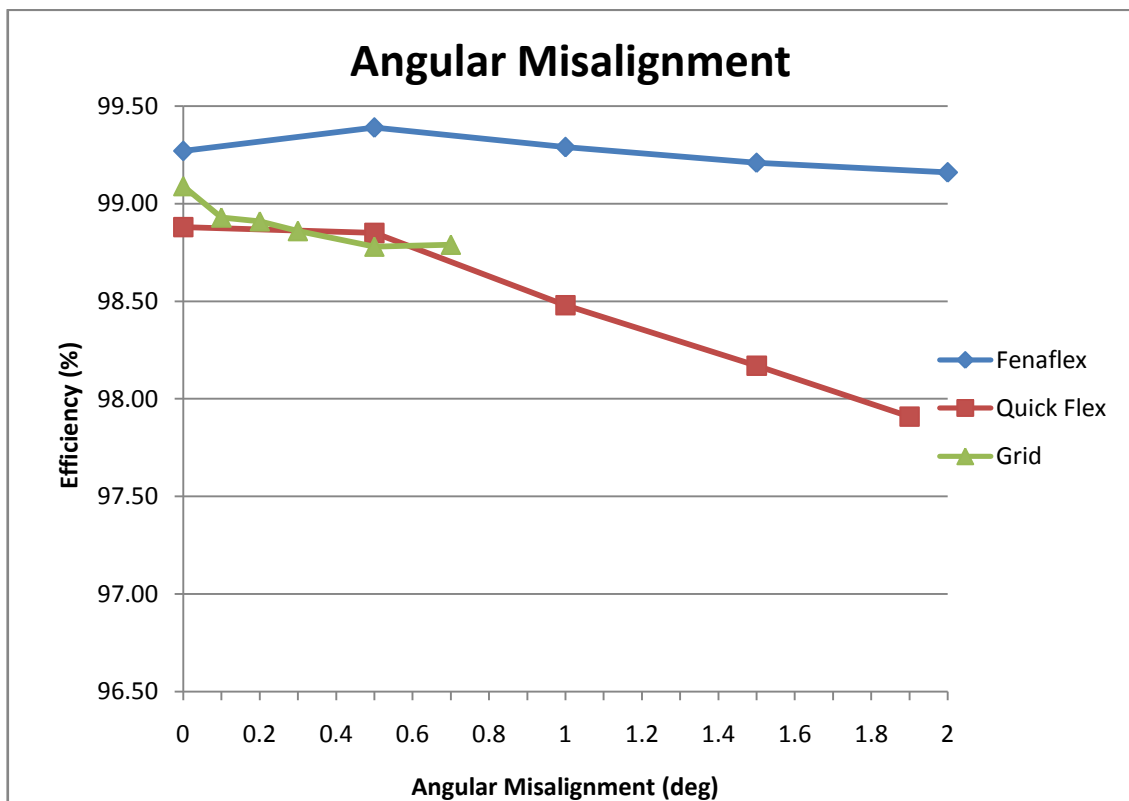

Figure 4-46: Graph of angular misalignment vs. efficiency

The Fenaflex® coupling loses very little efficiency, as the only loss in this coupling was the widening and narrowing of the tyre as it rotated under angular misalignment. This had much less movement and material distortion, due to the thin cross section, than the Quick-Flex® coupling. The Quick-Flex® coupling element was compressed during each rotation, and the stresses on this caused significant loss. The Quick-Flex® coupling also underwent considerable friction. This is due to the sliding of the teeth inside the element. The Fenagrid® coupling under misalignment generated a significant amount of vibration during rotation. This was due to the resistance of the steel grid inside the coupling. This grid was required to flex and slide under misalignment. Without any dampener separating the two flanges, the vibration caused by the flexing was transmitted through the coupling to the other shaft.

4.3   Belt testing

4.3.1   Testing procedure

This test required a comparison of the Fenner® SPB V-belts, the Fenner® Poly V ™ belt, and the Gates® Poly Chain® GT2. Each belt had a different tensioning method and value, and therefore each test was run at full load at the correct belt tension. The tension was then dropped in 25% steps of the full tension of the specific belt. Each belt was run-in for a specified amount of time, as stated in the catalogue, before the actual testing tension was set. The effects of noise, vibration, and temperature were noted during testing. Correct alignment was achieved using lasers to avoid any unnecessary efficiency loss or run-off. The belt to be tested was set up on the drive side of the test rig, while the load side was connected with a Poly Chain® GT2 synchronous belt for all the tests.

4.3.2   Test setup

The setup began with ensuring the pulleys were aligned with the motors. This was to prevent the misalignment of belts from affecting the efficiency of the belt under different tensions. The lay shaft was set in position, and the two motors were independently aligned to this. A belt alignment laser tool was used to accomplish this. Once alignment was achieved, the belts were tensioned correctly, while ensuring the alignment wasn't changed. The belts were then run for a set time period, and the tension was checked, and adjusted if required. It was noted that although the operation instructions required a second tensioning after a set run-in time, the tension did not change sufficiently to require re-tensioning of the belt.

Each test was conducted three times to ensure consistent results, and temperature was recorded at set intervals. After the full tension test was completed, the tension was reduced by 25%, and the test set was redone. The results in the graph are plotted as percentages of full tension.

4.3.3   Results

The belts tested were the SPB V-belt, the Poly V ^{TM} and the Poly Chain® synchronous belt. These belts each had their own unique properties, as discussed in section 2.2.2, resulting in different efficiency reactions. These results are described below.

4.3.3.1   Poly Chain® GT2

The Poly Chain belt is a synchronous belt, meaning that the teeth run perpendicular to the belt. From this it was assumed that the belt tension would not affect the efficiency significantly as each tooth in the belt resulted in the same rotational displacement of the pulley. The results, shown in Figure 4-47 below, confirmed this point. Unfortunately, at low tension, the belt was very unstable, and may run off due to the excessive vibration and bouncing of the slack side. Each test was conducted three times to ensure consistent results. These graphs can be found in Appendix B, Figure B-8.
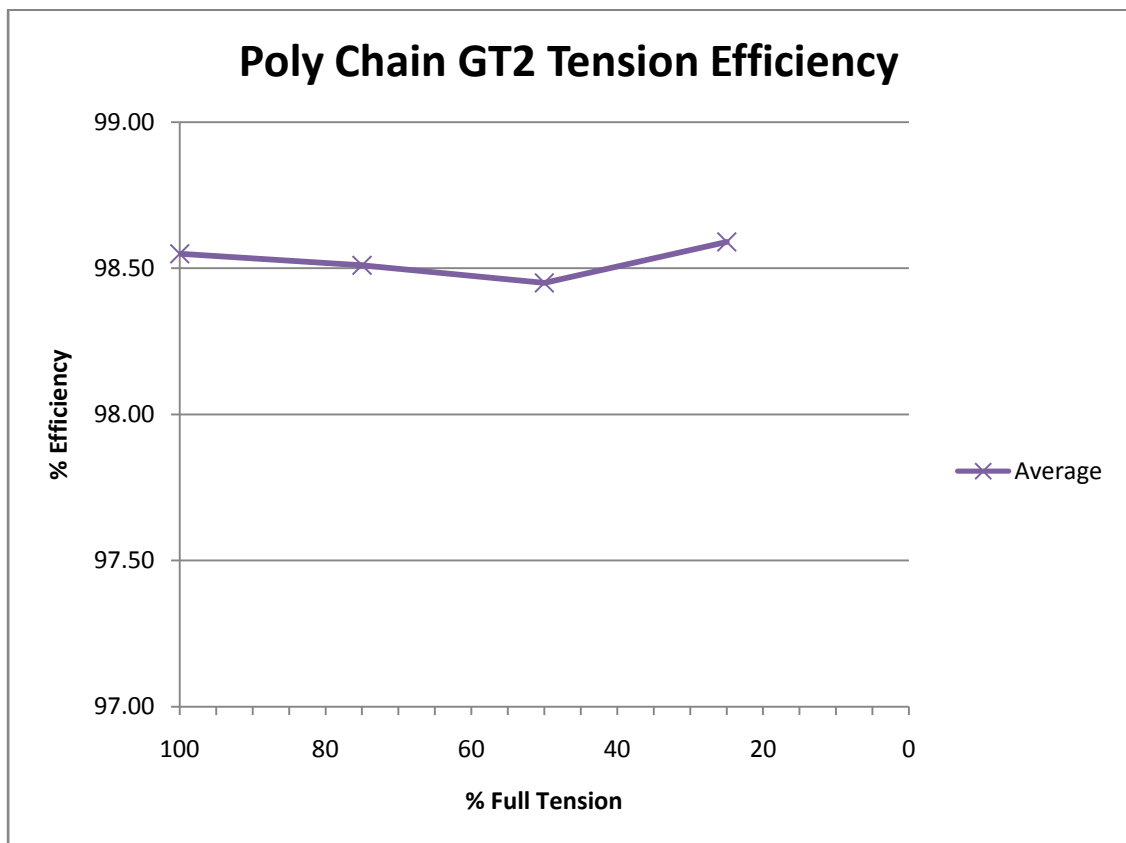

Figure 4-47: Graph of Poly Chain® GT2 belt efficiency vs. belt tension

This belt was also very difficult to align as it needed to run squarely in the grooves of the pulley, and any misalignment caused it to run off the pulley. Run off for this type of belt can also be caused by unbalanced pulleys, where the pulleys wobble during rotation. A high rising key may also cause the taper lock to sit off-centre on the shaft, resulting in eccentric pulleys.

The belt efficiency was also tested when it was 25% over-tensioned, although this result is not plotted on the graph. The efficiency remained within the same range, but the belt was severely damaged. It can be seen in Figure 4-48 below that the top layer of the belt flaked away, revealing the belt fibre. Figure 4-49 shows the belt flakes covering the motor.
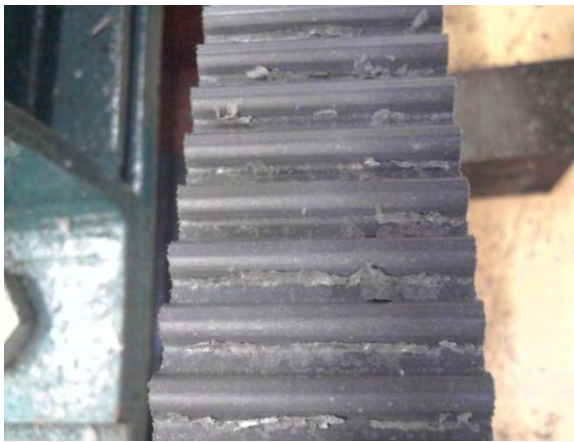

Figure 4-48: Flaked surface on Poly Chain® GT2   **Figure 4-49: Motor surface with flaked Poly Chain® GT2 belt**

Figure 4-50 below shows an increase of the belt surface temperature during testing to 10° above ambient. This temperature increase was caused by the friction of the belt teeth moving in and out of the pulleys. This friction generated heat, resulting in an efficiency loss and a temperature increase.
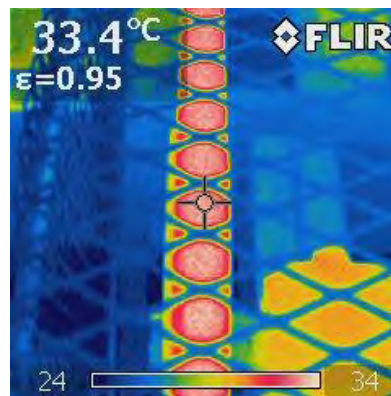

Figure 4-50: Temperature of Poly Chain® GT2 belt running at full load and full tension

4.3.3.2 SPB V-Belt

The SPB V-belt set selected ran in a three groove pulley. The graph shown in Figure 4-51 below shows an increase in efficiency at lower tension. It was noted that the graph shows an initial decrease in efficiency at 75% of full tension. This loss was very small and could be attributed to the inaccuracy of the test rig. The increase in efficiency was due to the reduced "wedging" effect. As the pulleys rotate, the belt was wedged into the groove. At high tension the belt goes further into the groove. This extra wedging caused heat generation, and thus a small amount of efficiency loss. As the belt was de-tensioned, it did not settle into the wedge as far and thus less energy was lost. It is noted that as the belt is run, the tension can decrease over time due to the stretching effect of the belt, and thus the initial tension is very important. Each test was conducted three times to ensure consistent results. These can be found in Appendix B, Figure B-9.
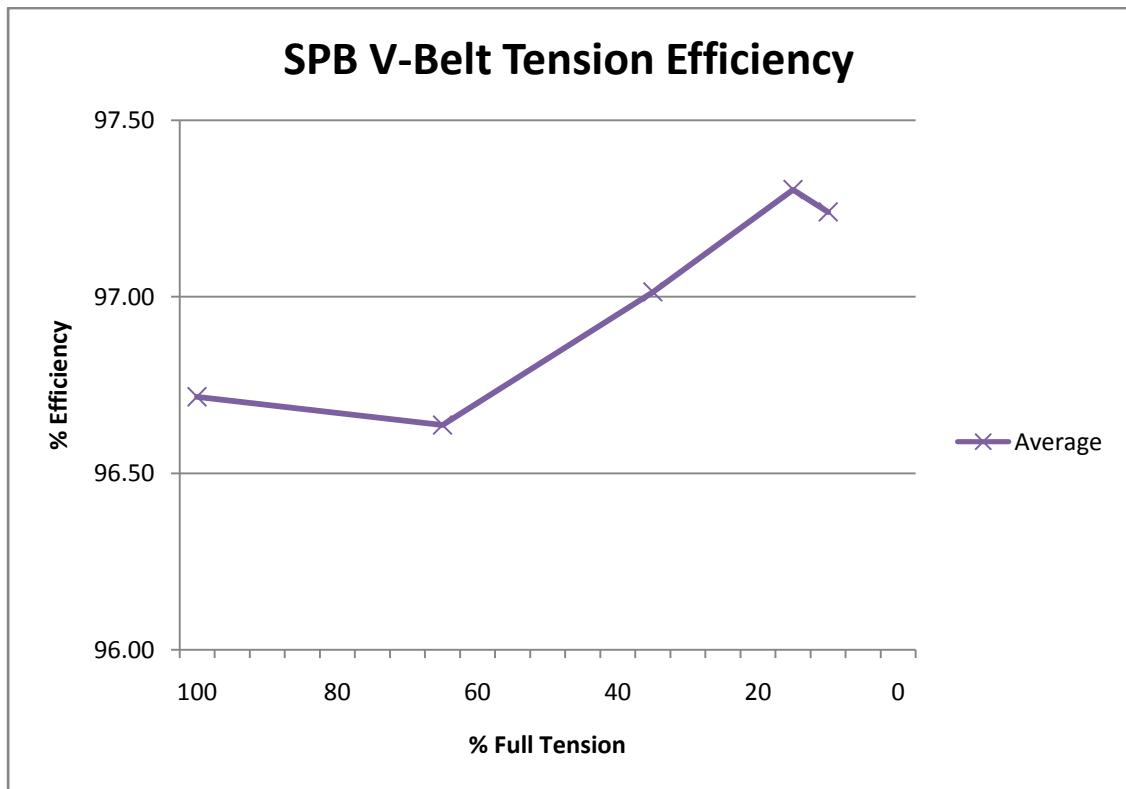

Figure 4-51: Graph of SPB V-Belt efficiency vs. belt tension

At a much lower tension, the efficiency began reducing again. This was caused by the slip of the belts in the pulleys. The slip was caused by the reduced friction force between the belt and pulley due to low tension. The efficiency dropped further from this point due to the wear caused by the slippage. It was noted that the side of the belt, and the inside of the pulley, had become "polished" due to the slipping of the belt inside the pulley. This effect can be seen in Figure 4-52 and Figure 4-53 below. The use of the OST self tensioning motor base can alleviate this effect as it will keep the belt at the correct tension by rotating the motor.

This motor base is ideal for Poly V ^{TM}, and V-Belts as these belts can withstand small amounts of misalignment without effecting performance. Unfortunately this base may not work with the Poly Chain® synchronous belt as the small amounts of rotation may cause slight misalignment of the pulleys, causing the belt to run off.
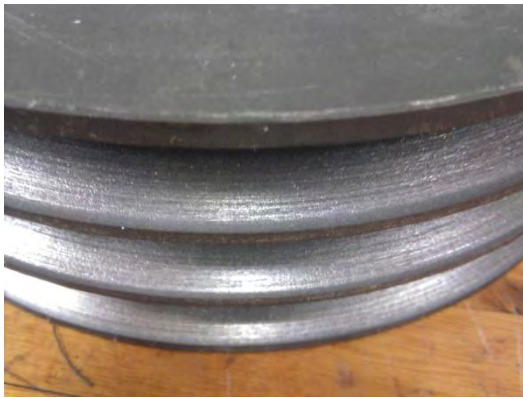

Figure 4-52: Polished V-Belt pulley

Figure 4-53: Polished V-Belt

Figure 4-54 and Figure 4-55 below show the temperature difference of the SPB V-belt at the reduced tension. As the graph implies, there was an efficiency increase as the belt was de-tensioned. The temperature readings also show a temperature drop at this point, confirming the readings on the graph, as less heat was generated, less energy was lost, and therefore the efficiency increased.
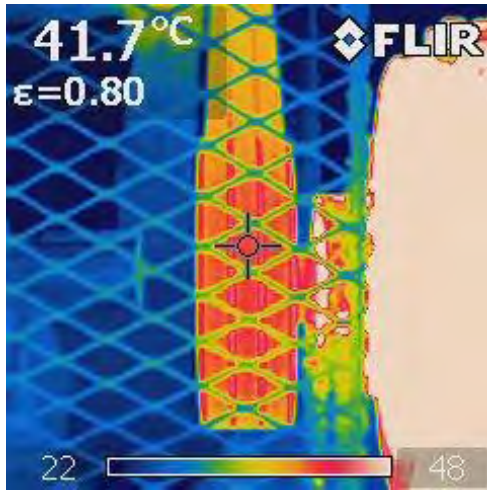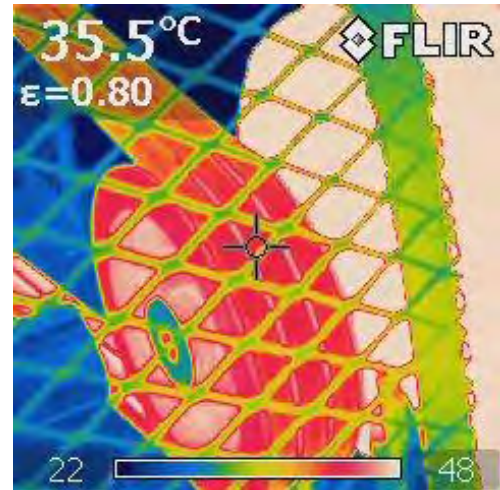
Figure 4-54 : Belt temperature at full tension

Figure 4-55: Belt temperature at 25% of full tension

4.3.3.3   Poly V ^{TM} belt

The Poly V ^{TM} belt is a wide belt with Parallel V grooves in it. These grooves were designed to increase the friction surface of the belt. It can be seen from Figure 4-56 below that the efficiency of this belt decreased as the tension decreased. This decrease in efficiency was caused by the reduced friction between the V-grooves and the pulley. Because this belt is a single belt, with many V's, the belt was never tightly wedged into the grooves. The decrease in tension then resulted in the V's not sitting in the grooves correctly, reducing the friction, and thus not transmitting as much power. Each test was conducted three times to ensure consistent results. These graphs can be found in Appendix B, Figure B-10.
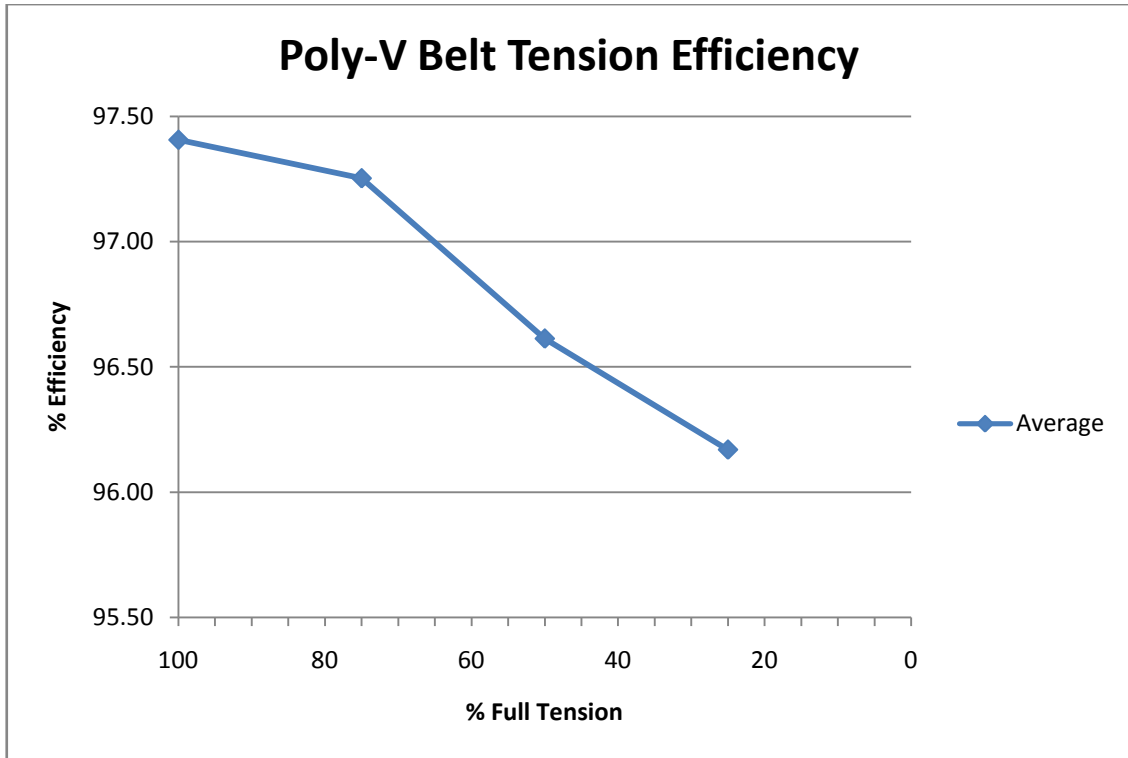
Figure 4-56: Graph of Poly V ^{TM} belt efficiency vs. belt tension

Figure 4-57 and Figure 4-58 below show the temperature increase due to the slip of the belt on the pulley. At the correct tension, the belt sits at 35.5°. The temperature increased to 46.5° when the belt tension was reduced to 25% of full tension. This coincides with the results given in the graph, as the efficiency decreases, the temperature due to slip increases.
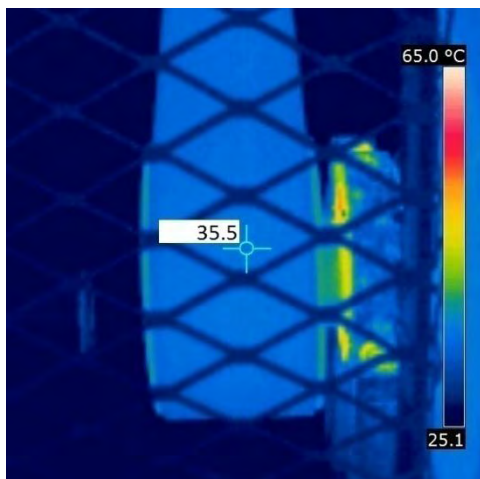

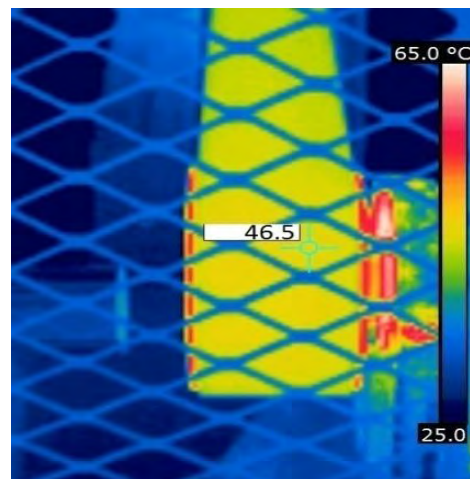**Figure 4-57: Temperature of Poly V ^{TM} Belt at correct tension**

Figure 4-58: Temperature of Poly V ^{TM} belt at 25% tension

Figure 4-59 below plots the efficiency of all the belts on the same set of axis. This shows the efficiency advantage of each belt compared to the others. It can be seen that the Poly Chain® GT2 belt had a much higher efficiency than the other belts, but the disadvantages of this belt is the difficulty involved with alignment. The Poly V ™ belt allows for more flexibility than the V-belt. The thin cross section of the Poly V ™ belt allows this belt to wrap around smaller pulleys, and change direction easily, but the efficiency loss at lower tensions is significant. The V-belt set, if maintained correctly, can allow misalignment, and is the easiest belt to install. The slight increase in efficiency shows the belts ability to run at decreased tension, but allowances must be made for the stretching of this belt.
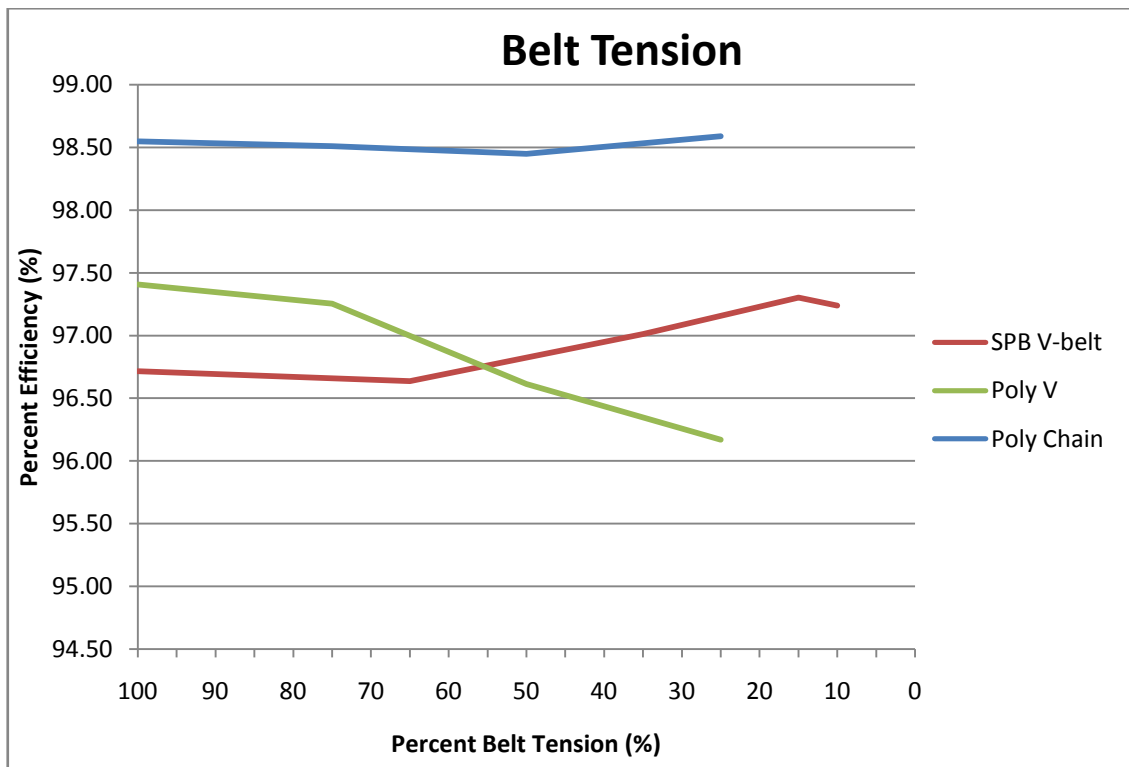

Figure 4-59: Graph of percent belt tension vs. efficiency for all the belts

A comparison of the belt tension graph shows that each belt has individual advantages and disadvantages. This makes it difficult to state which is better in practice. The situation should be analysed, and the appropriate belt chosen. From what was studied during this testing, it can be said that the Poly Chain® GT2 belt was significantly better at transmitting load, but was difficult to align, and may damage machinery if exposed to shock loading. The Poly V ™ belt has an increased efficiency, but must be maintained at the correct tension. It is also useful for smaller pulley diameters. The V-belt is able to withstand misalignment, and has flexibility to reduce damage to machinery if exposed to shock loading. Unfortunately, this belt requires regular maintenance, as it loses tension quickly during operation.

4.4   Fluid coupling

4.4.1   Testing procedure

The testing of the fluid coupling was carried out using the slow start-up, and the direct-on-line start-up capabilities of the test rig. The coupling connected the drive and load motors by means of a shaft. For the running efficiency of the coupling, the coupling was run up to speed, and then a load slowly applied to it. The temperature of the coupling was then allowed to settle, and the efficiency readings were taken. For the DOL start-up tests, the system was rapidly accelerated to full speed, and the torque and rotational displacement recorded. Due to the high rate of the acceleration, the data readings were set to record every 5ms. The system was required to overcome the inertia of the two motors (0.302 kgm^2 each), and the inertia of the whole fluid coupling (0.501 kgm^2). When a comparison test was conducted by directly coupling the motors, only the inertia of the drive and load motor acted as a load, as the fluid coupling was removed. This resulted in a lower start-up inertia which, for the purposes of this dissertation, was adjusted by calculations.

4.4.2   Test setup

This test required a new shaft to be fitted, and the frame bearing supports to be moved due to the size of the fluid coupling. The motors were aligned accurately to each other. The shaft was then placed between them and aligned. The fluid coupling was filled with oil to the correct level, and allowed to run for a short time. The oil level was then checked again, to ensure that any oil that had filled the air spaces was replaced.

4.4.3   Results

Figure 4-60 shows a graph of the start-up torques of the drive motor with a fluid coupling, and without a fluid coupling under DOL. It can be seen from this graph that the effect of the fluid coupling was to increase the time taken for the torque to be transmitted to the rest of the system. This indicates that the time taken to get the load motor to full speed was increased. The DOL start without the fluid coupling accelerated the inertial load to full speed in a much shorter time. This is confirmed in Figure 4-62.
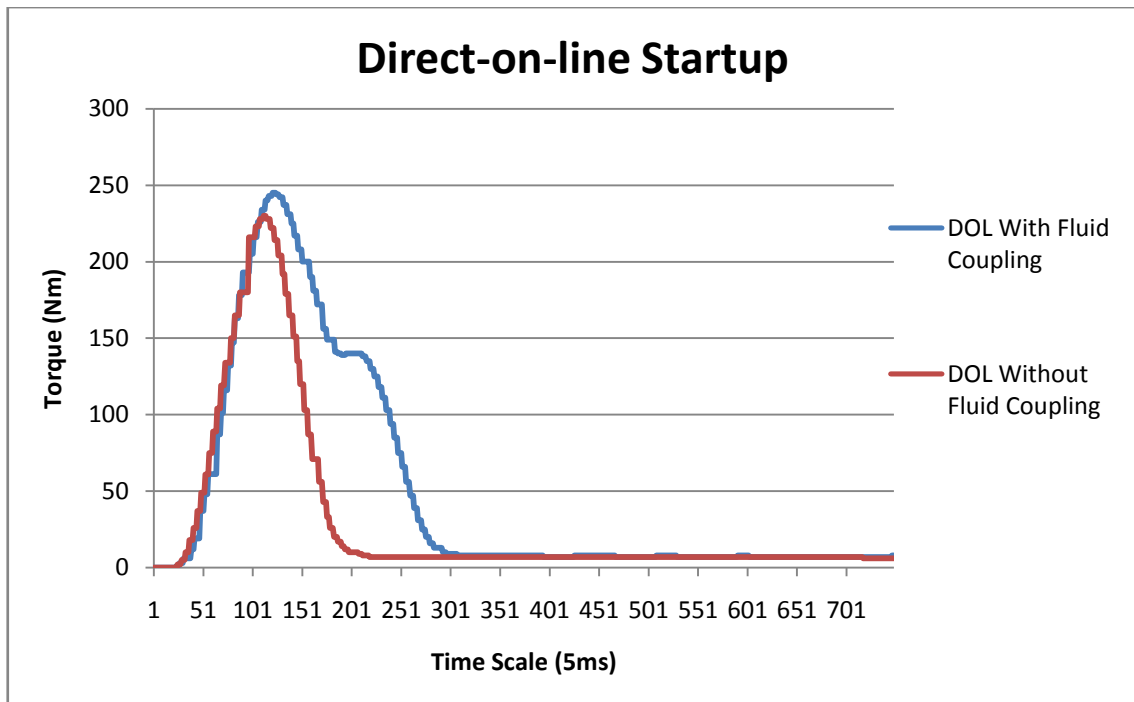
Figure 4-60: Direct on line start with fluid coupling and without fluid coupling

It is noted from Figure 4-60 that the maximum torque with the fluid coupling was higher than the maximum torque without the fluid coupling. This seems to be an anomaly as the fluid coupling was supposed to reduce the start-up torque. The maximum torque these motors can put out under DOL is 500Nm. When the fluid coupling was removed for the standard DOL, the inertia of the system had decreased from $1.105kgm^2$ to $0.604kgm^2$. This resulted in a lower peak on the standard DOL. If the system had much higher inertia, e.g. including a gearbox, resulting in the inertia of the fluid coupling being negligible, the graph would look more like Figure 4-61. This shows that the fluid coupling is only beneficial if used in a high inertia system, and in such a situation it can substantially decrease the start-up torque of the system. If the fluid coupling adds significantly more inertia to the system than originally exists, it is no longer beneficial.
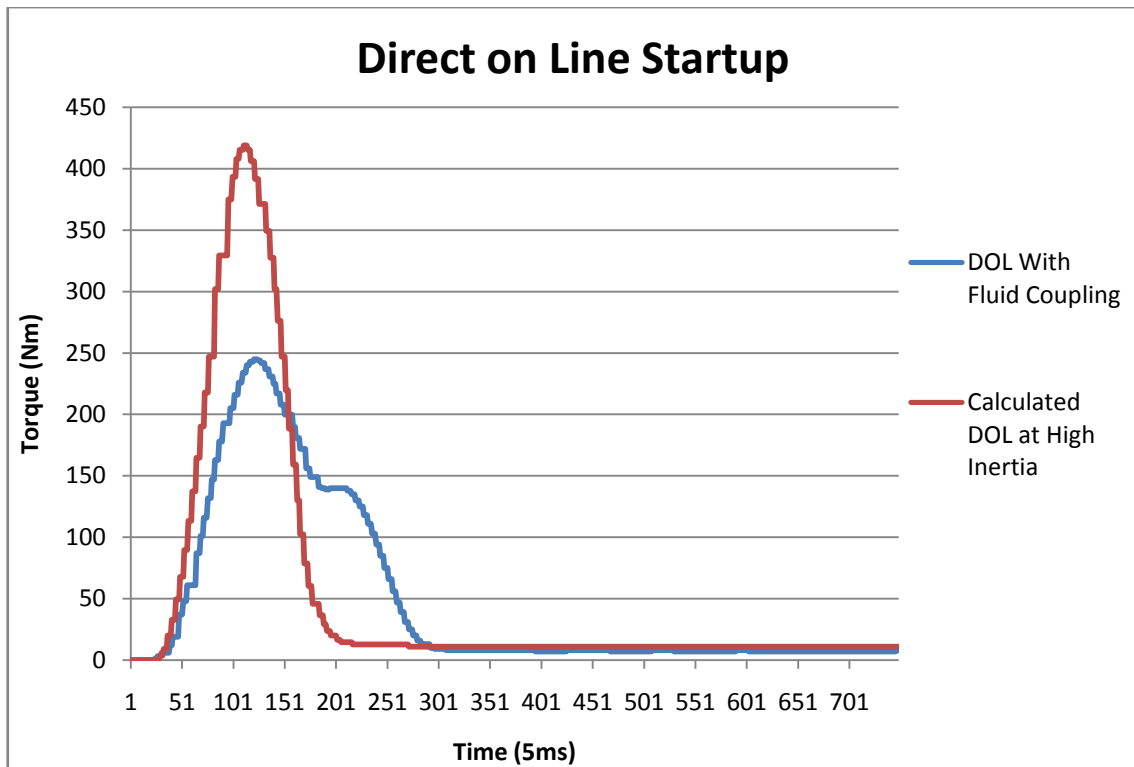
73

Figure 4-61: Calculated torque graph

The area under the graph is the angular momentum of the test rig. The two cases, if the inertia of the fluid coupling is negligible compared to the rest of the system, should have an equal area under the graph. The angular momentum was calculated as the product of the inertia of the system and the angular velocity. The final velocity was the same in both cases; therefore, the angular momentum was the same. The fluid coupling increased the time taken to reach the required velocity, and therefore, to maintain the same area under the curve, reduced the peak torque applied. The reduced peak torque resulted in a lower initial power influx, resulting in the motor running at a higher efficiency, and therefore reducing the electricity used at start-up. If there are multiple start-ups in a system, this reduced power influx, although short lived, can result in decreased power consumption. This can also results in lower stress on the motor, thus increasing the life of the motor.

Figure 4-62 shows the difference in rotational displacement of the two motors with and without the fluid coupling. It must be noted that the relative position of the drive motor and the load motor, without the fluid coupling, are identical since there is very little angular flexibility in the system (the red and blue curves are on top of each other). When the fluid coupling was included in the system, the displacement of the load motor lagged the displacement of the drive motor. This showed that the load motor was gradually accelerated while the drive motor, with minimal inertia, was accelerated quickly. The acceleration of the load was measured from this graph, and is noted to be 377 rad/s^2 without the fluid coupling, and 221.76 rad/s^2 with the fluid coupling. The acceleration of the drive motor with the fluid coupling was reduced as the fluid coupling completely separated the drive motor from the rest of the system. This means that the start-up inertia of the drive motor was only required to rotate the motor and half of the fluid coupling.
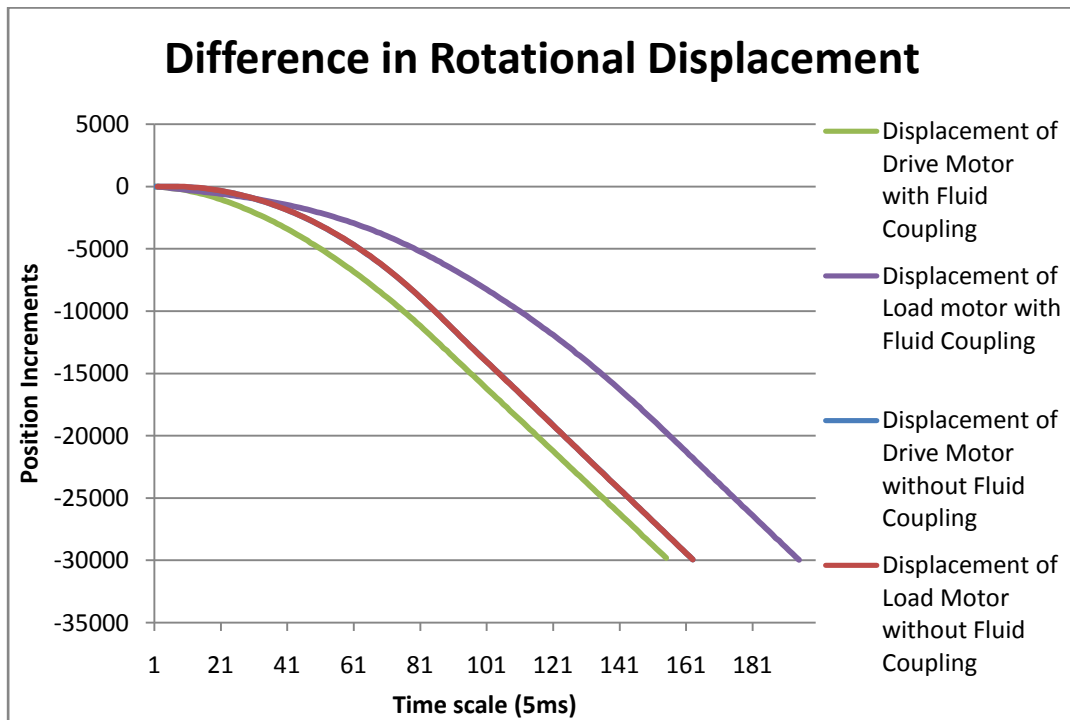

Figure 4-62: Relative displacement of load and drive motor with and without the fluid coupling

The efficiency of the system while running was significantly reduced when the fluid coupling was used. Figure 4-63 shows that the efficiency of the fluid coupling is very low when compared to the efficiency of the Quick-Flex® coupling, meaning that if a system is to be run for long periods of time, it is more beneficial to use a direct drive coupling as opposed to a fluid coupling. This leads to a conclusion that a fluid coupling is more suited to an application where there are a large number of high inertial load starts, and where it does not run for extended periods of time.
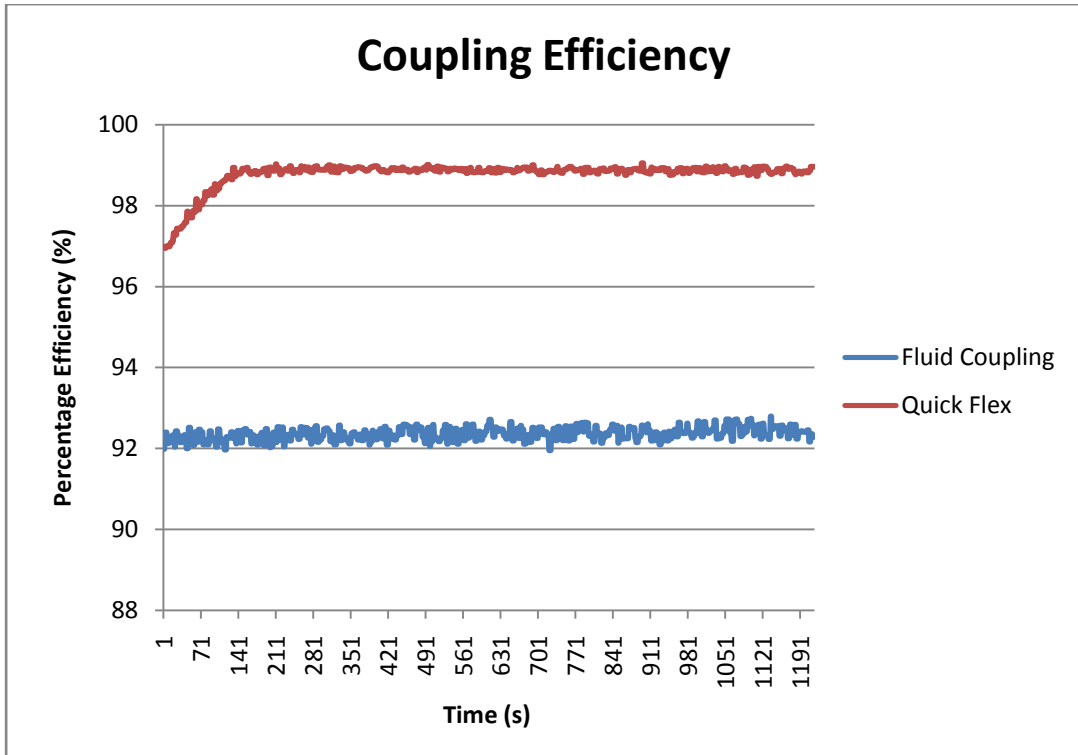
Figure 4-63: Efficiency of fluid coupling and Quick-Flex® coupling

An inspection of the fluid coupling shows large cooling fins around the coupling as can be seen in Figure 4-64 below. While the coupling was run, significant warm airflow was noticed. The large cooling fins show that the fluid coupling needs significant cooling. This heat generation is a consequence of the low efficiency of the fluid coupling.

Figure 4-64: Transfluid CKRG type fluid coupling [40]

4.5   Practical example

To put this research into financial terms, a simple example of a common system is provided. This system compared the efficiency of a common badly maintained system with standard equipment versus a well maintained system using high efficiency equipment. The overall power and, therefore cost saving of the system, was calculated using the results obtained in this dissertation. The cost of the usable power in each system was calculated to show the value lost if high efficiency equipment was not used.

A simple system of a 30kW motor driving a Warman 6/4 DAH centrifugal slurry pump via a coupling was investigated. This system is commonly used in mines, and is therefore a good example to use to apply the results. It will be assumed that the power input to the motor running the pump is 30kW.

4.5.1   Low efficiency condition

The first situation had a standard 30kW Fenner® motor running at full load, and a Quick-Flex® coupling with 1.2mm radial misalignment. The misalignment is not a significant amount, and could be easily accepted if aligned by an inexperienced operator. The results obtained in this work show that the motor has an efficiency of 89.1%, while the Quick-Flex® coupling has an efficiency of 97.7%. Using an average cost of South African electricity as 40c per kW (as stated on the ESKOM website), the total system efficiency (η_s) is calculated as follows:

$\eta_s = Motor\ Efficiency\ X\ Coupling\ Efficiency$

$\eta_s = 89.1\%\ X\ 97.7\%$

$\eta_s = 87.05\%$

The input electrical cost (E_i) is calculated as follows:

$E_i = Motor\ Power\ (kW)X\ Working\ Time\ (Hours)XCost\ per\ kW\ (Rands)$

$E_i = 30\ X\ (24\ Hours\ X\ 340\ days)X\ R0.4/kW$

$E_i = R97920\ per\ year$

The result of the calculation shows a total electrical cost of R97920 per year, per pump unit. If there were multiple pump units in the mine, this cost will be increased by that number.

The value of the useful electrical output cost (E_u) is:

$$E_u = E_i \; X \; \eta_s$$

$$E_u = 97920 \; X \; 0.8705$$

$$E_u = R85239.36 \; per \; year$$

4.5.2   High efficiency condition

The second situation had a high efficiency 30kW Fenner® motor running at full load, and a Quick-Flex® coupling with no misalignment. The results from this dissertation show that the motor has an efficiency of 91.2%, while the Quick-Flex® coupling has an efficiency of 98.8%. Using the same calculation method as above, the total system efficiency is calculated as:

$$\eta_s = Motor \; Efficiency \; X \; Coupling \; Efficiency$$

$$\eta_s = 91.2\% \; X \; 98.8\%$$

$$\eta_s = 90.1\%$$

The value of the useful electrical output cost (E_u) is:

$$E_u = E_i \; X \; \eta_s$$

$$E_u = 97920 \; X \; 0.901$$

$$E_u = R88225.92 \; per \; year$$

These results show a cost waste of R2986.56 per year if the high efficiency system is not used. The price of the standard 30kW motor used in this dissertation was R11 156.01 and the price of the high efficiency motor was R14 175.14, which gives a price difference of R3019.13. This calculation shows that the cost difference of the high efficiency motor can be recouped in about 1 year. The alignment tool is expensive, but if there are multiple systems running in this sector, the cost will be absorbed relatively soon.

CONCLUSION

The test rig design and manufacture was achieved, and all relevant testing was completed successfully. The test rig was able to test all the different aspects required for this dissertation, and more. It was easily adjusted to test the different equipment and therefore the testing procedure time was reduced. The system could not only test the required belts, motors, and couplings, but could also be used to test gearboxes and other equipment if required with just a few minor adjustments. The test rig was fully capable of meeting the requirements of the proposed tests.

The decision to use the Exigo EcoDyn system over a standard Dynamometer was made due to the nature of research. The price difference between a standard dynamometer and the EcoDyn was negligible, so the decision had to be based on other standards. As this project was created to reduce energy consumption, it seemed the logical choice that energy should be conserved during testing as well. This would also increase outside interest in the project as it was a new system.

The design of the gimbal system was extremely valuable to the overall design, allowing for more accurate measurements of the power losses in the system. This reduced the complexities involved in calculating efficiencies, as well as increasing the accuracy of the readings. As very small reading changes were expected in certain tests, the accuracy resulting from the usage of the load cells was a very important aspect.

The results obtained were useful in understanding the theory of efficiency loss in industrial equipment. As described in the theory section of the dissertation, there are many modes of power loss in a system. The testing allowed the variables to be controlled and tested to view the effects each one had on the equipment tested. The information revealed will allow Industry to reduce their energy consumption, and thus reduce their expenses.

The motor testing showed the benefits a high efficiency motor can have as opposed to a standard motor. The price difference between these two motors is not large compared with the running costs, and therefore the cost can be recovered quickly in Industry.

The results clearly show the sufficient efficiency losses that can be avoided with preventative maintenance. The coupling misalignment testing showed that significant energy can be lost due to flexing of the rubber element cross section. The flexing of the rubber results in a hysteresis loss, and thus energy is lost. This energy is all lost as heat, which is demonstrated in the thermal figures provided in this dissertation. Heat is an undesirable result, due to safety and efficiency, and should be avoided at all costs.

The results also showed that coupling misalignment can result in excessive vibration. Vibration in rotating machinery should be avoided. If a motor is run with significant vibration, it is indicative of misalignment or shock loading on a system. This can cause the motor to be damaged if the cause of the problem is not investigated and rectified.

The belt testing gave interesting results on the properties of each belt, and how the different tensions affected the belt efficiency. The results showed the clear efficiency advantage of the Poly Chain® belt, but there were some disadvantages which were discussed in comparison to the other belts. The Poly V ™ belt and the V-belt differences were discussed, and the efficiency results were explained. These results showed the two efficiencies graphs intersect. This was a result of the decreased wedging of the V-belt into the pulley grooves, resulting in a higher efficiency, and the decreased friction force of the Poly V ™ belt as the tension was decreased, resulting in a reduced efficiency.

The results from the fluid coupling testing show that there can be improvements in power consumption by reducing the start-up torque of high inertial systems. This also benefits sensitive equipment by cushioning it from shock loading start-ups. The fluid coupling is only beneficial in systems where the inertia of the fluid coupling does not significantly affect the total inertia. The running efficiency of this coupling was very low compared to other couplings tested. This low running efficiency reduces the advantage of the fluid coupling if run for long periods of time.

The testing performed for this dissertation was performed as accurately as possible, given the equipment supplied. The results obtained have been explained, and discussed. The testing covered an adequate variety of belts, coupling and motors to draw the conclusions discussed in each section.

REFERENCES

[1]   Department of Minerals and Energy. Digest of South African Energy Statistics 2006
        [Online]
        Available at: www.dme.gov.sa/pdfs/energy/planning/2006%20digest.pdf
        [Accessed 20 November 2009]

[2]   Department of Minerals and Energy. National Energy Efficiency Strategy October 2008
        [Online]
        Available at: www.dme.gov.za/pdfs/energy/efficiency/strategy.pdf
        [Accessed 20 November 2009]

[3]   Oladiran, M.T. & Meyer J.P. 2007. Energy and Exergy analyses of energy consumption
        in the industrial sector in South Africa. *Applied Energy.* Vol.84, 2007, p.1056-1067.

[4]   Sebitosi, A.B. 2008. Energy Efficiency, security of supply and the environment in
        South Africa: moving beyond the strategy documents. *Energy.* Vol.33, 2008, p.1591-
        1596.

[5]   Prakash, V. et al. 2008. Energy for Sustainable Development. Vol XII No.2. A Novel
        efficiency improvement measure in three-phase induction motors, its conservation
        potential and economic analysis. P.78-87.

[6]   Saidur, R. 2009. A Review on electrical motors energy use and energy savings.
        *Renewable and Sustainable Energy Reviews.*2009

[7]   Teschler, L. 2008. Green Technology. More-efficient motors. [Online]
        Available at: http://web.ebscohost.com
        [Accessed 1 July 2009]

[8]   Almeida, A.D & Greenberg, S. 1995. Technology assessment: energy-efficient belt
        transmissions. *Energy and Buildings,* Vol.22, 1995, p.245-253.

[9]   Shieh, C. & Chen, W. 2002. Effect of angular speed on behaviour of a V-Belt drive
        system. *International Journal of Mechanical Sciences.* Vol.44, 2002, p.1879-1892.

[10]   Chen, T.F. Lee, D.W. & Sung C.K. 1996. An experimental study on transmission efficiency of a rubber V-belt CVT. *Mech.Mach. Theory*, Vol.33, No. 4, 1998, p.351-363.

[11]   Firbank, T.C. 1970. Mechanics of belt drive. *International Journal of Mechanical Sciences,* Vol.12, 1970, p.1053-1063.

[12]   WordNet Search - 3.0 [Online]
         Available at: http://wordnetweb.princeton.edu/perl/webwn?s=efficiency
         [Accessed 13 January 2009]

[13]   Piotrowski, J. 2007. Shaft alignment handbook. 3rd ed.
         USA: CRC Press, Taylor & Francis group.

[14]   Al-Hussain, K.M. 2002. Dynamic stability of two rigid rotors connected by a flexible coupling with angular misalignment. *Journal of Sound and Vibration*,Vol.266, 2003, p.217-234.

[15]   Lees, A.W. 2007. Misalignment in rigidly coupled motors. *Journal of sound and vibration,* Vol.305, 2007, p.261-271.

[16]   Lorenzen, H., Niedermann, E.A. & Wattinger, W. 1989. Solid couplings with flexible intermediate shafts for high speed turbo compressor trains, proceeding the 18th Turbo machinery Symposium, Texas, 1989, p. 101-110.

[17]   Moon, J., Wickert, J.A. 1999. Radial boundary vibration of misaligned V-belt drives. *Journal of Sound and Vibration*, 225, 1999, p.527-541.

[18]   Connel, J.E., Rorrer, R.L. 1992. Friction-induced vibration in rubber v-belt applications. *Friction-induced Vibration, Chatter, Squeal and Chaos. p.*75-85.

[19]   Harrington, H.I., 1991. Save Energy With Synchronous Belts. *GatesFacts[TM] Technical Information Library.* Gates Compass[TM] Power Transmission CD-ROM version 1.2.

[20]   Belt Drive Efficiencies. *GatesFacts[TM] Technical Information Library.*
         Gates Compass[TM] Power Transmission CD-ROM version 1.2.

[21]   Sachs, N.W., 2000. Coaxing V-Belts to Operate More Efficiently. [Online]
         Available at: http://motionsystemdesign.com
         [Accessed 19 October 2010]

[22]   Tarr, W., 2009. Switching to Synchronous Belt Drives for Energy Savings. [Online]
         Available at: http://www.mt-online.com
         [Accessed 19 October 2010]

[23]   US Department of Energy Efficiency and Renewable Energy, 2005. Replace V-Belts
         with Cogged or Synchronous Belt Drives. *Energy Tips – Motor Systems.*

[24]   Körfer, W., Lacy, F., 2006. Timing Belt Drives and their Advantages Regarding Engine
         Efficiency and NVH Characteristics. *MTZ 07-08|2006.* P.538.

[25]   Energy Loss and Efficiency of Power Transmission Belts. *Advanced Engineering
         Research, Belt testing Centre, Springfield, Missouri.* [Online]
         Available at: http://www.carlislebelts.com
         [Accessed 19 October 2010]

[26]   Fenner® Drive selection & Maintenance Manual, 3rd Edition Catalogue.

[27]   Transfluid, Fluid Coupling catalogue.

[28]   Gates Design Manual, Ploy Chain GT2 catalogue.

[29]   Caborgan, R., et al. 2010. Thermomechanical Analysis of Natural Rubber Behaviour
         Stressed at Room Temperature.

[30]   Figure 2-1: Squirrel cage induction motor [Online]
         Available at: http://www.daviddarling.info
         [Accessed 24 November 2009]

[31]   Figure 2-2: Schematic of 3-phase, 4 pole electric motor [Online]
         Available at: http://www.ibiblio.org/kuphaldt/electricCircuits/AC/AC_13.html
         [Accessed 07 June 2011]

[32]   Figure 2-5: V-belt [Online]
         Available at: http://www.gates.com
         [Accessed 15 January 2011]

[33]   Figure 2-6: Synchronous belt [Online]
         Available at: http://www.fennerindia.com
         [Accessed 15 January 2011]

[34]   Figure 2-8: Poly V ^{TM} belt [Online]
         Available at: http://www.stationaryengineparts.com
         [Accessed 15 January 2011]

[35]   Figure 2-9: Fluid coupling [Online]
         Available at: http://www.doppstadtus.com
         [Accessed 20 January 2011]

[36]   Figure 2-10: Fluid flow within a fluid coupling [Online]
         Available at: http://www.cadillacforums.com
         [Accessed 20 November 2009]

[37]   Figure 2-12: Quick-Flex® coupling [Online]
         Available at: http://www.bsc.com.au
         [Accessed 04 February 2011]

[38]   Figure2-13: Fenaflex® coupling [Online]
         Available at: http://www.eriks.co.uk
         [Accessed 19 January 2011]

[39]   Figure 2-14: Fenagrid® coupling [Online]
         Available at: http://www.eng-tips.com
         [Accessed 19 January 2011]

[40]   Figure 4-64: Transfluid CKRG type fluid coupling [Online]
         Available at: http://www.bmgworld.net
         [Accessed 04 February 2011]

APPENDICES

Appendix A – Design Calculations

A-1   Load arm

To design the distance from the centre axis of the gimbal shaft to the load cell, the motor torque was required. This was calculated as follows, using equation (1):

$$W = \frac{2\pi N M_t}{60}$$
(1)

Where: W = Power (W)

M$_t$ = Torque (Nm)

N = Rotation Speed (rpm)

$$M_t = \frac{(30 X 10^3)(60)}{2\pi \, (1440)}$$

$$M_t = 198.94 \; Nm$$

The intention of the load arm design was to allow the full capacity of the load cell (250kg) to be used during testing to increase the resolution of the readings taken. This means that there were to be two mounting points on the load arm, one for soft start tests, where the applied torque was as calculated above, and one for DOL, where the applied torque was estimated to be up to three times this amount.

To simplify the placement of the load cell, it was proposed that the same set of mounting holes be used for both cases, but the load cell be flipped around for the DOL test, allowing for an extension of the lever arm of 198mm. A value of 87.5mm from the centre axis was chosen for the soft start mounting point. This can be seen in Figure X-X below.

198   87.5
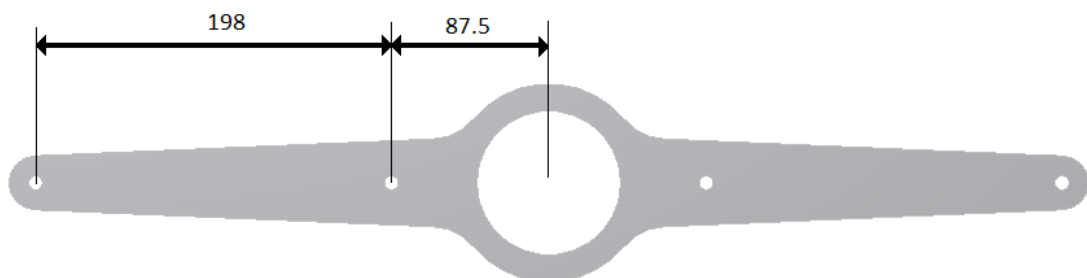
Figure A-1-1: Load arm dimensions

A simple calculation using equation (2) shows the maximum force that was applied to the load cell at this point at a torque rating of 198.94 Nm.

$$M_t = Fd \qquad\qquad\qquad (2)$$

Where F = force applied to load cell (N)

　　　d = Distance from centre of rotation to force (m)

$$F = \frac{M_t}{d}$$

$$F = \frac{198.94}{87.5 X 10^{-3}}$$

$$F = 2273.6 \ N$$

If gravitational acceleration was taken as g = 9.81 m/s^2, the weight applied to the load cell was calculated as follows, using equation (3):

$$w = \frac{F}{g} \qquad\qquad\qquad (3)$$

Where w= Weight (kg)

$$w = \frac{2273.6}{9.81}$$

$$w = 231.76 \ kg$$

This weight calculated showed that almost the entire range of the load cell was used. Similarly, calculating for the DOL scenario, with the torque applied being 596.82 Nm, and the distance from the centre axis being 285.5mm, the maximum load on the load cell was 213.1 kg. This value was again within the range of the load cell, while also allowing almost the full capacity of the load cell to be used.

A-2   Direct shaft

Given:

Material En8

$S_u = 540$ MPa

$S_y = 280$ MPa

$K_f = 1.25$ for rectangular keys

Assumptions:

Bending can be neglected as there were no external loads on this shaft.

Design for DOL loading ($M_t = 596.82$ Nm)

All keys are rectangular

Shaft is a straight shaft with no stress concentrations (other than keyways), therefore K_{ts} can be assumed to be 1

Substituting known values into equation (4), the minimum allowable diameter of the shaft can be calculated.

$$d = \left[\frac{32RF}{\pi} \left\{ \left(\frac{MK_t}{S_y} \right)^2 + \left(\frac{M_t K_{ts}}{S_u} \right)^2 \right\}^{\frac{1}{2}} \right]^{\frac{1}{3}} kf \qquad (4)$$

Where: M = bending moment (Nm)

K_t = concentration factor for bending

K_{ts} = concentration factor for torsion

Su = Ultimate tensile strength

Sy = Yield strength

$$d = \left[\frac{32(1)}{\pi} \left\{ (0)^2 + \left(\frac{596.82 \, X10^3}{280} \right)^2 \right\}^{\frac{1}{2}} \right]^{\frac{1}{3}} 1.25$$

$$d = 34.87 \; mm$$

The minimum diameter for this shaft was calculated as 34.87mm, therefore a diameter of 55mm was chosen as the bearing sizes were convenient and readily available, allowing for a safety factor of 1,6. Fatigue was not taken into account for the shaft calculations, as the run time was restricted to the duration of testing required by the dissertation.

A-3   Lay shaft

The lay shaft was designed as shown in Figure X-X below. A more detailed section can be seen in Figure X-X below. The support bearings sat on the 70mm diameter section, up against the abutment. For calculation purposes, this resulted in the centre of the bearing being 154.5mm from either end, which can be seen in the free body diagram in Figure X-X below. The pulleys were mounted at either end of the shaft.
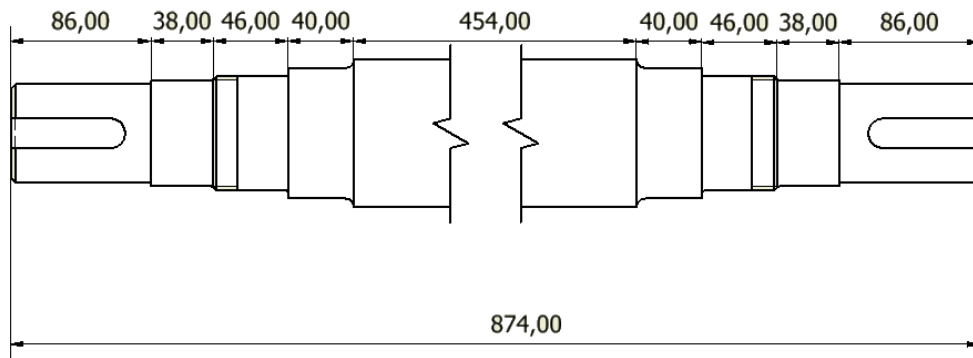
Figure A-3-1: Lay shaft dimensions
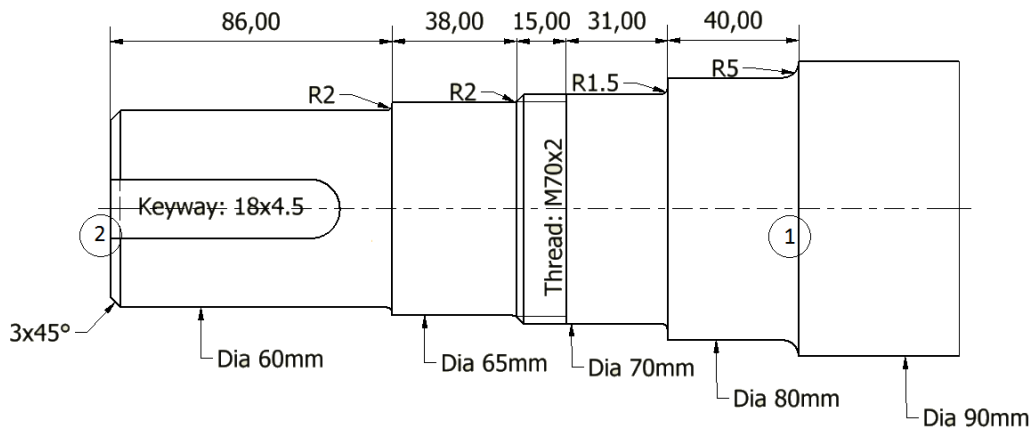
Figure A-3-2: Detailed view of lay shaft

The lay shaft had both bending and torsional loads applied to it. Due to the variety of belts tested, a worst case scenario was selected to set the design parameters. The belts which had the highest tension during testing were the synchronous belts, which had a static tension of 1205N. This was calculated from the catalogue. Using the following formula:

$$T_{st} = 425\frac{P}{V} + mV^2 \tag{5}$$

Where T_{st} = Static tension of belt (N)

P = Power transmitted (kW)

m = mass (kg/m)

V = Velocity

The velocity was calculated using equation (6). The diameter of the small pulley can be obtained from the catalogue using the number of teeth (56) and the pitch (8mm). This results in a diameter of 142.6mm.

$$V = \frac{\pi d N}{60} \tag{6}$$

$$V = \frac{\pi(142.6 X 10^{-3})(1440)}{60}$$

$$V = 10.75\ m/s$$

Substituting V = 10.75m/s and m=0.167 kg/m into equation (5), the static tension was calculated to be as follows:

$$T_{st} = 425\frac{30}{10.75} + (0.167)(10.75)^2$$

$$T_{st} = 1205\ N$$

The free body diagram and bending moment diagram of the lay shaft is shown in Figure X-X below. The bending moment diagram was easily determined by first resolving the reaction forces at A and thus B. Due to the simplicity of the shaft and loading, it can easily be seen that the reaction forces at the bearings are going to be equal to the forces applied to the shaft. Thus reaction R_A and R_B are both 1205N. The bending moment
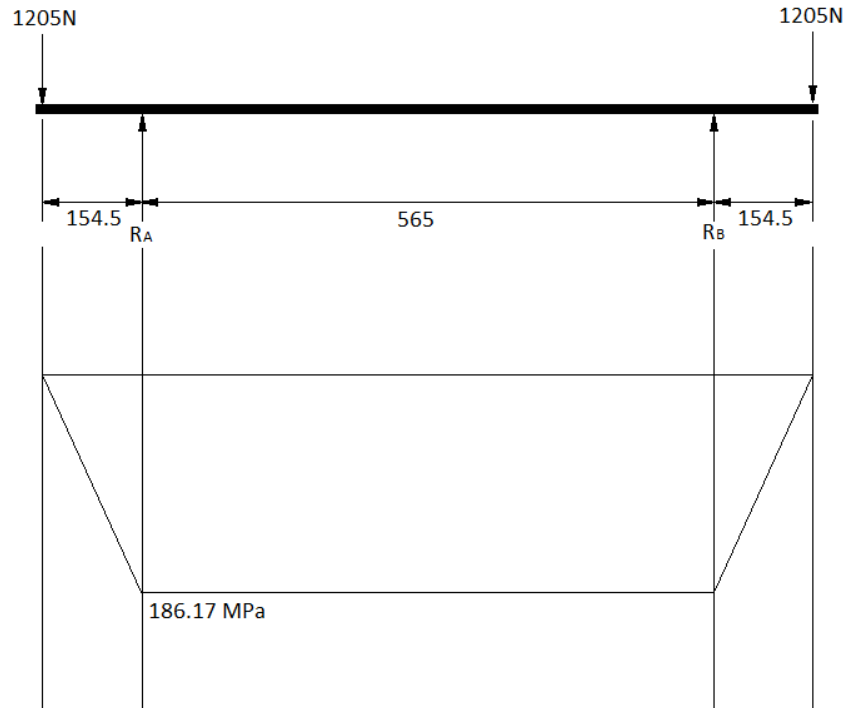
The lay shaft had a much higher torque applied to it as the pulleys were all 2.5:1 step down ratios. This ratio reduced the speed of the lay shaft to 576 rpm, and increased the torque to 497.35Nm. The minimum diameter of the shaft at critical section 1 was then calculated.

Given:

Material En8

$S_u = 540$ MPa

$S_y = 280$ MPa

$K_f = 1.25$ for rectangular keys

Assumptions:

All keys are rectangular

Shaft has many abutments, therefore K_t and K_{ts} can be taken as 1.5 and 1.3 respectively at all critical sections.

Using equation (4) and referring to figure X-X above for section numbering, the minimum shaft diameters can be calculated as follows:

At section 1(highest stressed area):

$M = 186.17$ Nm

$M_t = 497.35$ Nm

$$\text{kf} = 1$$

$$d_1 = \left[\frac{32}{\pi}\left\{\left(\frac{(186.17 X 10^3)(1.5)}{280}\right)^2 + \left(\frac{(497.35 X 10^3)(1.3)}{540}\right)^2\right\}^{\frac{1}{2}}\right]^{\frac{1}{3}} \quad (1)$$

$$d_1 = 25.13 mm$$

The minimum diameters for the other sections of the shaft did not need to be calculated as the result will only be smaller than this calculated value. All machined diameters are greater than this diameter, and thus the shaft will not fail under loading. The stresses at the end of the shaft were different to the rest of the shaft as there is a keyway which increases the stress concentration at this. There is no bending at this point, but the stress concentration factor caused by the key may result in an increased stress on the shaft.

At section 2 (key way):

$$M = 0$$
$$M_t = 497.35 \text{ Nm}$$
$$\text{kf} = 1.25$$

$$d_2 = \left[\frac{32}{\pi}\left\{(0)^2 + \left(\frac{(497.35 X 10^3)(1.3)}{540}\right)^2\right\}^{\frac{1}{2}}\right]^{\frac{1}{3}} (1.25)$$

$$d_2 = 28.77 \text{ mm}$$

The designed diameter of the shaft is greater than the minimum calculated diameter, and thus will not fail under loading.

Appendix B – Graphs
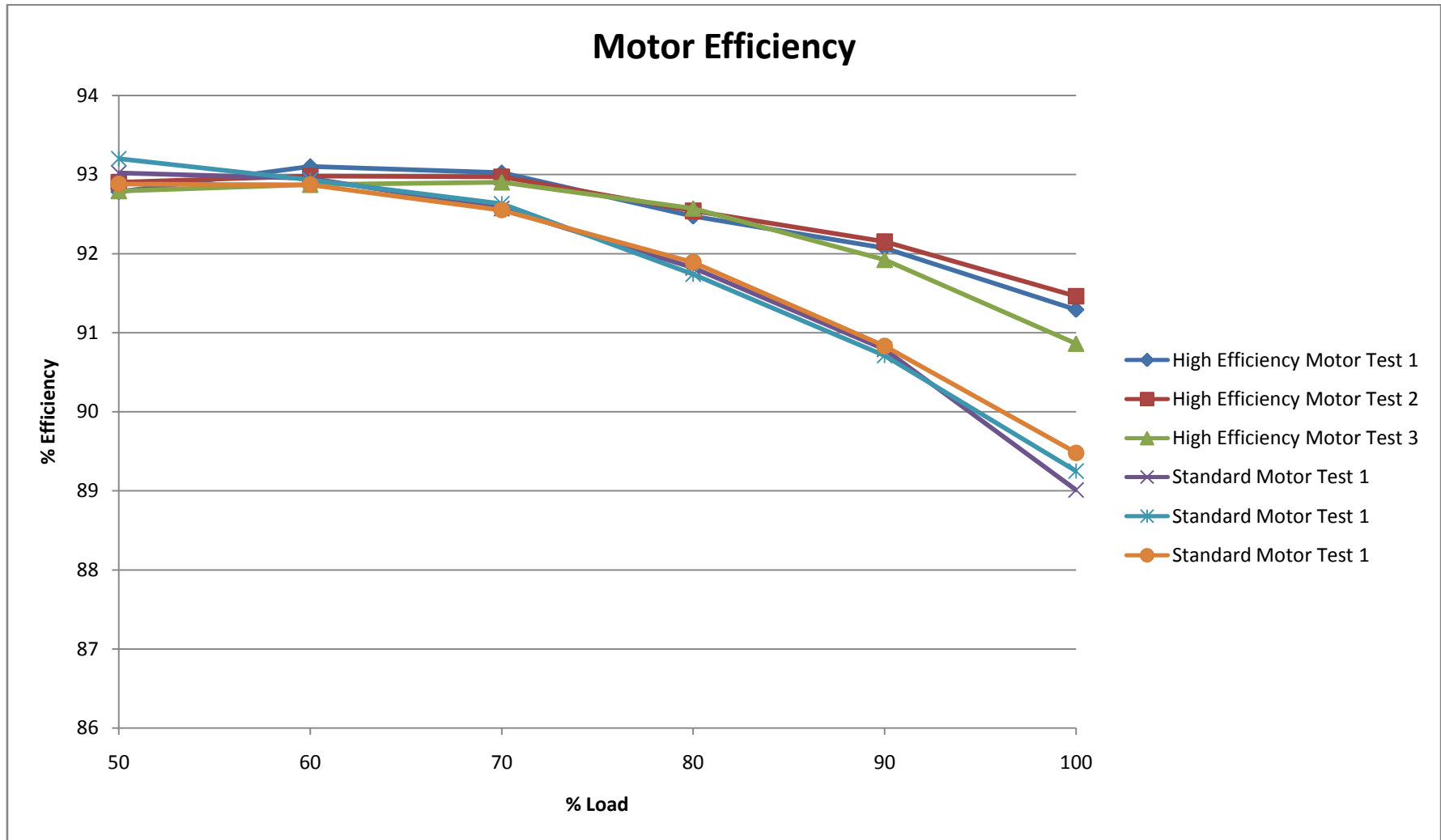
Figure B-1: Graph of efficiency of high efficiency motor and standard motor

B-2   Quick-Flex® coupling radial misalignment
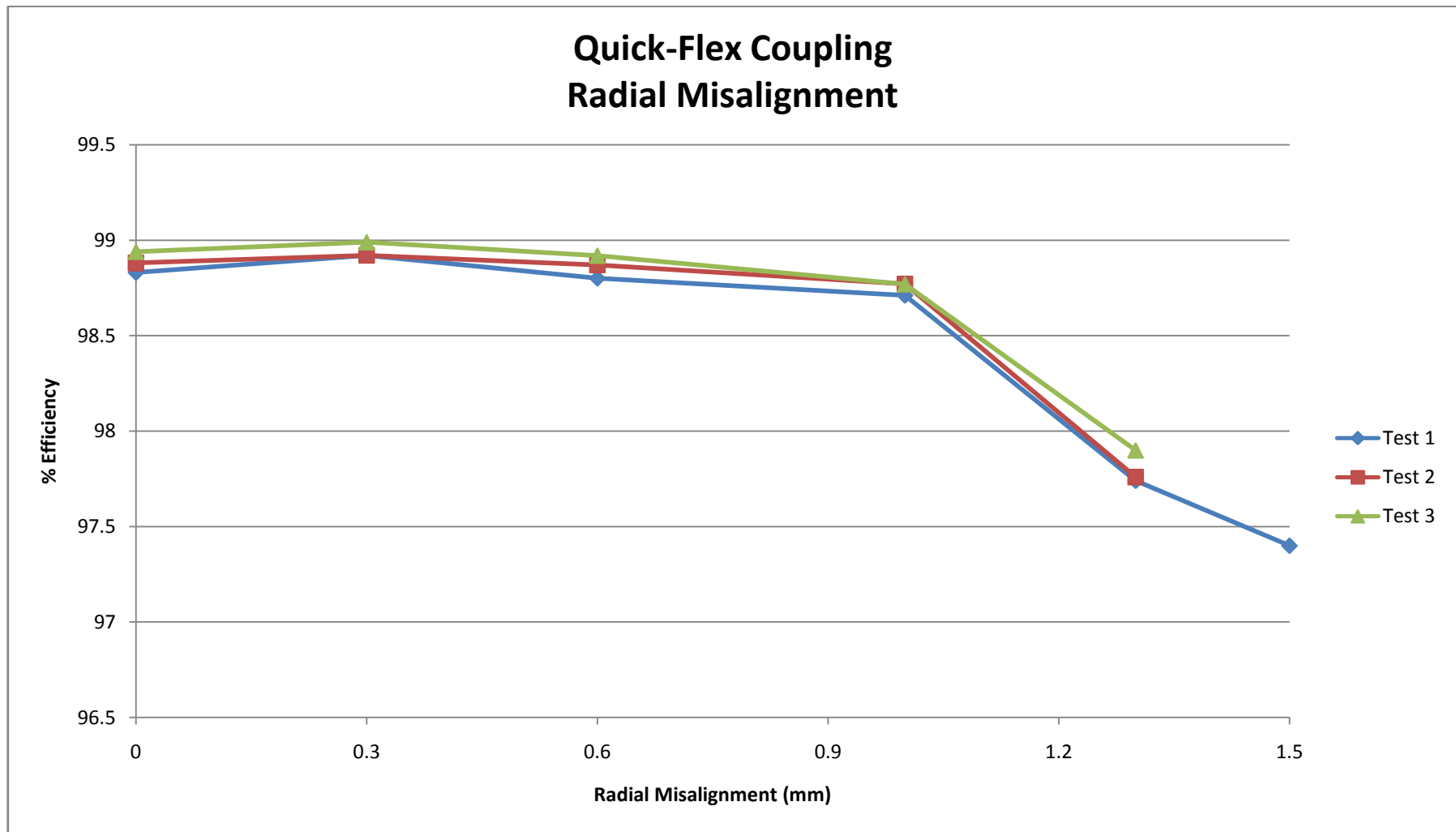
Figure B-2: Graph of radial misalignment vs. efficiency of the Quick-Flex® coupling

B-3   Fenaflex® coupling radial misalignment
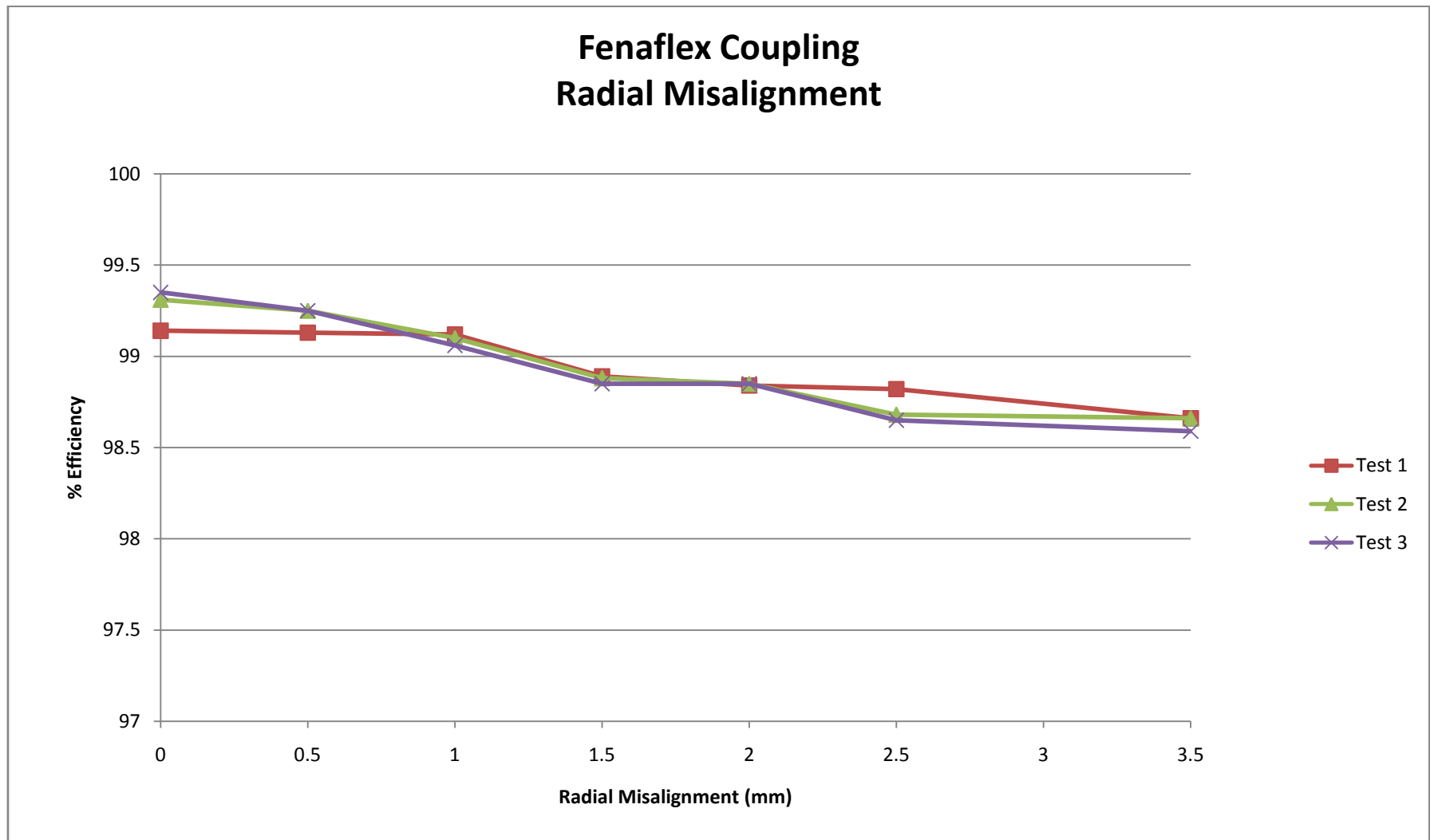
Figure B-3: Graph of radial misalignment vs. efficiency of the Fenaflex® coupling

B-4   **Grid coupling radial misalignment**
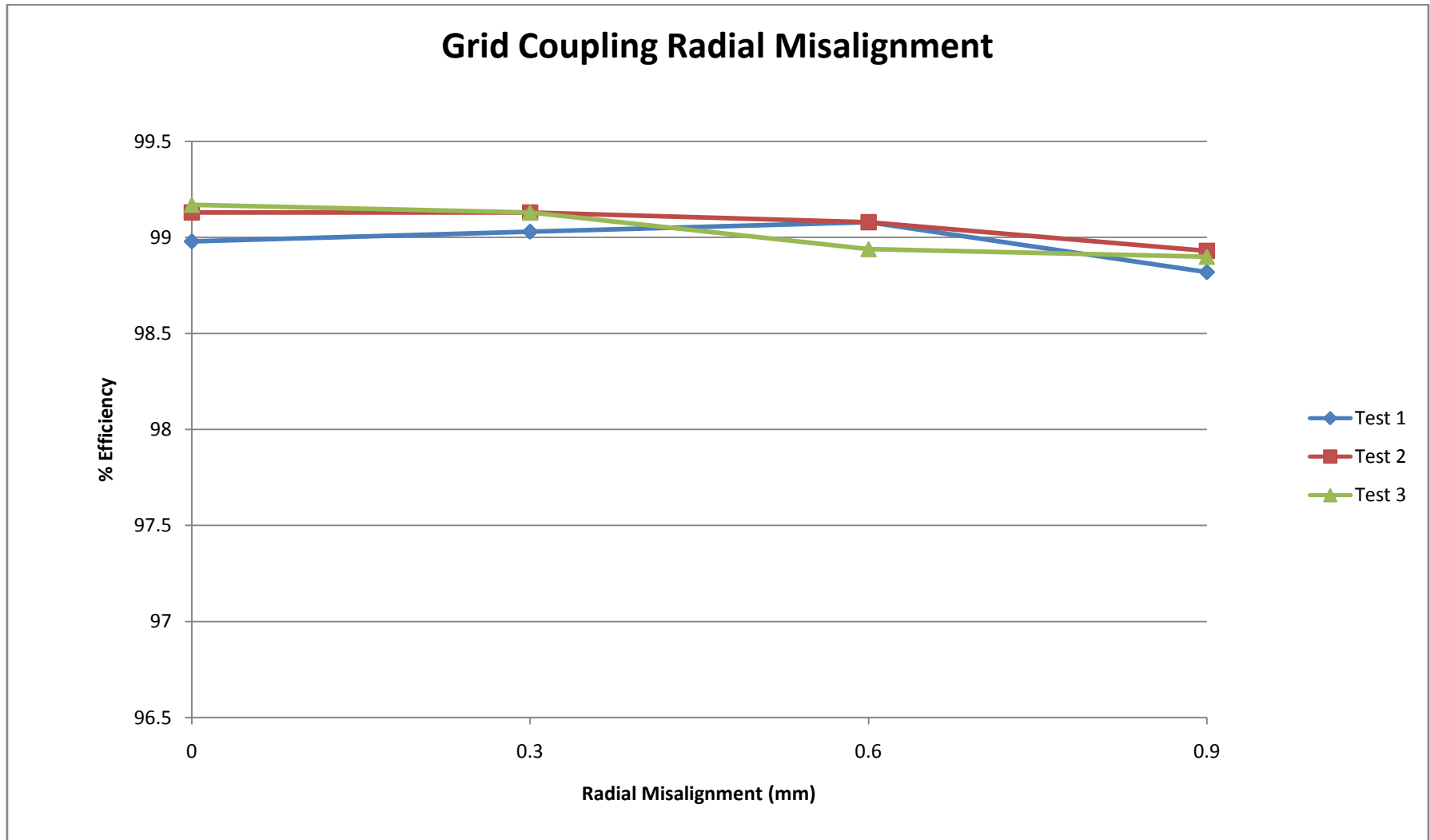
Figure B-4: Graph of radial misalignment vs. efficiency of the Grid coupling
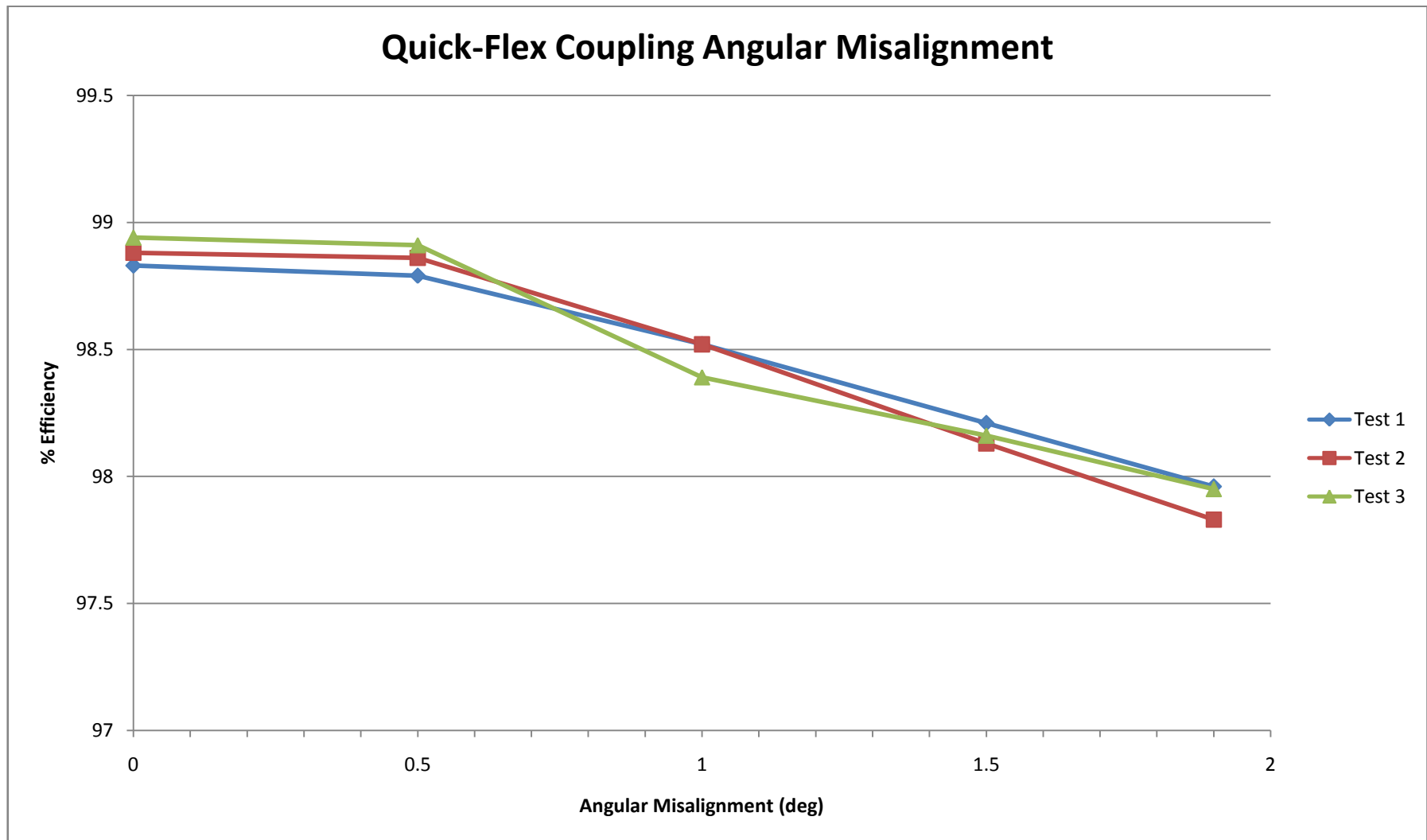
Figure B-5: Graph of angular misalignment vs. efficiency of the Quick-Flex® coupling

B-6   **Fenaflex® coupling angular misalignment**
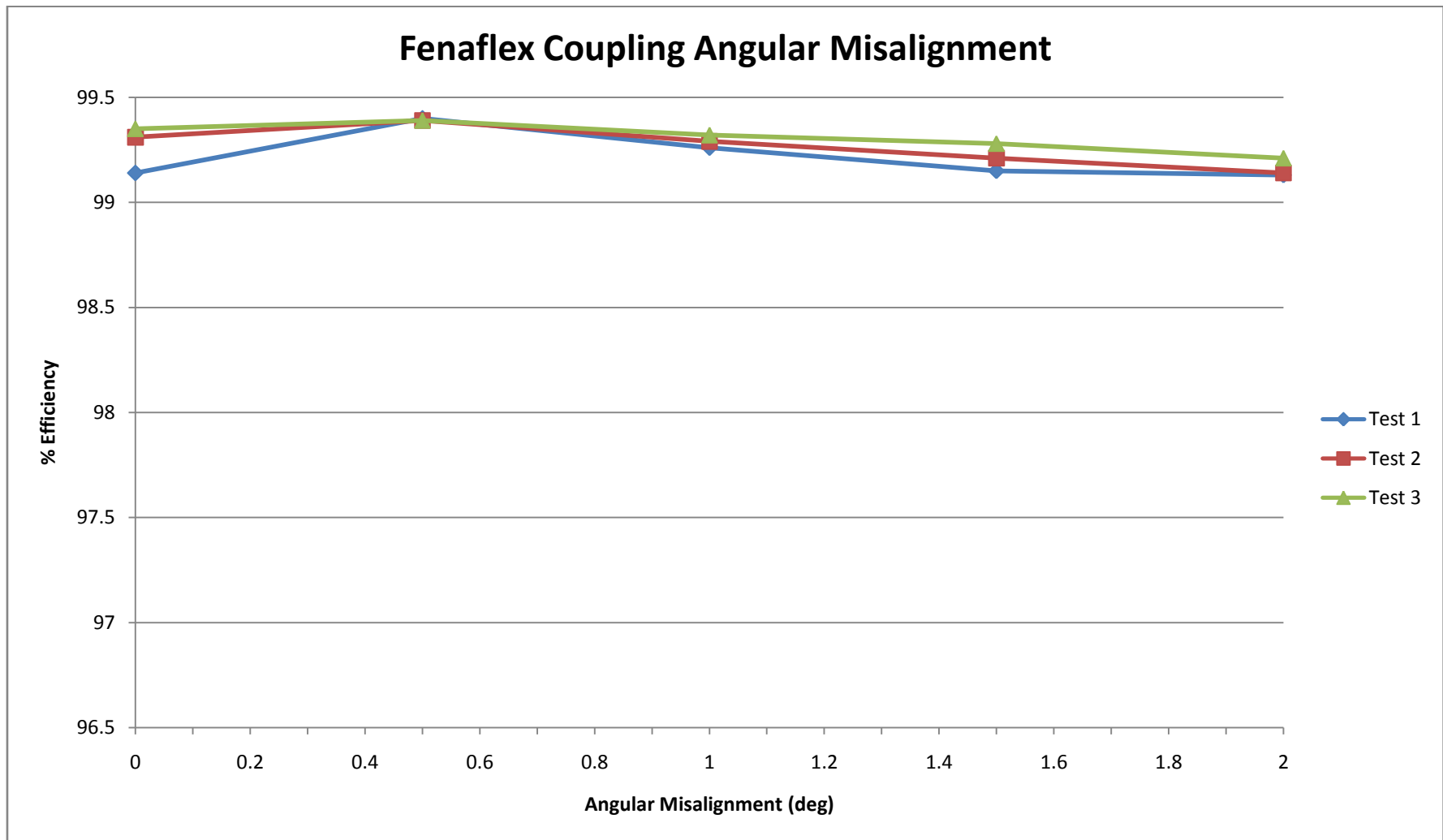
Figure B-6: Graph of angular misalignment vs. efficiency of the Fenaflex® coupling
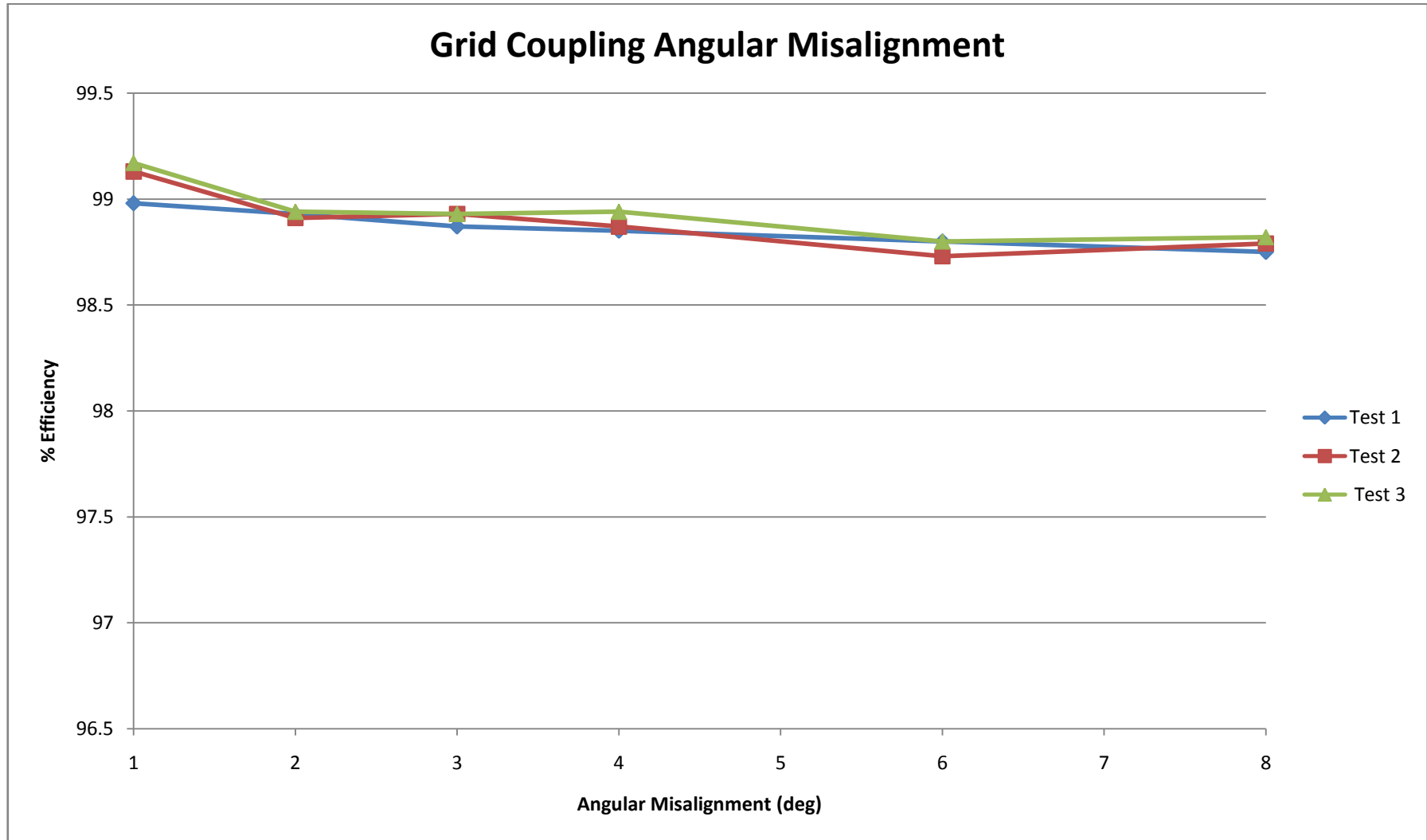
Figure B-7: Graph of angular misalignment vs. efficiency of the Grid coupling
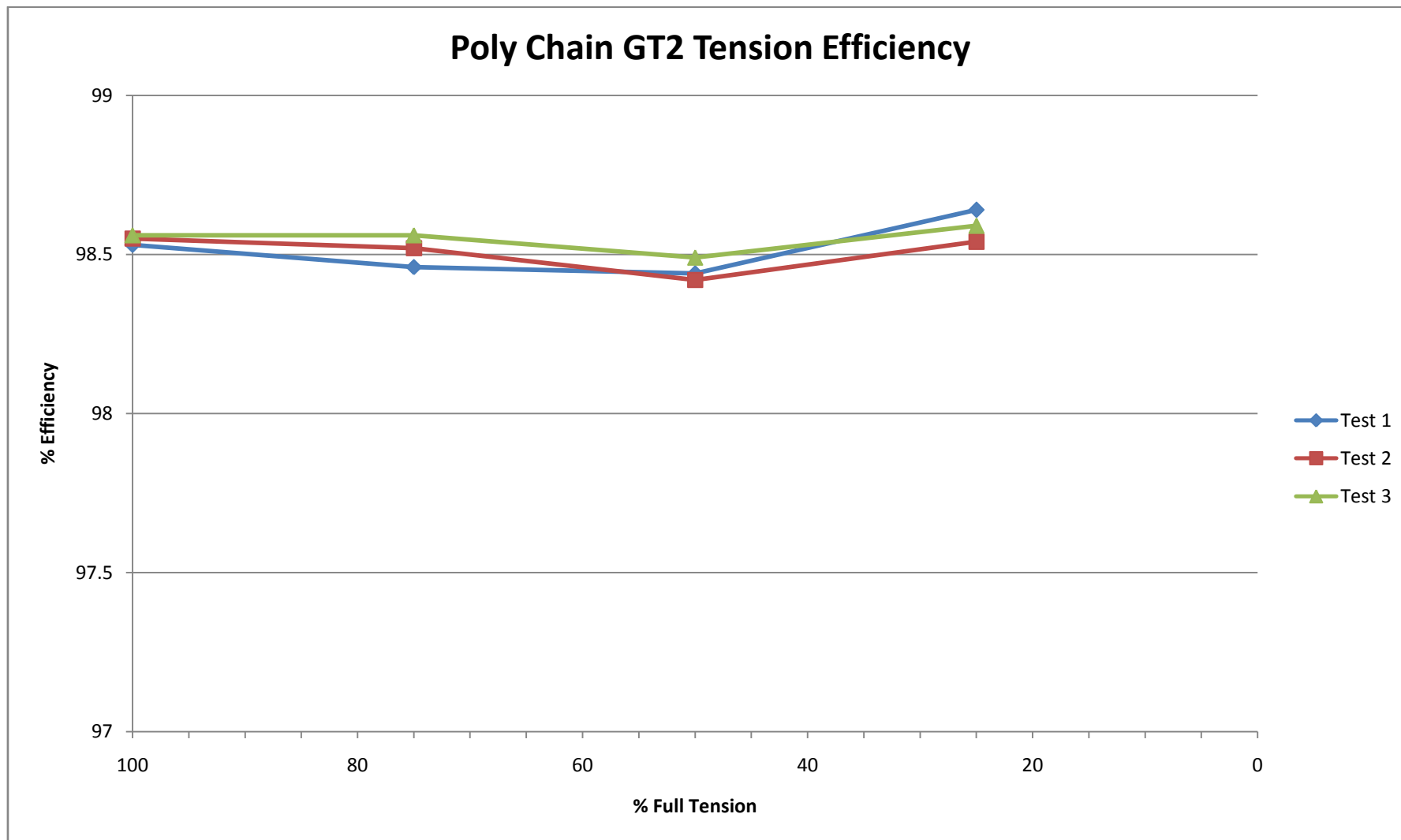
Figure B-8: Graph of Poly Chain[®] **GT2 belt efficiency vs. belt tension**

Figure B-9: Graph of SPB V-Belt efficiency vs. belt tension

B-10   Poly V ™ belt tension efficiency
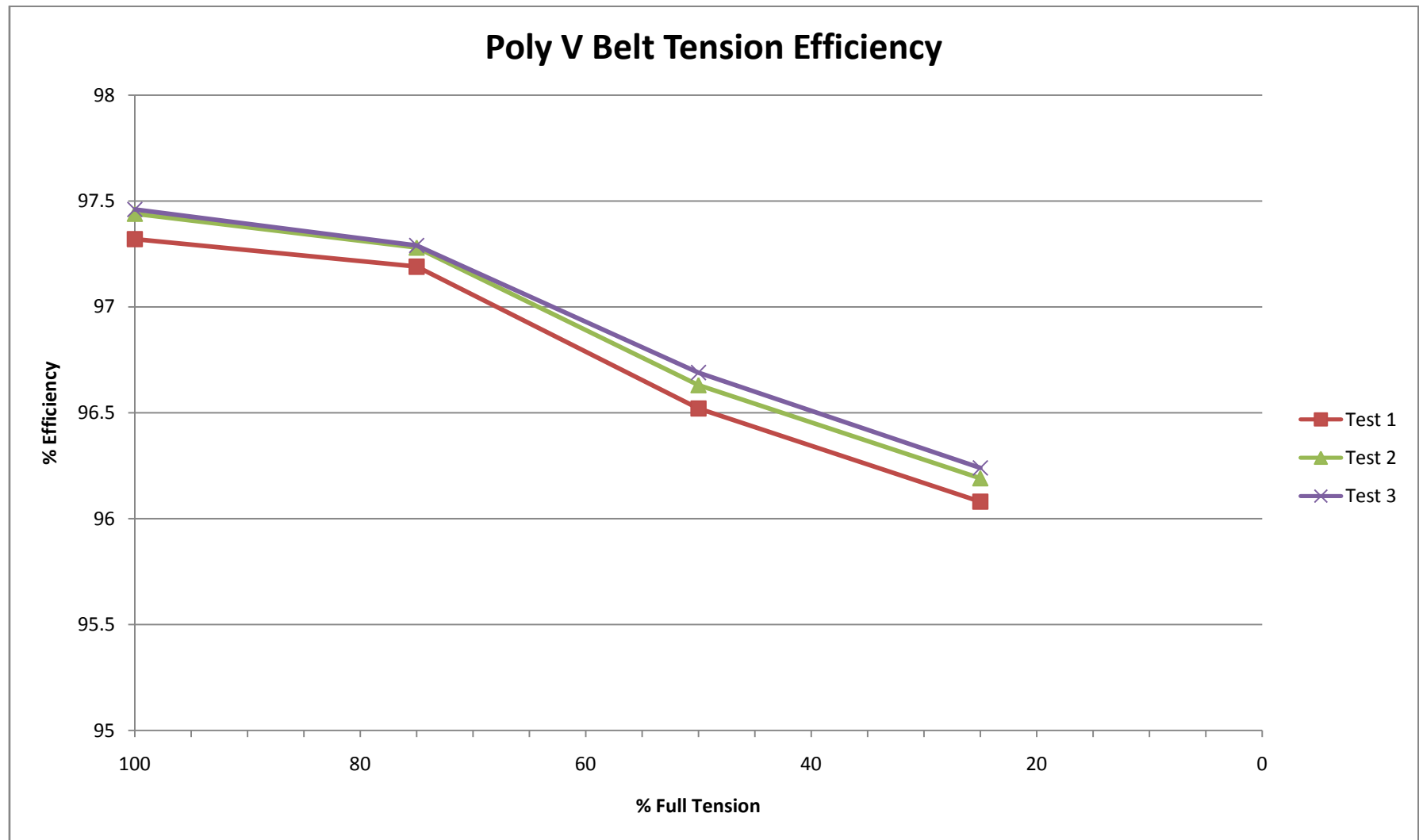
Figure B-10: Graph of Poly V ™ belt efficiency vs. belt tension

B-11   Direct on line start-up with fluid coupling
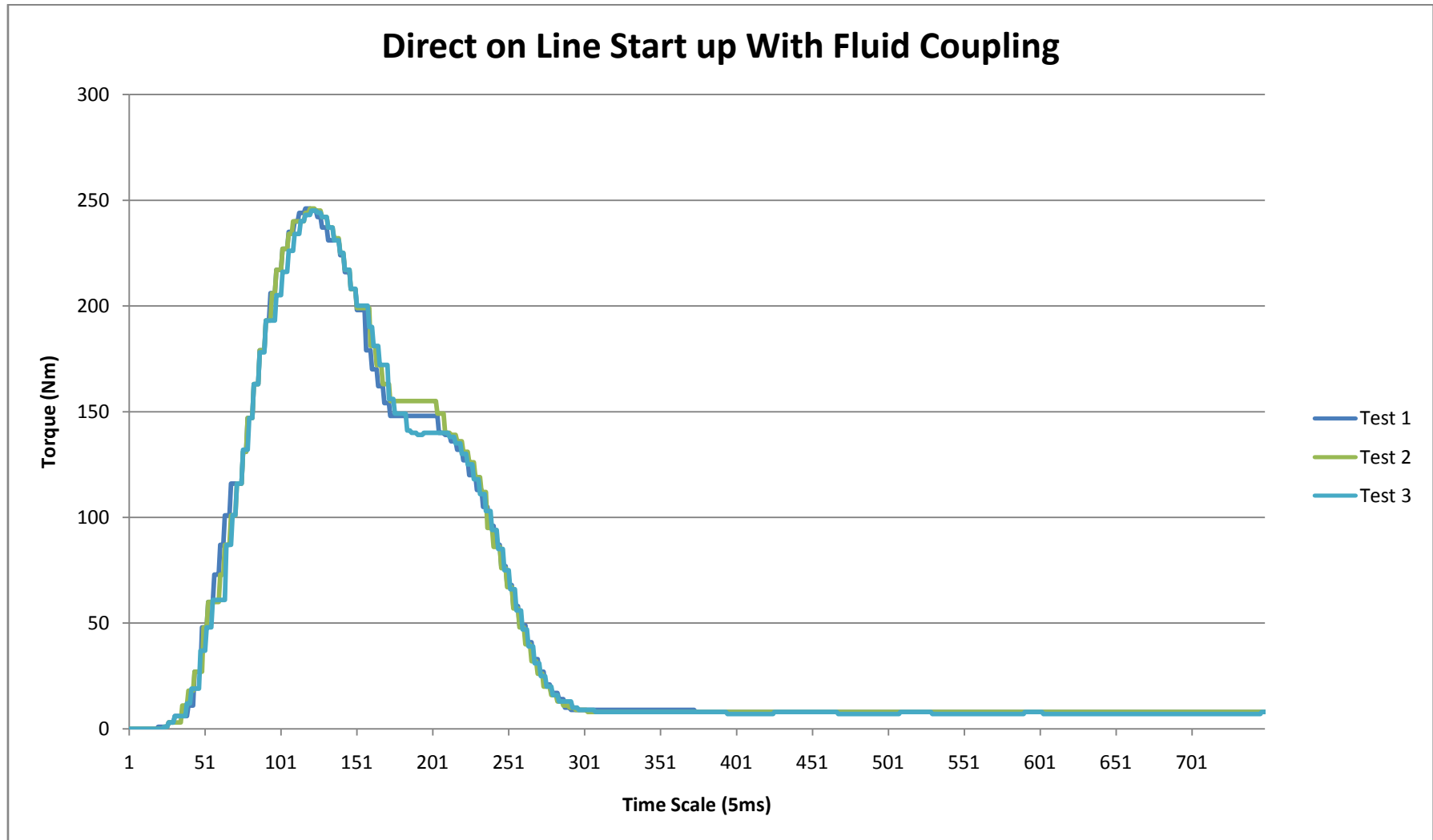
Figure B-11: Graph of DOL start with fluid coupling

B-12   Direct on line start with Quick-Flex® coupling
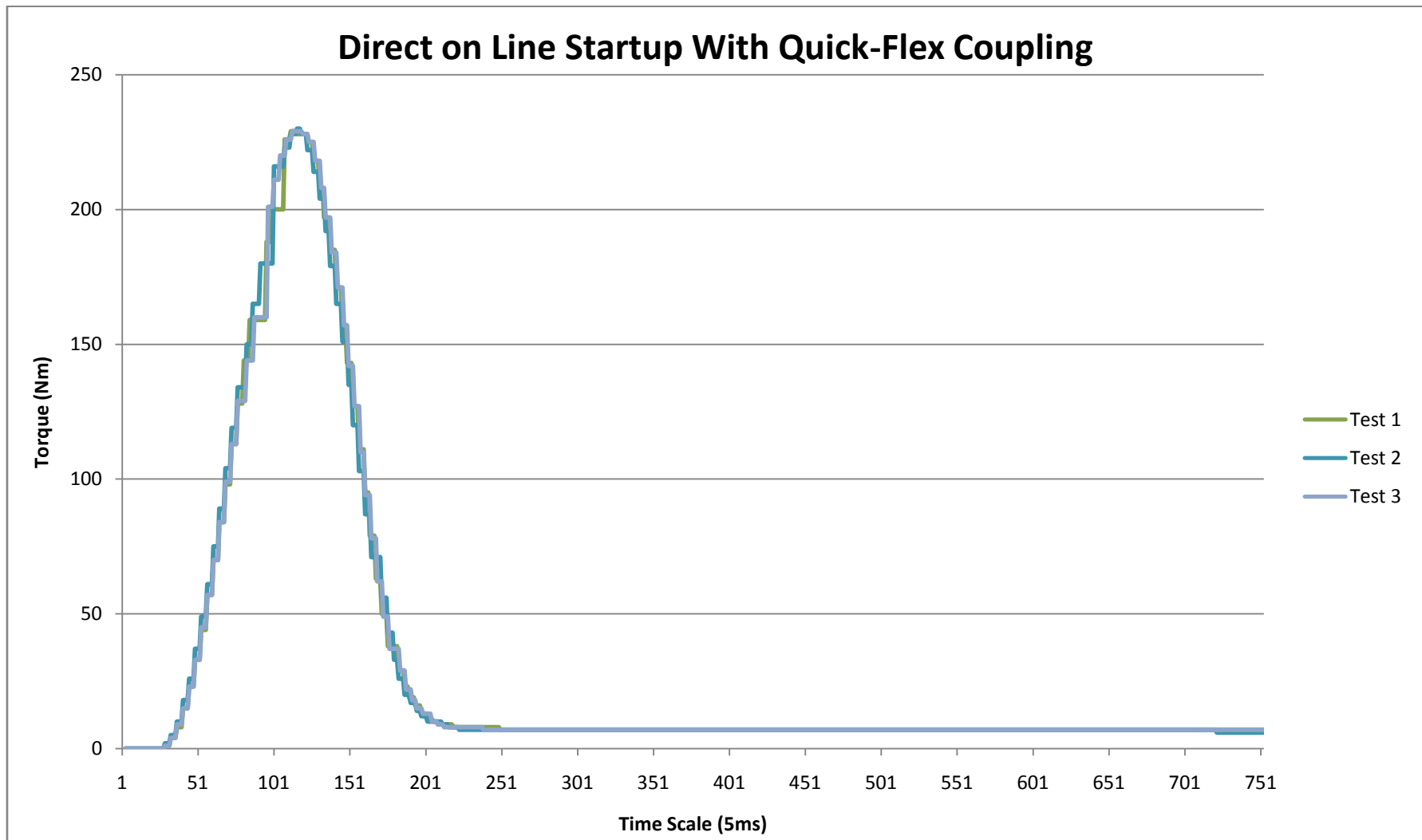
Figure B-12: Graph of DOL start with Quick-Flex® coupling

105

Appendix C − Alignment Certificates

C-1   Motor alignment
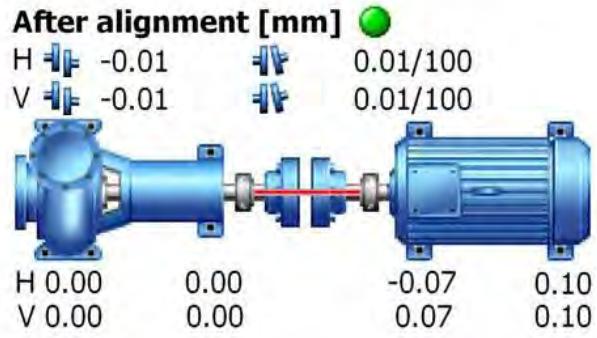
Figure C-1-1: Motor alignment certificate

C-2   Direct shaft alignment
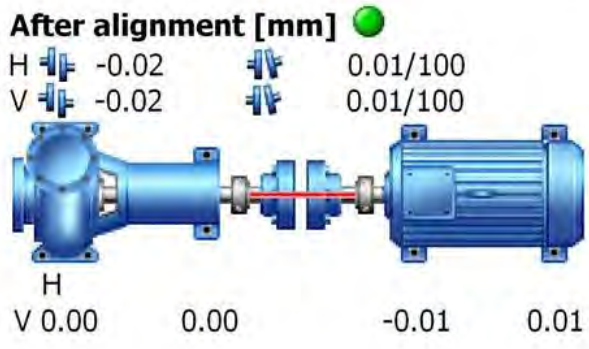
Figure C-2-1: Direct shaft alignment certificate

C-3 Quick-Flex® coupling, radial misalignment
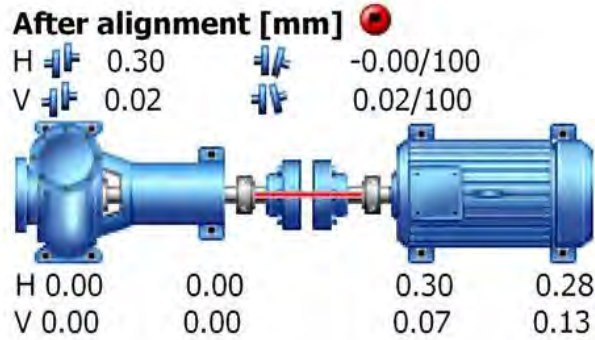
Figure C-3-1: Quick-Flex® coupling, 0.3mm radial misalignment certificate

Figure C-3-2: Quick-Flex® coupling, 0.6mm radial misalignment certificate

SPM • • •
● ● ● ● ● ● ●

Horizontal shaft alignment - 2010-08-08 16:32:25

1 mm mis

After alignment [mm] 🔴

H	0.97		-0.02/100
V	0.02		0.02/100
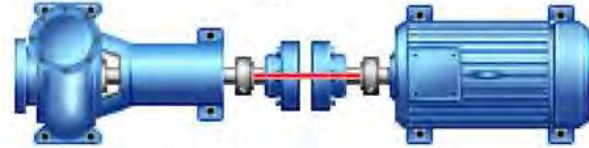
H	0.00	0.00	0.93	0.81
V	0.00	0.00	0.06	0.18

Figure C-3-3: Quick-Flex® coupling, 1mm radial misalignment certificate

SPM • • •
● ● ● ● ● ● ●

Horizontal shaft alignment - 2010-08-09 11:14:15

1.3

After alignment [mm] 🔴

H	1.31		-0.01/100
V	0.02		0.02/100
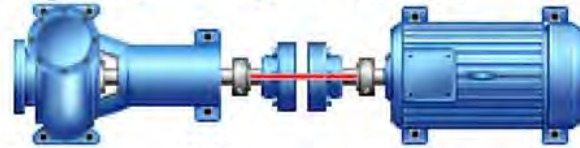
H	0.00	0.00	1.30	1.28
V	0.00	0.00	0.06	0.18

Figure C-3-4: Quick-Flex® coupling, 1.3mm radial misalignment certificate
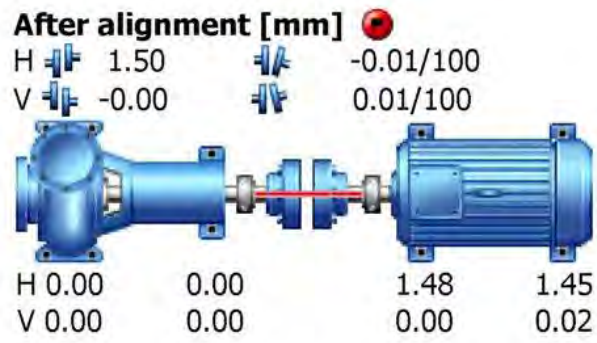
Figure C-3-5: Quick-Flex® coupling, 1.5mm radial misalignment certificate

C-4   Fenaflex® coupling, radial misalignment
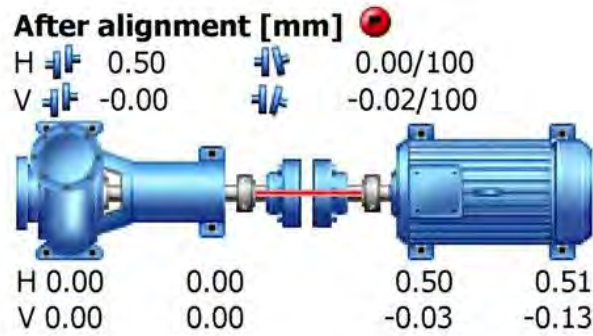
Figure C-4-1: Fenaflex® coupling, 0.5mm radial misalignment certificate
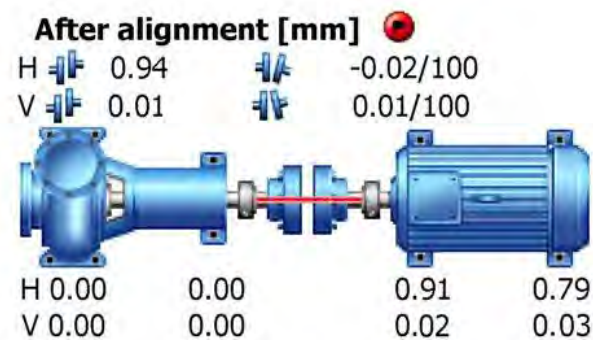
Figure C-4-2: Fenaflex® coupling, 1mm radial misalignment certificate
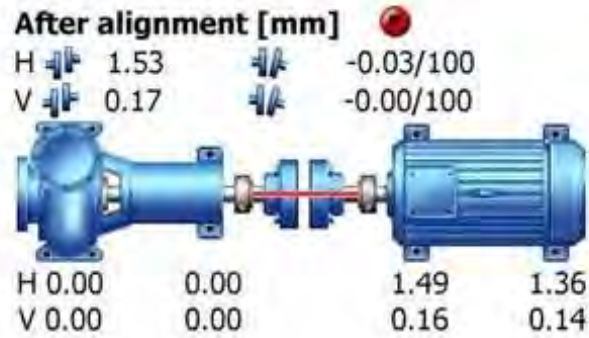
Figure C-4-3: Fenaflex® coupling, 1.5mm radial misalignment certificate
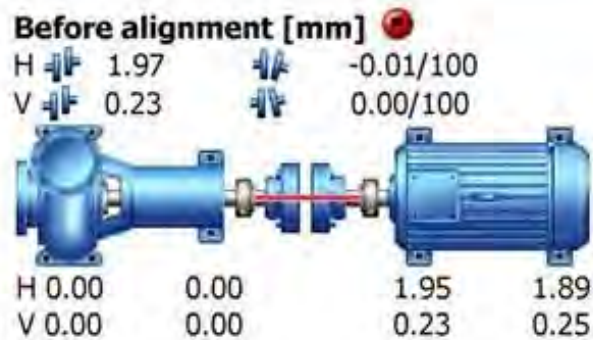
Figure C-4-4: Fenaflex® coupling, 2mm radial misalignment certificate
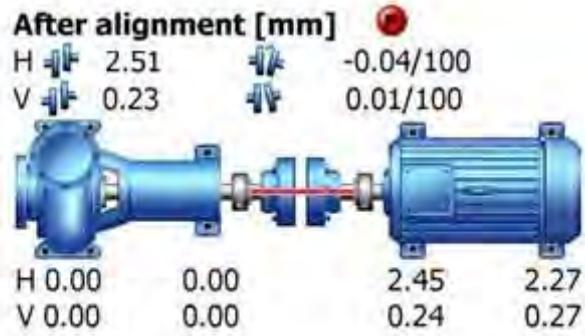
Figure C-4-5: Fenaflex® coupling, 2.5mm radial misalignment certificate
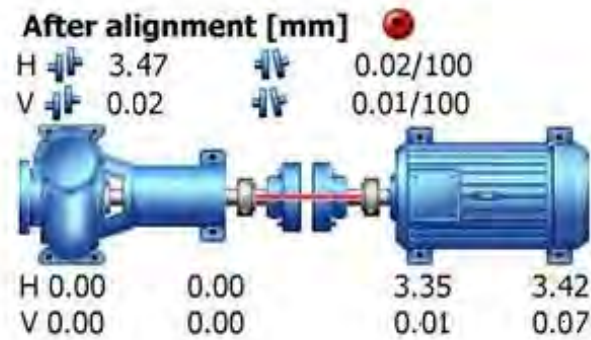
Figure C-4-6: Fenaflex® coupling, 3.5mm radial misalignment certificate

C-5   Grid coupling, radial misalignment
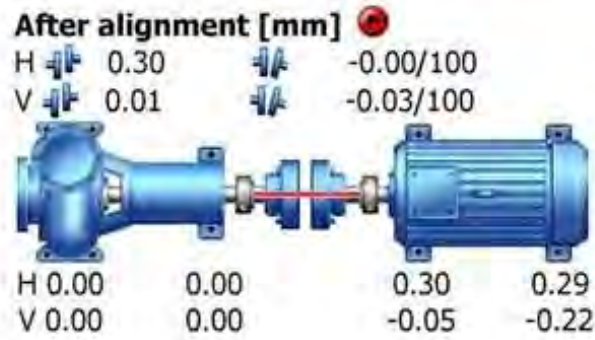
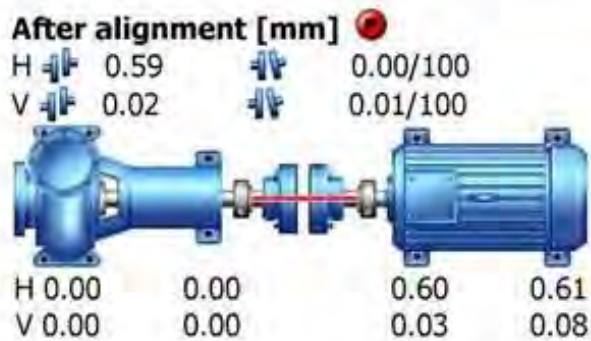**Figure C-5-1: Grid coupling, 0.3mm radial misalignment certificate**

Figure C-5-2: Grid coupling, 0.6mm radial misalignment certificate

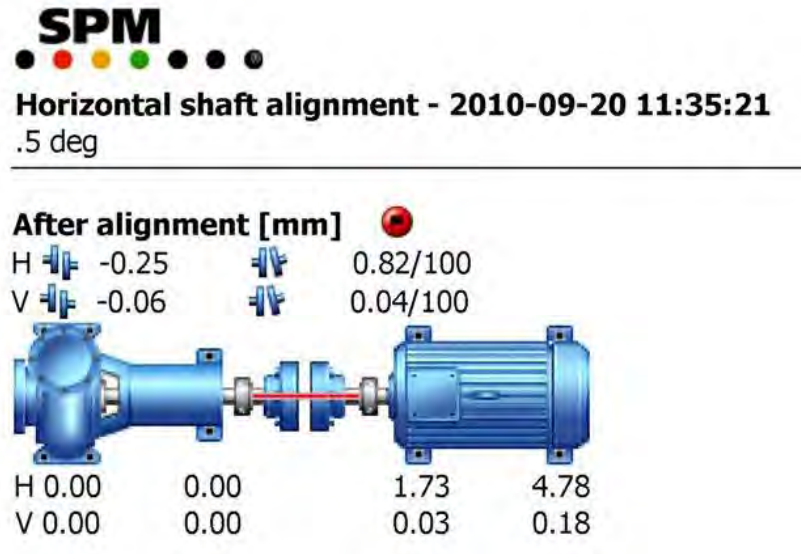## C-6 Quick-Flex® coupling, angular misalignment

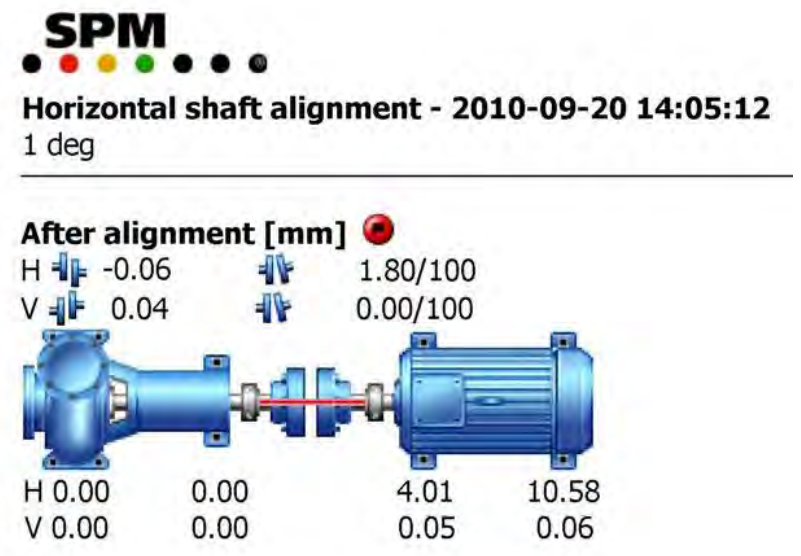**Figure C-6-1: Quick-Flex® coupling, 0.5° angular misalignment certificate**

Figure C-6-2: Quick-Flex® coupling, 15° angular misalignment certificate
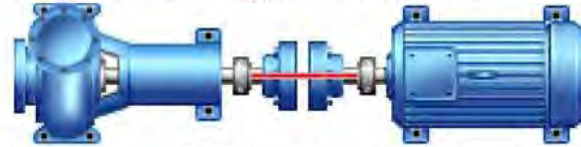
Figure C-6-3: Quick-Flex® coupling, 1.5° angular misalignment certificate
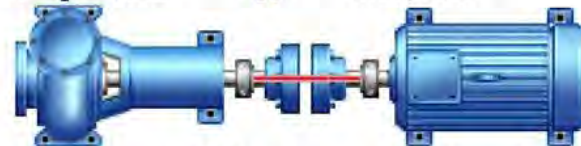
Figure C-6-4: Quick-Flex® coupling, 1.9° angular misalignment certificate

C-7   Fenaflex® coupling, angular misalignment

Figure C-7-1: Fenaflex® coupling, 0.5° angular misalignment certificate

Figure C-7-2: Fenaflex® coupling, 1° angular misalignment certificate

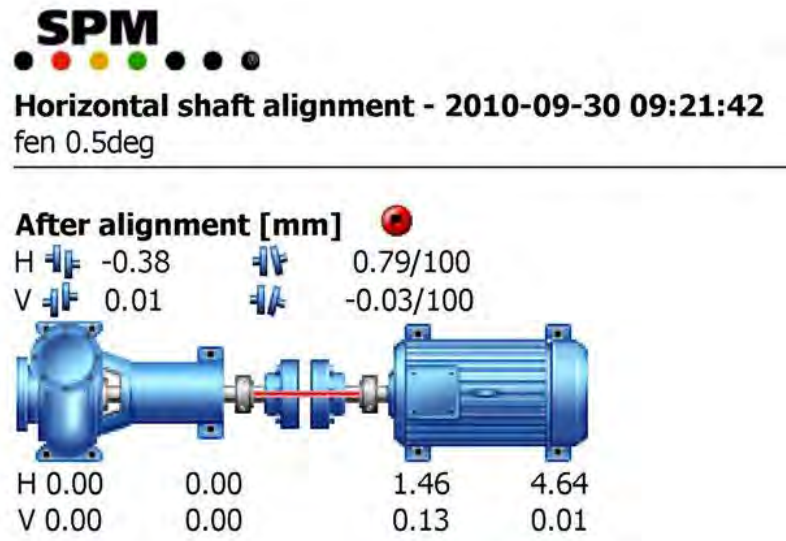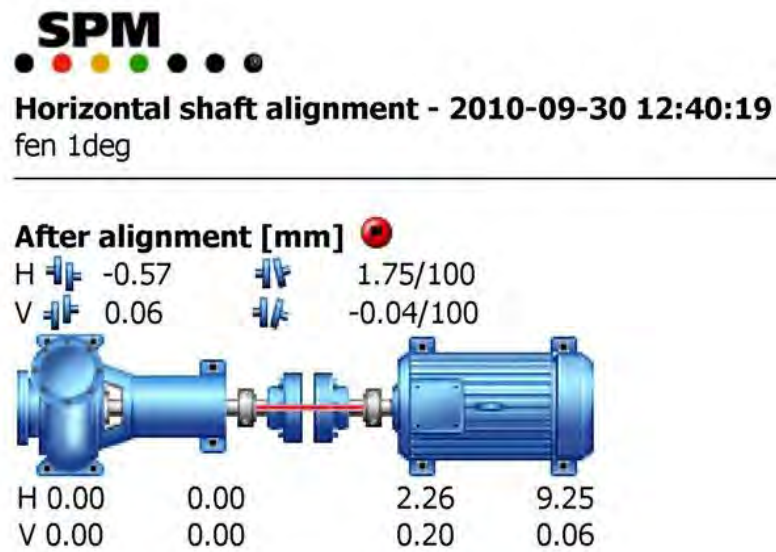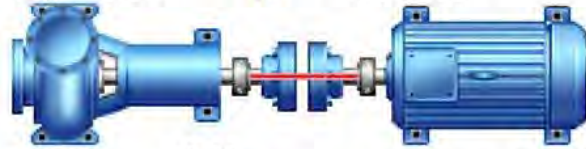**Figure C-7-3: Fenaflex® coupling, 1.5° angular misalignment certificate**
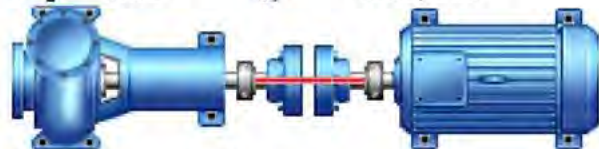
Figure C-7-4: Fenaflex® coupling, 2° angular misalignment certificate

Appendix D - Motor Results

Table D-1: Standard motor power readings, test 1

Standard Motor Test 1						
Load Out (%)	50	60	70	80	90	100
Load Out (W)	15	18	21	24	27	30
Voltage (V)	360	364	363	362	353	349
Frequency (Hz)	50	50	50	50	50	50
Current (A)	31	36	41	47	55	64
Speed (rpm)	1485	1482	1477	1472	1464	1453
Input Power (W)	16000	19400	22700	26100	29500	34000
Reactive Input Power (W)	10300	11300	12200	13600	16100	18100
Apparent Input Power (W)	19000	22500	25800	29500	33700	38600
Shaft Output Torque (Nm)	96.5	116	135.8	155.7	175.9	197.1
Shaft Output Power (W)	15005	18004	20996	23993	26968	29994
Temp Probe 1 (°C)	48.1	53.6	62.1	68.7	75	86.5

Table D-2: Standard motor power readings, test 2

Standard Motor Test 2						
Load Out (%)	50	60	70	80	90	100
Load Out (W)	15	18	21	24	27	30
Voltage (V)	365	363	363	363	356	353
Frequency (Hz)	50	50	50	50	50	50
Current (A)	30	35	41	47	54	63
Speed (rpm)	1484	1482	1477	1472	1464	1453
Input Power (W)	16100	19200	22700	26300	29700	33500
Reactive Input Power (W)	10300	11300	12300	13800	15500	18600
Apparent Input Power (W)	19100	22200	25900	29700	33500	38300
Shaft Output Torque (Nm)	96.5	116.1	135.8	155.7	176.2	197.6
Shaft Output Power (W)	15003	18021	21000	24010	27010	29995
Temp Probe 1 (°C)	50	54.6	60.2	68.1	76.5	87.4

Table D-3: Standard motor power readings, test 3

Standard Motor Test 3						
Load Out (%)	50	60	70	80	90	100
Load Out (W)	15	18	21	24	27	30
Voltage (V)	366	365	362	356	355	355
Frequency (Hz)	50	50	50	50	50	50
Current (A)	30	36	41	48	55	62
Speed (rpm)	1487	1482	1477	1473	1465	1455
Input Power (W)	16200	19400	22800	26000	29700	33600
Reactive Input Power (W)	10200	11500	12300	14100	15900	18000
Apparent Input Power (W)	19200	22500	25900	29600	33700	38100
Shaft Output Torque (Nm)	96.4	116.1	135.8	155.7	175.9	196.9
Shaft Output Power (W)	15006	18017	21017	24020	26993	30000
Temp Probe 1 (°C)	38.8	48.8	58.6	48.6	65.7	89.48

Table D-4: High efficiency motor power readings, test 1

High efficiency Motor Test 1						
Load Out (%)	50	60	70	80	90	100
Load Out (W)	15	18	21	24	27	30
Voltage (V)	367	366	364	363	358	357
Frequency (Hz)	50	50	50	50	50	50
Current (A)	31	36	41	47	53	59
Speed (rpm)	1487	1484	1480	1478	1473	1467
Input Power (W)	16200	19300	22500	25900	25900	32600
Reactive Input Power (W)	11100	11900	13100	13700	14600	16900
Apparent Input Power (W)	19700	22700	26000	29300	32900	36700
Shaft Output Torque (Nm)	96.2	115.8	135.4	155.1	175.2	195.6
Shaft Output Power (W)	15003	17995	20988	24000	26996	29951
Temp Probe 1 (°C)	74.7	74.4	75	77.6	77.9	85.9

Table D-5: High efficiency motor power readings, test 2

High efficiency Motor Test 2						
Load Out (%)	50	60	70	80	90	100
Load Out (W)	15	18	21	24	27	30
Voltage (V)	370	368	366	365	364	358
Frequency (Hz)	50	50	50	50	50	50
Current (A)	31	36	41	46	52	59
Speed (rpm)	1486	1483	1482	1478	1471	1466
Input Power (W)	16200	19200	22700	25700	29300	32800
Reactive Input Power (W)	11500	12200	12500	14000	15200	15800
Apparent Input Power (W)	19800	22800	26000	29300	32800	36400
Shaft Output Torque (Nm)	96.1	115.7	135.6	15.1	175	195.1
Shaft Output Power (W)	14956	17980	21044	24018	26935	29979
Temp Probe 1 (°C)	82.6	79.6	79.2	80	83.9	88.6

Table D-6: High efficiency motor power readings, test 3

High efficiency Motor Test 3						
Load Out (%)	50	60	70	80	90	100
Load Out (W)	15	18	21	24	27	30
Voltage (V)	361	358	358	354	353	345
Frequency (Hz)	50	50	50	50	50	50
Current (A)	31	36	42	48	54	61
Speed (rpm)	1487	1484	1481	1475	1472	1464
Input Power (W)	16200	19200	22700	25600	29300	32900
Reactive Input Power (W)	11100	11700	12600	14000	14800	16400
Apparent Input Power (W)	19600	22500	26000	29200	32800	36800
Shaft Output Torque (Nm)	96.4	116	135.4	155.1	175.4	195.9
Shaft Output Power (W)	15008	18036	21001	23951	27033	30041
Temp Probe 1 (°C)	72.7	73.5	75.3	78.1	83.3	91.9

Appendix E – Manufacturing Drawings
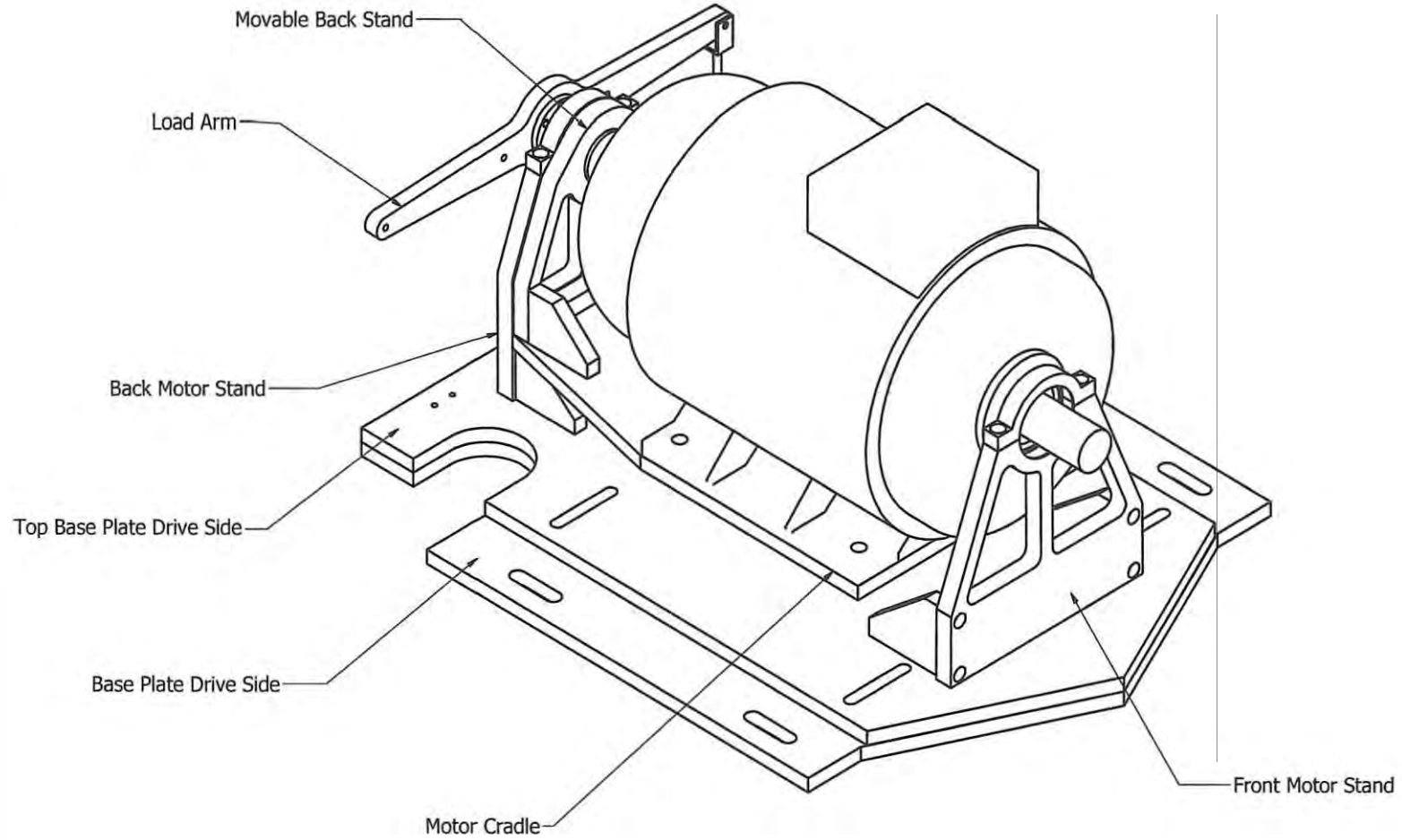
Movable Back Stand

Load Arm

Back Motor Stand

Top Base Plate Drive Side

Base Plate Drive Side

Motor Cradle

Front Motor Stand

124

Load Arm

Movable Back Stand

Back Motor Stand

Front Motor Stand

Top Base Plate Load Side

Motor Cradle

Base Plate Load Side

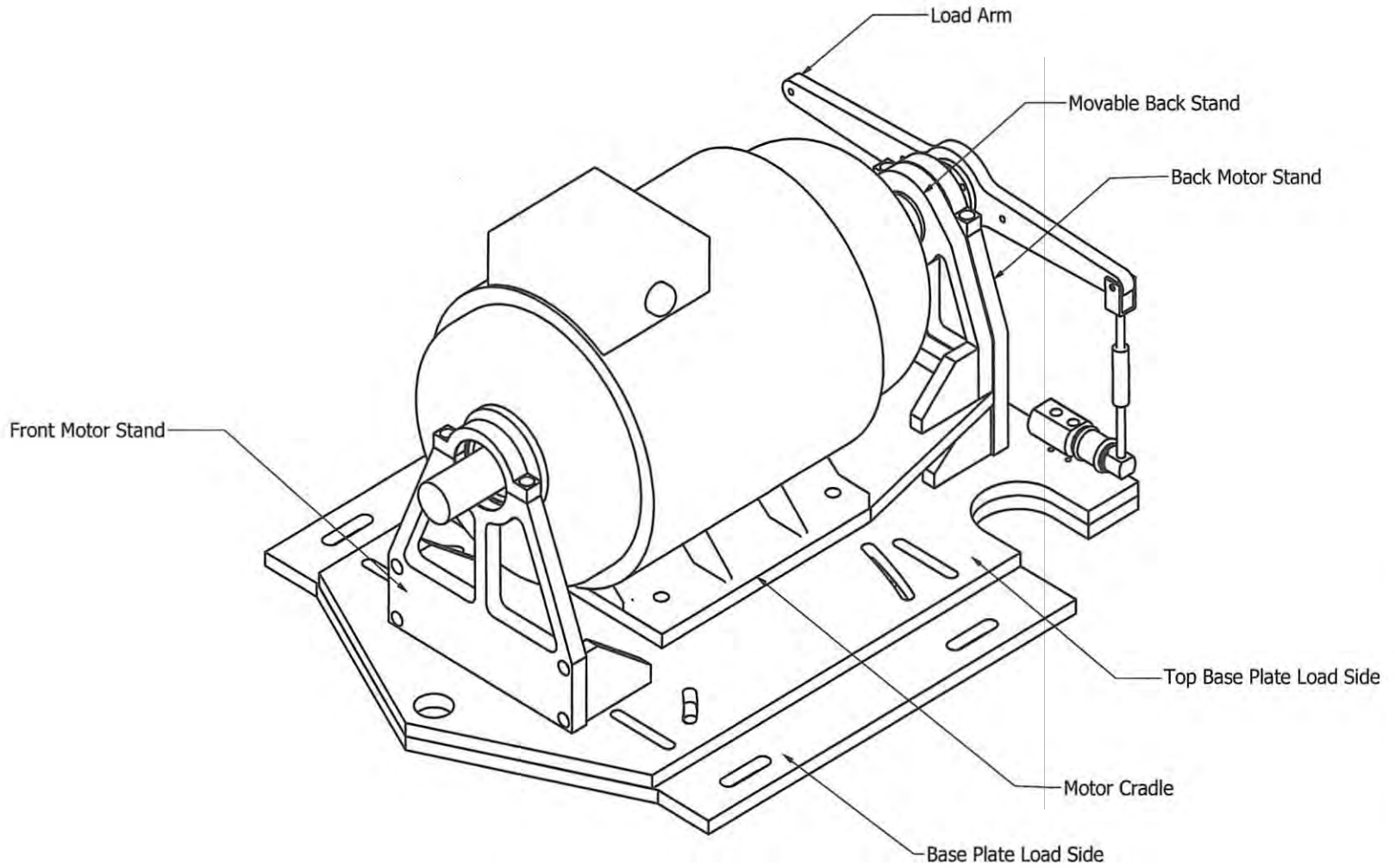| UNIVERSITY OF KWAZULU-NATAL School of Mechanical Engineering	Orthographic Projection ⊲⊙ SCALE 1:5 UNITS : mm	QUANTITY:	PROJECT: Power Efficiency Test Rig	DRAFTPERSON: Kirsty Veale
		MATERIAL:	TITLE: Gimbal Assembly Load	DRAWING No: DATE:

Main Support Base

Bearing Support

Cross Beam

Slider Rail

Lay Shaft Support Base

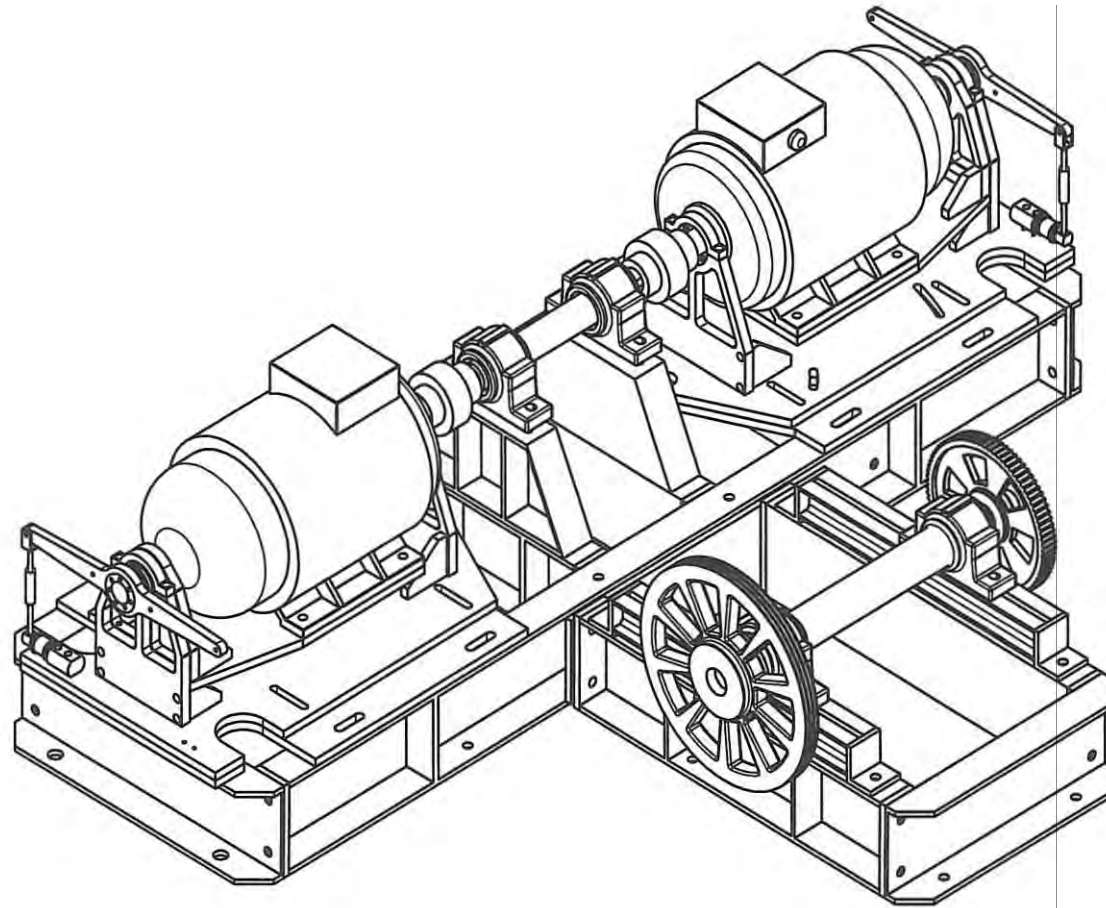|	UNIVERSITY OF KWAZULU-NATAL School of Mechanical Engineering	Orthographic Projection SCALE 1:10 UNITS : mm	QUANTITY:	PROJECT: Power Efficiency Test Rig	DRAFTPERSON: Kirsty Veale	
			MATERIAL:	TITLE: Base Frame	DRAWING No:	DATE:

UNIVERSITY OF KWAZULU-NATAL School of Mechanical Engineering	Orthographic Projection ⊲◯◉ SCALE 1:10 UNITS : mm	QUANTITY:	PROJECT: Power Efficiency Test Rig	DRAFTPERSON: Kirsty Veale	
		MATERIAL:	TITLE: Assembled Test Rig	DRAWING No: DATE:	